CR-166150
(K. Aoyagi)

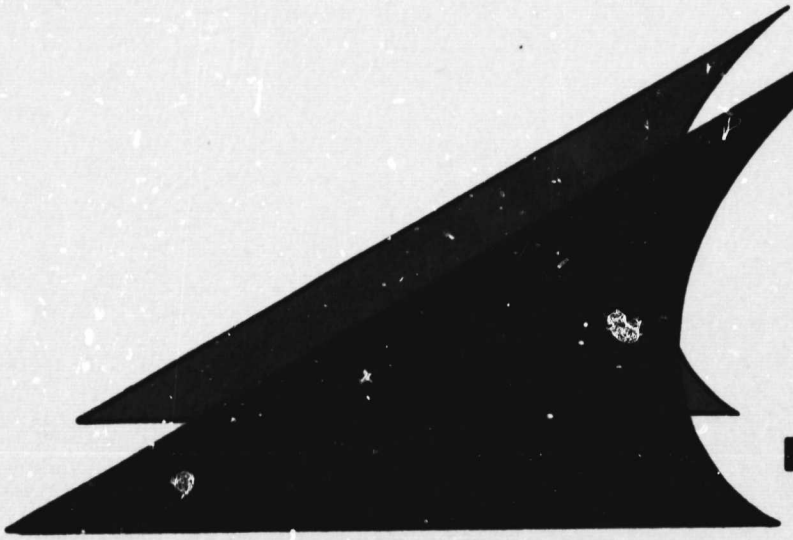

NIELSEN ENGINEERING AND RESEARCH, INC.

OFFICES: 510 CLYDE AVENUE / MOUNTAIN VIEW, CALIFORNIA 94043 / TELEPHONE (415) 968-9457

COPY NO. 8

1 Report No NASA CR-166150	2 Government Accession No	3 Recipient's Catalog No
4 Title and Subtitle A STUDY OF REAL JET EFFECTS ON THE SURFACE PRESSURE DISTRIBUTION INDUCED BY A JET IN A CROSSFLOW		5 Report Date March 1981 6 Performing Organization Code 563/C
7 Author(s) Stanley C. Perkins, Jr. and Michael R. Mendenhall		8 Performing Organization Report No. NEAR TR 237 10. Work Unit No.
9 Performing Organization Name and Address Nielsen Engineering & Research, Inc. 510 Clyde Avenue Mountain View, CA 94043		11 Contract or Grant No. NAS2-10623 13. Type of Report and Period Covered Final 5/1/80 - 3/1/81
12 Sponsoring Agency Name and Address National Aeronautics and Space Administration Ames Research Center Moffett Field, CA 94035		14 Sponsoring Agency Code

15 Supplementary Notes

Ames Technical Monitor, D. Koenig

16. Abstract

Results of a study of jet exit profile, exit Mach number, swirl and turbulence level on jet-induced loadings for jets exhausting from a surface into a crossflow are presented. The importance of each of these "real jet" characteristics has been assessed using available data. Where adequate surface pressure distribution data are available, a correlation method to predict surface pressure for a jet exhausting from an infinite flat plate has been used either to attempt to develop a correlation based on the real jet characteristics or to model the effects of that characteristic. Data comparisons are presented for selected cases. Also, a summary of information on surface pressure distribution data for jets exhausting from flat plates into a subsonic crossflow is presented.

17. Key Words (Suggested by Author(s))	18. Distribution Statement
Subsonic Crossflow Jet in a Crossflow Initial Velocity Profile	Approved for public release; distribution unlimited

19. Security Classif. (of this report)	20 Security Classif. (of this page)	21. No. of Pages	22. Price*
Unclassified	Unclassified	156	

*For sale by the National Technical Information Service, Springfield, Virginia 22161

A STUDY OF REAL JET EFFECTS ON THE SURFACE PRESSURE DISTRIBUTION INDUCED BY A JET IN A CROSSFLOW

by

Stanley C. Perkins, Jr.

and

Michael R. Mendenhall

NEAR TR 237

March 1981

Prepared under Contract No. NAS2-10623

for

NATIONAL AERONAUTICS AND SPACE ADMINISTRATION
Ames Research Center
Moffett Field, CA 94035

by

NIELSEN ENGINEERING & RESEARCH, INC.
510 Clyde Avenue, Mountain View, CA 94043
Telephone (415) 968-9457

TABLE OF CONTENTS

TABLE OF CONTENTS (Concluded)

A STUDY OF REAL JET EFFECTS ON THE SURFACE PRESSURE DISTRIBUTION INDUCED BY A JET IN A CROSSFLOW

by

Stanley C. Perkins, Jr. and Michael R. Mendenhall

SUMMARY

Results of a study of jet exit profile, exit Mach number, swirl and turbulence level on jet-induced loadings for jets exhausting from a surface into a crossflow are presented. The importance of each of these "real jet" characteristics has been assessed using available data. Where adequate surface pressure distribution data are available, a correlation method to predict surface pressure for a jet exhausting from an infinite flat plate has been used either to attempt to develop a correlation based on the real jet characteristic or to model the effects of that characteristic. Data comparisons are presented for selected cases. Also, a summary of information on surface pressure distribution data for jets exhausting from flat plates into a subsonic crossflow is presented.

INTRODUCTION

A considerable amount of research over the past several years has been devoted to understanding the interaction of a jet exhausting from a plane surface into a crossflowing stream. This flow problem is applicable to V/STOL configurations which utilize turbofan or lift-fan engines mounted in the wing, pod, or fuselage. The interaction of the jet and the free stream, which occurs during transition from hovering to horizontal

flight, can result in undesirable aerodynamic loading characteristics influencing lift and stability. Numerous experimental investigations of jets exhausting from a flat plate into an uniform crossflow (refs. 1-13) have been made to study the basic flow problem. In most of these investigations, jets with uniform initial velocity profile are used and the jet velocity ratio (ratio of jet exit velocity to free-stream velocity) is considered the dominant flow parameter for determining jet-induced effects on the surface pressure distribution on the plate.

Jets from turbofan and lift-fan engines and vectored thrust nozzles, utilized by full-scale V/STOL configurations, exhibit nonuniform exit velocity profiles, wide variations in turbulence level, and swirl. These characteristics influence the path of the jet, its entrainment and spreading rate, and the subsequent decay of the jet centerline velocity and dynamic pressure. These real jet characteristics influence the surface pressure distribution in the region of the jet, thereby influencing the overall loads on the airframe surface. Scale effects, which are normally related in aerodynamic flow phenomena to Reynolds number, can also be considered as "real jet" effects. Such effects may be important when extrapolating results from experimental to full-scale configurations.

This report presents the results of a study of real jet effects on jet-induced loadings for jets exhausting from a surface into a crossflow. An assessment of the importance of jet exit profile, jet exit Mach number, swirl, and turbulence level effects on the jet-lift interaction problem is carried out using available data. For cases in which adequate surface pressure data are available, an empirical method developed by Nielsen Engineering & Research, Inc. (refs. 14 and 15) is used in an attempt to develop a correlation based on the real jet

characteristics. This method consists of an inviscid analytical jet model and empirically-derived factors to account for viscous effects. These factors, obtained from a correlation of the difference between predicted surface pressures and measured results, are presented as a function of jet velocity ratio and position on the plate and are defined as follows:

$$\Delta C_p = C_p\Big|_{\text{experimental}} - C_p\Big|_{\text{potential}}$$

For cases in which surface pressure data showing the effects of a particular real jet characteristic are not available, other data are used to infer effects of that characteristic. Finally, recommendations are given for an experimental program to provide data required for further understanding of real jet effects on the induced pressures on adjacent surfaces.

SYMBOLS

A_j	jet exit area, πr_o^2
A_{plate}	total area of circular flat plate used to determine forces and moments
C_m	pitching-moment coefficient, $\frac{\text{pitching moment}}{q_\infty r_{max} A_{plate}}$, see figure 1(b)
C_N	normal-force coefficient, $\frac{\text{normal force}}{q_\infty A_{plate}}$, see figure 1(b)
C_p	pressure coefficient, $p - p_\infty/q_\infty$
D	jet diameter at the exit plane
D_{eff}	jet equivalent idealized diameter
L	lift on circular flat plate or streamwise length of flat plate
ℓ	distance from leading edge of plate to center of jet
M	pitching moment on circular flat plate
M_j,MJ	Mach number of jet at the exit plane
M	free-stream Mach number
p	static pressure
q_j	jet dynamic pressure at exit plane, $\frac{1}{2} \rho_j V_j^2$
q_s	local maximum centerline dynamic pressure of the jet
q_∞	free-stream dynamic pressure, $\frac{1}{2} \rho_\infty V_\infty^2$
R	jet velocity ratio, see equation (1)
Re_D	Reynolds number based on jet diameter at the exit plane, $\rho_\infty V_\infty D/\mu_\infty$
Re_ℓ	Reynolds number based on distance from leading edge of plate to center of jet, $\rho_\infty V_\infty \ell/\mu_\infty$
r	radial distance along the plate from the center of the jet to any field point on the plate

SYMBOLS (Continued)

r_{max}	radius of the circular plage (used in normal force and pitching moment calculations), see figure 1(b)
r_o	jet radius at the exit plane
s	curve length of the jet axis
T	jet thrust
T_j	jet temperature at the exit plane
T_∞	free-stream temperature
t	local jet radius
u'/V_j	turbulence intensity of the jet
V_j	jet velocity at the exit plane
V_m	local maximum centerline velocity of the jet
V_∞	constant free-stream velocity
W	width of flat plate
x,y,z	plate coordinate system fixed at the center of the jet exit plane, positive x is upstream
x_j,y_j,z_j	jet coordinate system fixed at center of the jet exit plane, positive x_j is downstream
β	polar angle, measured clockwise from the positive x-axis in the plate x-y plane, see figure 1(a)
ξ	curve length of the jet axis multiplied by the potential core length of a free jet divided by the potential core length of the jet at jet velocity ratio R
δ_j	initial inclination angle of jet centerline, measured from the positive x-axis in the x-z plane, $\delta_j = 90° - \theta$; see figure 1(a)
θ	initial inclination angle of jet centerline, measured from the positive z_j axis in the x_j-z_j plane, $\theta = 0°$ for a jet issuing normal to the free stream, see figure 1(a)

SYMBOLS (Concluded)

δ_{bl}	boundary-layer thickness
μ_∞	absolute viscosity of free stream
ρ_j	jet density at exit plane
ρ_∞	free-stream density
ζ	jet centerline velocity decay rate, $\frac{V_m - V_\infty}{V_j - V_\infty}$

Subscripts

j	jet quantity
m,max	maximum value
∞	free-stream quantity

APPROACH

A sketch of an expanding jet of initial velocity V_j and initial inclination angle θ emerging from an infinite plate into a subsonic crossflow of velocity V_∞ is shown in figure 1(a). The overall effect of the jet on the plate is to produce a region of positive pressures upstream of the jet and a region of negative pressures laterally and downstream of the jet. In most experimental investigations (refs. 1-9), the dominant flow parameter influencing the surface pressure distribution on the plate is considered to be jet velocity ratio, R, defined below:

$$R = \left[\frac{\int_{A_j} \rho_j V_j^2 dA}{\rho_\infty V_\infty^2 A_j} \right]^{1/2} \tag{1}$$

This ratio reduces to a velocity ratio (V_j/V_∞), a Mach number ratio (M_j/M_∞) or the square root of a dynamic pressure ratio ($\sqrt{q_j/q_\infty}$) depending on the particular experimental flow parameters

As a part of the present investigation, a literature search was carried out for references containing surface pressures and additional data for jets exhausting into a crossflow. References of interest were studied to determine the range and type of data available. A summary of information on available surface pressure distribution data is presented in Appendix A. The additional data, some of which

is for jets without adjacent surfaces, include measurements of jet potential core length, trajectories, temperature, and spreading rate. These data can be used to infer effects of a given parameter on the surface pressure distribution. The main parameters of interest are jet velocity ratio, jet exit and free-stream Mach numbers, jet turbulence level, exit velocity profiles and swirl. Data are available for examining jet exit Mach number and exit velocity profile effects on surface pressure distributions. Surface pressure data are not available for jets with swirl; however, data showing effects of swirl on other jet quantities, such as jet centerline decay, are available. Also, jet turbulence data are not presented in any of the references with surface pressure data; however, information on jet potential core length and/or centerline decay rates can be indicative of jet turbulence level.

In the following sections, an assessment of the importance of each of the aforementioned jet characteristics on surface pressures for a jet exhausting into a crossflow is carried out. If adequate data are available for a particular jet characteristic, the current prediction method with viscous correlation factors (refs. 14 and 15) can be used to develop a correlation for that characteristic. It is noted here that the nature of real jet characteristics often does not allow sufficient separation of effects for correlation factors to be obtained. For example, nonuniform exit profile jets usually have different potential core lengths, decay rates, and centerline trajectories than uniform exit profile jets. In this situation, a correlation based on a single jet characteristic cannot be obtained, and the current prediction method is used in conjunction with available jet data (e.g., jet decay rates, centerline trajectories) to attempt to model the effects of nonuniform exit profile.

In addition to the sections on nonuniform exit profile, jet exit Mach number, turbulence, and swirl, a general section is included. This section contains information on jet temperature/density effects and plate boundary-layer effects. Limited information is available on these jet characteristics which are nevertheless of interest for the jet in a crossflow problem.

Jet Exit Velocity Profile

In most experimental investigations of a jet exhausting from a flat plate into a crossflow, jets with a uniform initial velocity profile are considered. This is not the type of initial profile to be expected in general in full-scale V/STOL aircraft which employ turbofan and lift-fan engines and vectored thrust nozzles. Experimental investigations of the effects of nonuniform exit velocity profiles on surface pressures are reported in references 10 through 13. Reference 12 incorporates cylindrical centerbodies submerged in the jet nozzle to alter the jet exit dynamic pressure profile (plugged jets), while reference 11 uses an annular nozzle with a high velocity core, a dead air core, and a vaned nozzle. The equivalent ideal nozzle concept of Ziegler and Wooler (ref. 13) is used to reduce data in both references. This procedure, used for jets with a nonuniform exit velocity profile, determines an effective jet dynamic pressure and effective jet diameter corresponding to a jet with the same thrust and mass flow, but having a uniform exit velocity profile. The effective diameter and effective jet dynamic pressure are used to nondimensionalize distances and to obtain the desired jet velocity ratio, respectively.

In the following sections, comparisons of surface pressure distribution data for uniform and nonuniform exit profile jets are presented. For the plugged jets, comparisons of forces and moments on the plate are also presented. In addition, attempts

are made to model the effects of nonuniform exit profile on surface pressures using the empirical correlation method of references 14 and 15 in conjunction with jet centerline trajectory and decay rate data. Comparisons of measured and predicted surface pressures are presented for a limited number of jet velocity ratios.

Plugged jets.- Jet centerline trajectories, jet exit dynamic pressure profiles, jet centerline dynamic pressure decay rates, surface pressures, and forces and moments are presented in references 10 and 12 for a rounded tip and flat tip centerbody positioned at various depths below the jet exit plane (see sketch). Data are for a jet exit Mach number (based on

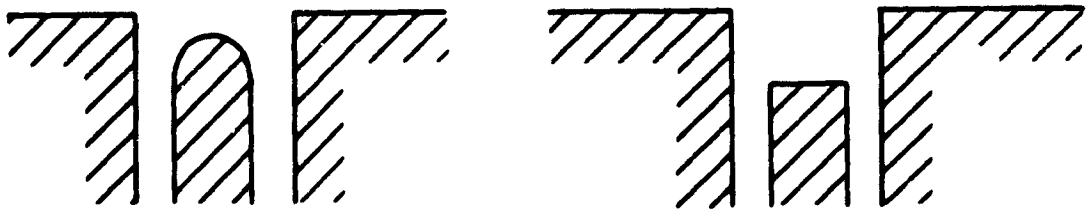

Round plug centerbody Flat plug centerbody

effective velocity) of 0.40 and jet velocity ratios (based on effective velocity) of 2.2 to 10.0.

Jet-induced lift loss and pitching moments are obtained by integrating surface pressure distributions over a circular area on the plate with the jet at the center. The positive sense of the normal force (and lift) and pitching moment is shown in figure 1(b). Results for an area on the plate equal to 43 times the jet effective exit area are presented in figures 2 and 3 for various cases of centerbody type and position as a function of 1/R. In these figures, the lift loss is nondimensionalized by

the calculated thrust, and the pitching moment is nondimensionalized by the product of calculated thrust and jet effective diameter. The equivalent jet concept works reasonably well for forces and moments for high jet velocity ratios, but does not collapse the data at low jet velocity ratios. At a constant jet velocity, the centerbody causes a smaller jet-induced lift loss and pitching moment as compared to a jet with no centerbody. These results, which are obtained for a constant plate area to jet effective area ratio, do not indicate the effects of jet exit profile on loads for the same size plate. Figures 4 and 5 present lift loss and pitching moment for a circular area on the plate which is 43 times the actual jet exit area. Pitching moment is nondimensionalized by the calculated thrust times the actual jet exit diameter in these figures. Use of the same physical area collapses the moment curves very well and does a better job on the lift force. On this basis, the jet exit profile effect on moments is small and is still appreciable on lift force at low jet velocity ratios.

Note that the differences in lift loss for R = 4 and 10 between the "no plug" data from references 4 and 12 are larger than the differences between the "no plug" and "plug" data of reference 12. This indicates that the effects on surface pressures and loads due to jet exit profile may be no greater than the differences caused by scatter between different sets of data for uniform exit profile jets. Force data comparisons for a wider range of jet velocity are needed to verify these conclusions.

Examination of figures 2 through 5 reveals that the largest effects on lift loss are for cases in which the jet decay rates of the plugged jets are most different from those of the clean (no plug) jets; i.e., the flat plug flush and round plug flush cases. Jet dynamic pressure decay rates for R = 2.5 and

8.0, shown in figures 6 and 7, respectively, indicate much faster decay rates for the aforementioned cases than for the clean jet case. Also, more rapid decay rates result in more rapid deflection of the jet in the free stream direction as shown in figures 8 and 9. Due to the multiple effects of the jet exit profile on other jet quantities, a correlation based on this jet characteristic would have little meaning. Therefore, the present prediction method, in conjunction with data on jet decay rates and centerline trajectories, is used to predict surface pressures for R = 2.5 and 7.8.

In the following sections, jet models for determining the effects of nonuniform exit profile on surface pressures are obtained in a systematic fashion. First, uniform exit profile data for a given R are compared with predicted results obtained using the correlation method of references 14 and 15. Agreement between the different sets of available data and between measured and predicted results should be reasonably good over the entire plate. Second, the same predicted results (with original correlation factors) are compared with the no-plug and plugged jet data from reference 12 to determine the effects of nonuniform exit profile on surface pressures. In regions on the plate where these effects are large, the present method will not accurately predict pressures for the nonuniform profile jets. In such cases, the present potential flow model for the jet is modified using available jet centerline trajectory and dynamic pressure decay data presented in reference 12. New predicted results obtained using the modified potential flow models are compared with nonuniform exit profile data for the region ahead of the jet. In this region of the plate, viscous effects are believed to be small ($0^{\circ} < \beta < 60^{\circ}$) based on experimental observations (ref. 7). Data comparisons in this region are a true test of the ability of the potential flow model to accurately predict pressures on the plate in the absence of

large viscous effects. If reasonably good agreement is obtained between measured and predicted results in the region ahead of the jet, the original correlation factors (refs. 14 and 15) are used in conjunction with the modified potential flow models to obtain "corrected" predicted results. Comparisons of these predicted pressures and measured pressures are made for the entire plate.

Effects of nonuniform exit profile on surface pressures may be different for low and high jet velocity ratios, since blockage effects are dominant at low R values and entrainment effects are dominant at high R values. Jet models for plugged jets are presented for a low and a high jet velocity ratio ($R \approx 2.5$ and 7.8).

Uniform velocity profile, low velocity ratio: Comparison of measured and predicted (with original correlation factors) surface pressures for $R \approx 2.5$ are shown in figure 10 for several radial positions around the jet. The uniform exit profile data of reference 12, which are not included in the correlation factors, are compared with data from references 1 and 9 in the same figure. Agreement between the different sets of data and between measured and predicted results is reasonably good over most of the plate; however, pressures along $\beta = 180^{\circ}$ indicate that the jet of reference 12 may exhibit a more rapid decay rate than the jets of references 1 and 9.

Nonuniform velocity profile, low velocity ratio: Figure 11 presents a comparison of the same predicted results with data from reference 12 for the "no plug," "round plug down .5D" (RP1), and "round plug down 1.0D" (RP2) cases. The effects of jet decay rate on surface pressures for $R \approx 2.5$ are reasonably small ahead of the jet ($\beta < 30^{\circ}$) and generally increase to the side of and behind the jet. The surface pressures for the

plugged jets generally show a more rapid decay to $C_p = 0.0$ than the no plug jet. These effects can be explained in part by the more rapid deflection of the RP1 and RP2 jets in the free-stream direction due to more rapid decay rates than those of the "clean" jets. This results in a decrease in the blockage effect and a lowering of pressures ahead of the jet, as exhibited by the RP2 data in figure 11.

The pressures behind the plugged jets may be affected by a weakening of the vortex pair associated with the jet, as suggested by Kuhlman (ref. 10). This phenomena is discussed by Taylor (ref. 8) for jets initially inclined to the crossflow. Reference 8 suggests that the generation of vorticity decreases as the jet inclination angle (θ, see figure 1) increases, thereby causing a lowering of the vortex-induced entrainment rate. In fact, trends exhibited by the $\beta = 0^{\circ}$ data of reference 10 are similar to those exhibited by the inclined jet data of reference 8. For example, for $R < 4$, an increase in inclination angle from the normal and a more rapid dynamic pressure decay rate cause the pressure level along $\beta = 0^{\circ}$ to decrease. For $R > 4$, the pressure level along $\beta = 0^{\circ}$ increases with an increase in inclination angle and decay rate. The "free-jet" type entrainment may also be reduced for the RP1 and RP2 jets, since the centerline velocities decay much faster than those of the clean jet. Such effects would give rise to higher pressures behind the jet, as exhibited by the data of RP1 and RP2 in figure 11.

Modified potential flow model, low velocity ratio: The potential flow model developed in reference 14 utilizes jet centerline decay data from reference 16 to determine jet spreading rates for jet velocity ratios 4.0, 6.0, and 8.0. Spreading rates for other jet velocity ratios are presently obtained by interpolating or extrapolating these rates. The

centerline velocity decay data for R = 4, 6, and 8 are shown in figure 12, where V_m is the maximum centerline velocity and s is the distance along the jet axis. The dynamic pressure decay data presented in references 10 and 12 can be used to obtain jet centerline velocity decay rates, assuming the locus of maximum jet dynamic pressures coincides with the locus of maximum velocities. Since the jet exit temperature is nearly the same as that of the free stream, this assumption is valid. Jet centerline velocity decay rates, based on the data shown in figure 6, are presented in figure 13 for the clean, RP1, and RP2 jets.

Jet centerline trajectory data are used in the potential flow model to set up the jet blockage and entrainment models. The centerline data for the three jets being modeled (fig. 8) are utilized in the following manner. First a smoothed curve is obtained for the region between the first and last data points. The centerline shape between the jet exit and the first data point is obtained for two cases. For jet model A, centerlines are obtained using Margason's equation (ref. 17) for a range of jet velocity ratios ($1.5 < R < 2.2$) and the curve which best fit the data in the region near each jet is used. Keffer and Baines (ref. 16) note that for $R < 4$, jets enter the free stream at an angle less than 90° to the plate. Such effects may also be exhibited by nonuniform exit profile jets, since these jets show a more rapid deflection in the free-stream direction than uniform profile jets. For jet model B, a jet centerline which is slightly inclined to the normal and which passes through the first data point is used.

Comparisons of measured and predicted (without correlation factors) results for the region ahead of jet for jets RP1 and RP2 are shown in figures 14 and 15, respectively. Jet models A and B are described above, and model C utilizes the centerlines

from B and a slightly smaller expansion rate. Each successive case represents a reduction in blockage effects which improves agreement between data and theory, especially in the region near the jet. These comparisons indicate that the predicted results are very sensitive to the jet centerline shape/jet expansion rate combination in the region near the jet. Data on these jet quantities in the region of the jet are necessary to better assess the jet model utilized by the present prediction method.

Modified jet model, low velocity ratio: Predicted results obtained using the original correlation factors from references 14 and 15 are compared with data for jets RP1 and RP2 in figures 16 and 17. It is interesting to note that the predicted results obtained using jet model B and the correlation factors agree very well with experiment in the region ahead of the jet. The correlation factors for the region behind the jet (figs. 16(c) and 17(c)) greatly overcorrect the theoretical results for RP1 and RP2. Reducing entrainment effects in the potential flow model, obtained by reducing the jet velocity ratio while keeping all other jet quantities the same, showed improved agreement between data and theory everywhere except in the region immediately ahead of the jet.

Experimental data from reference 3 for R = 3.3 exhibit trends similar to those of the RP1 and RP2 jets when compared to data from references 1 and 4. The jet in reference 3 has a very rapid decay rate, resulting in a potential core length of only .5 jet diameters. This more rapid jet decay for the jet of reference 3 may explain the disagreement between these data and data from other sources. The surface pressure data from reference 2 for R = 2, 4, and 8 decay more rapidly than data for other uniform profile jets. This suggests that the dynamic pressure decay rates of the reference 2 data are more rapid than those present in other experimental investigations.

Uniform velocity profile, high velocity ratio: Attempts to model the effects of nonuniform exit profile on surface pressures were also carried out for R = 8.0. Comparisons of measured and predicted (with original correlation factors) surface pressures for R = 8.0 are shown in figure 18. The uniform profile jet data from reference 12 agrees reasonably well with most of the data except along $\beta = 0^{\circ}$ and in the region behind the jet (fig. 18(d)), where there are large differences between different sets of data.

Nonuniform velocity profile, high velocity ratio: Comparisons of predicted results and data from reference 12 for the no plug and round plug down 0.5D (RP1) cases are shown in figure 19. The effects due to jet decay rate are largest directly ahead of and in the region behind the jet. The plugged jet data shows less blockage (lower pressures) ahead of the jet (fig. 19(a)) and less entrainment (higher pressures) behind the jet (fig. 19(d)), as did the R = 2.5 data (fig. 11).

Modified potential flow model, high velocity ratio: Jet centerline velocity decay rates for R = 8, determined from the dynamic pressure decay rates (fig. 7), are presented in figure 20 for the no plug and RP1 jets. The clean and RP1 jets appear to have potential core lengths of 3.5 and less than 1.0 jet diameters, respectively. The potential core length affects the modeled jet spreading rate, and therefore may have a large effect on predicted pressures ahead of and near the jet. Several jet models were developed to predict the effects of jet decay rate on surface pressures for R = 7.76. Different models are obtained by varying one or more of the following parameters: potential core length, jet centerline description in region near jet, the value of ψ in potential core region, and distance along jet centerline at which jet expansion begins. Based on the results shown in figure 20, two baseline jet models were

developed. One baseline model is a jet with no potential core and $\psi = 1.0$ at $s/D = 0$, and the other is a jet with a potential core length of 2.5 jet diameters and $\psi = .815$ in the potential core region. The latter model assumes the value of ψ decays to .815 a very short distance downstream of the jet exit. Two centerline descriptions are also used; one approximates the centerline as a straight line between the jet exit and the first data point, and the other uses a faired curve between these two points. For cases in which the jet has a potential core, jet models having a constant radius ($r/r_o = 1.0$) for distances of 0.0, 1.25, and 2.05 jet diameters along the centerline are developed.

The jet models for which predicted results without correlation factors in the region ahead of the jet agree best with data are summarized as follows:

Jet Model	Potential Core Length	Jet ℄ Description Near Jet	ψ (Potential Core Region)	s/D at Which Jet Expansion Begins
A	0.0D	Straight line	1.0	0.0
B	2.5D	Faired curve	.815	1.25
C	Expansion rate is average of rates from Models A and B, with expansion beginning at s/D = 1.0.			

The expansion rates for each of these cases are shown in figure 21. Comparisons of predicted pressures without correlation factors and data for the RP1 jet are shown in figure 22. Results obtained using jet model A agree best with

data, although the data along $\beta = 0^{\circ}$ indicate less of a blockage effect than is predicted. These results are not unexpected since the uniform exit profile data of reference 12 show the same trend along $\beta = 0^{\circ}$ when compared with predicted results with correlation factors in figure 19(a).

Modified jet model, high velocity ratio: Predicted results with original correlation factors (refs. 14 and 15) are compared with RP1 data in figure 23 and show good agreement for $\beta \leq 90^{\circ}$ between the predicted results from jet models B and C and experiment. Much larger correction factors are needed for $x/D \leq 2.5$, $\beta = 0^{\circ}$ to improve the predicted results. With the exception of the $\beta = 0^{\circ}$ comparisons, the predicted results obtained using jet model A are overcorrected, as are all of the results for $\beta = 180^{\circ}$. Once again, the reduced entrainment behind the jet for plugged jets results in the large pressure differences between clean jets and jets with centerbodies. Reducing entrainment for jet model A improved agreement between theory and experiment in the region behind the jet, as it did for the R = 2.5 plugged jet data.

Summary, plugged jets: Based on the analysis of data from references 10 through 12, it appears that jet exit profile and jet centerline velocity decay rates are important parameters for determining jet-induced surface pressure distributions on surfaces adjacent to the jet. These jet parameters were found to affect jet centerline trajectory, potential core length, spreading rate and entrainment. Use of the equivalent ideal jet concept to correlate surface pressures was not successful in the regions to the side and behind the jet, nor was it successful in correlating loads on the plate. However, comparisons of measured and predicted results for R = 2.2 and 8.0 (refs. 10 and 12) indicate that the potential flow model developed in references 14 and 15 can be used to determine jet exit profile

effects on plate surface pressures in the region ahead of the jet, provided detailed data on jet centerline trajectories, expansion rates, and centerline decay rates are available. Correlation factors developed in references 14 and 15 tended to overcorrect the predicted results in the region to the side and behind the jet for the nonuniform exit profile jets; therefore, new correlation factors, possibly based on jet centerline decay rate, would have to be developed for these jets.

Annular jets.- References 11 and 13 present pressure distribution data for jets with uniform exit, annular (zero core flow) exit, and high-velocity-core profiles (see sketch). These

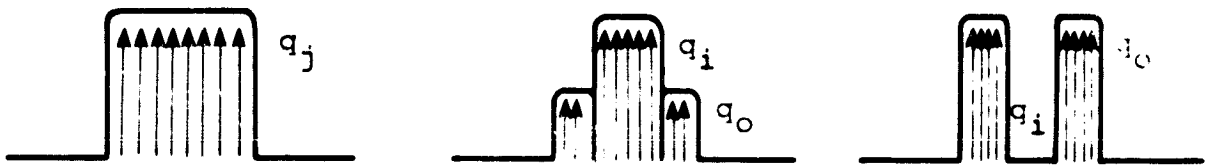

Uniform Exit Profile, q_j = constant

High-Velocity Core $q_i > q_o$

Annular Exit Profile, $q_i = 0$

jets are intended to be representative of jets from nozzles found on full-scale V/STOL vehicles; namely, lift-jet, lift-fan, and high by-pass ratio turbofan nozzles, respectively. The equivalent ideal nozzle concept of Ziegler and Wooler (ref. 13) is used to obtain jet velocity ratios and to nondimensionalize distances. Jet trajectory data are presented only for R = 8, and static entrainment data is also presented. Jet decay rate data is not presented; therefore, jet models for the jets with nonuniform exit profiles cannot be modeled in the same manner as was done for the data of references 10 and 12. Instead, comparisons of surface pressure distribution data are presented

for the different exit profiles and observations on the effects of jet exit profile, based on these data, are made.

Figures 18 and 24 show comparisons of surface pressure distribution data from reference 11 with data from other sources for uniform exit profile jets and with predicted results with correlation factors for R = 8.0 and 2.2, respectively. For R = 2.2 (fig. 24), the uniform exit profile data from reference 11 agrees well with data from reference 4 and with the predicted results. For R = 8 (fig. 18), agreement between data from reference 11 and that from other references is generally good except in the region ahead of the jet, where the pressure coefficients from references 6 and 11 decay less rapidly than that from other references. The cause of this difference could not be determined from available data; however, both sets of data (refs. 6 and 11) were obtained in the same wind tunnel using the same experimental apparatus (circular plate) and therefore would be expected to exhibit similar, and possibly identical, trends. It is noted that at some positions on the plate, differences between the data from references 6 and 11 are greater than differences between data obtained in different wind tunnel facilities. Such differences represent limits of accuracy in measuring jet-induced pressures on the plate.

Examination of figure 24 indicates that the largest effects of jet exit profile are for the regions ahead of and behind the jet. In the region ahead of the jet, the high-velocity-core (HVC) profile jet data resembles that of the annular exit profile (AEP) jet. Both jets exhibit lower pressure levels than the uniform exit profile (UEP) jet in the same fashion as was shown by the plugged jet data of reference 12. This would seem to indicate that the jet centerline decay rates for these jets (HVC and AEP) are more rapid than that for the UEP jet. It is unlikely that the HVC jet centerline decay

rate is more rapid than that of the UEP jet, since the dynamic pressure at the HVC jet exit is several times larger than that of the UEP jet. It appears that the core region of the HVC jet, which has an exit area equal to only 16-percent of the total jet exit area, does not influence the blockage effects on surface pressures ahead of the jet, resulting in jet effects which are similar to those for an annular exit profile jet with the same jet velocity ratio. In the region behind the jet (figs. 24(c) and (d)), the HVC jet exhibits lower pressures and the AEP jet exhibits higher pressures than those of the uniform profile jet. The AEP jet effects are again similar to those of the plugged jets from reference 12. The lower pressures produced by the HVC jet may be due to increased entrainment resulting from a stronger vortex pair, since this jet probably penetrates the free-stream more than either the AEP or UEP jets (jet centerline data are not available for R = 2.2 to determine if this is true). Also, the stronger core region of the HVC jet may increase free-jet type entrainment.

Jet-induced effects on surface pressures due to the AEP and HVC jets for R = 8, shown in figure 25, are similar to those exhibited by the data for R = 2.2. The largest effects appear in the region near the jet, as would be expected. In the region ahead of the jet, the pressures for the HVC jet are more like those exhibited by a jet at a lower jet velocity ratio; that is, an effective jet velocity ratio based on the exit dynamic pressure of the annular region. In the region aft of (figs. 25(c) and (d)) and near the jet, the AEP jet again exhibits higher pressures and the HVC jet exhibits lower pressures than the UEP data. Jet centerline data presented in figure 26 show that the HVC jet penetrates the free stream more than the UEP and AEP jets. As previously discussed in the section on the plugged jet data from reference 12, decreased penetration of a jet into the free stream may result in a weakening of the vortex

pair associated with the jet. This reduces entrainment effects behind the jet thereby increasing pressures in this region. It follows that stronger penetration into the free stream results in stronger vortices and an increase in the entrainment due to these vortices. This results in decreased pressures behind the jet, as exhibited by the HVC data in figure 25.

Analysis of the annular jet data from references 11 and 13 indicate that nonuniform exit profiles affect surface pressures and jet centerline trajectories. Effects on pressures are largest in the regions directly ahead of ($\beta = 0^{\circ}$) and behind ($\beta = 180^{\circ}$) the jet, as was the case for the plugged jet data. Effects on overall plate loads could not be obtained for the annular jets due to a lack of data in the region close to the jet ($r/D < 1.25$), where effects due to jet exit profile are usually the largest.

Jet Exit Mach Number

Surface pressure distribution data, as summarized in Appendix A, is available for a wide range of jet exit/free-stream Mach number combinations. Full-scale V/STOL configurations are also expected to exhibit a wide range of these parameters. Experimental studies of the effects of jet exit and free-stream Mach number on surface pressures are carried out in references 1, 4, 5, and 6. These studies also represent jet Reynolds number effects studies, since jet exit and free-stream Mach numbers were varied for constant jet velocity ratio R. Analysis of these data to determine if a correlation based on jet Mach number is possible or warranted, follows.

Measured surface pressures.- Figures 27 through 31 present plots of experimental pressure coefficient vs. r/D for constant β for a range of jet velocity ratios. These figures include data from the jet Mach number studies of references 1, 4, 5, and 6 and other experimental studies in references 2, 7, 9, and 12. These data indicate the effects of jet Mach number (M_j) and the trends of the effects exhibited by the different sets of data are often not consistent with one another. For example, data for $V_j/V_\infty = 2.5$ from reference 1 (fig. 27) show the highest C_p values for $M_j = .45$ and lower C_p values for $M_j = .18$ and .88. These trends are inconsistent with those exhibited by the $V_j/V_\infty = 3.0$ data from reference 5 (fig. 28), which show an increase in C_p with increasing M_j for $0^\circ < \beta < 120^\circ$ and a decrease in C_p with increasing M_j for $\beta = 180^\circ$. Similar trends are exhibited by the data of reference 5 for $V_j/V_\infty = 2$ and 4. Data for $V_j/V_\infty = 6$ from reference 4 (fig. 29) show the lowest C_p values for $M_j = .74$ and higher C_p values for $M_j = .46$ and .94. The reference 6 data exhibit trends which are different from those of both references 1 and 5. It should be noted that while the observed trends are often inconsistent, differences in C_p due to M_j are often of the same order as differences between different sets of data at the same jet Mach number. Figure 18 illustrates such differences at R = 8 for data from several sources.

The present prediction method is used to model the effects of jet Mach number on surface pressures in the following manner. It has been shown in experimental investigations on jets without crossflow that potential core length increases with Reynolds number (ref. 18) and with jet exit Mach number (ref. 19). Assuming similar behavior for jets in a crossflow, the effects of jet exit Mach number are modeled by varying the length of the potential core. Predicted results are obtained for jet velocity ratio 2.0 with potential core lengths 1.0, 2.0,

and 3.0, and for jet velocity ratio 6.0 with core lengths 2.0, 3.0, and 4.0. Varying the potential core length affects only the modeled jet expansion rate, and since this rate did not change appreciably, varying the potential core length had very little effect on surface pressures. These comparisons are not shown since the differences are barely discernable on a graph. It is noted, however, that a change in potential core in a real jet will affect penetration of the jet into the crossflow, thereby affecting jet blockage, expansion and trajectory. Such changes are not modeled in the above potential core length study because of an absence of data.

At low jet velocity ratios, where blockage effects dominate entrainment effects in the region ahead of the jet, increasing potential core length (for constant R) will decrease the deflection of the jet as it enters the crossflow. This action results in increased blockage effects, thereby increasing C_p ahead of the jet. The data of reference 5 for jet velocity ratios 2.0, 3.0, and 4.0 (figs. 30, 28, and 31, respectively) exhibit such effects. At high jet velocity ratios, where entrainment effects dominate blockage effects ahead of the jet, jet entrainment may be a function of M_j; however, data are not available to determine if such a relationship exists. Data showing the effects of jet Mach numbers on jet centerline trajectory, expansion and entrainment are required to more accurately predict the effects of M_j on surface pressures.

Measured and predicted surface pressures.- Based on differing trends exhibited by the aforementioned data, it is not evident that a correlation based on jet exit Mach number is possible. The following approach should determine the practicality of such a correlation. Using the current prediction method without viscous correlation factors, comparisons of predicted and measured surface pressures are made for the

region of the plate ahead of the jet. If predicted results are found to consistently agree best with data for a particular jet Mach number, a set of correlation factors can be obtained for that jet exit Mach number. Data for other jet exit Mach numbers can then be used in conjunction with predicted results (obtained using these correlation factors) to obtain a correlation for jet exit Mach number.

Figures 32 through 36 show comparisons of measured and predicted surface pressures for nominal jet velocity ratios 2.0, 3.0, 3.33, 4.0, and 6.0 for the region ahead of the jet. While there is generally good agreement between theory and data, there is no jet exit Mach number for which predicted results consistently agree best with experiment.

Forces and moments.- Analysis of available data indicates that a correlation based on jet exit Mach number effects on surface pressures cannot be modeled due to a lack of jet characteristics data. An effective means of determining the overall effects of jet exit Mach number is to compare the total loads on a finite plate in the same manner as was done for the jet exit profile study. Normal-force and pitching-moment coefficients obtained using data from references 4, 5, and 9 are presented in figure 37. Results are not presented for references 1 and 6 due to a lack of data in the region near the jet, where differences in C_p due to jet Mach number are the largest. Results from references 4 and 5 indicate that normal force is more sensitive to jet exit Mach number than pitching moment. This indicates that the change in pressure level due to jet Mach number is nearly constant around the plate.

The results from references 4 and 5 show a decrease in normal-force coefficient with increasing Mach number except for the $M_j = .46$ data from reference 4. This same result was

also shown by the surface pressure data comparisons in figures 29 and 36. The decrease in normal force at R = 10.0 for M_j = .94 (ref. 4) is also inconsistent with respect to the other data, thereby resulting in apparently large jet exit Mach number effects on normal force for this jet velocity ratio. In the parts of figure 37, the M_j = .74 results of reference 4 agree best with the high jet Mach number results (.63 < M_j < 1.0) of reference 5, and the M_j = .94 results of reference 4 agree best with the M_j = .95 results of reference 9. In general, the effect of jet exit Mach number on normal force is usually no greater than the differences caused by scatter between different sets of data. Based on these results, a correlation for jet exit Mach number does not appear to be warranted. In fact, a correlation based on jet velocity ratio R and developed using all of the available data would probably be more accurate than a correlation based on jet exit Mach number.

Swirl

Swirling the jet exhaust of turbofan and turbojet engines as a means of reducing jet noise has been investigated for the past several years. Swirling exhaust flows may induce loadings on V/STOL aircraft that are different from those induced by flows without swirl. Data showing the effects of swirl on surface pressure distribution for jets in a crossflow are not available. Most of the swirling jet studies are for jets exhausting into queiscent air and the data are acoustical in nature; however, jet quantities such as jet spreading rates and dynamic pressure decay rates have also been obtained in some of the studies. Data of this nature can be used to infer effects of swirl on surface pressures, assuming that effects on jet quantities due to swirl for jets exhausting into a crossflow are similar to those for jets exhausting into queiscent air. A summary of swirled jet results from several references and comments on the

effects of swirl for a jet in a crossflow, based on these results, follow.

Schwartz (refs. 20-22) has done a considerable amount of acoustical research on swirling-jet flows in turbofan and turbojet engines. Of particular interest are results indicating that swirl in a hot jet exhaust without crossflow increases the rates of turbulent mixing, thereby increasing spreading rates and entrainment of flow into the jet. It was also found that the axial velocity component of the flow in a swirling jet decays at a greater rate than that in a nonswirled jet. In addition, data show that the effect of swirling flow on the turbulent modes of the jet structure increases as density and temperature gradients increase. These latter results indicate that swirling is more effective in high thrust engines whose exhausts exhibit larger density and temperature gradients than those of low thrust engines. In the aforementioned tests, swirl is introduced into the flow by solid-body rotation in the engine exhaust nozzle.

An experimental study of the effects of swirl and initial velocity profile on jet quantities for a jet exhausting from a pipe are presented in reference 23. A number of different methods for producing swirl in the jet are investigated. In addition, a swirling jet with an exit velocity profile with a minimum at the center of the jet is investigated. Results indicate that introducing swirl in a jet usually increases the jet expansion rate and the jet centerline velocity decay rate. One method of producing swirl does result in a reduction in both of these rates. The jets with the greatest amounts of swirl have the greatest levels of turbulence intensity and produce the largest effects on jet spreading and centerline decay rates. More importantly, it was found that for a jet with swirl, a radial gradient of axial velocity that is positive outwards from the jet axis can result in a reduction of jet expansion and

centerline velocity decay rates as compared with an axial velocity gradient which is negative outwards. For a jet without swirl, the positive outwards gradient produces an increase in jet expansion and causes the centerline velocity to decay more rapidly.

From the effects of swirl on jet quantities for jets exhausting into queiscent air, the following effects due to swirl may be inferred for the jet in a crossflow:

- more rapid deflection of the jet in the free-stream direction due to shortening of the potential core.

- decrease in blockage effects (lower surface pressures) ahead of the jet due to more rapid deflection of jet in free-stream direction.

- increase in blockage effects (higher surface pressures) ahead of the jet due to an increase in jet expansion.

- increase in entrainment effects (lower surface pressures) in the region behind the jet due to an increase in "free-jet" type entrainment.

In addition, it can be inferred that a swirled jet with a velocity deficit in the center at the exit will probably penetrate the crossflow more than one with a uniform exit velocity profile, due to more rapid centerline velocity decay rates for the latter jet. This would result in an increase in blockage effects, or higher surface pressures, ahead of the jet.

The combination of all the above effects for a jet with swirl may substantially change any given effect. For instance,

the increase in blockage effects ahead of the jet due to an increase in jet expansion may be offset by the effects due to centerline changes and increased entrainment. Swirling the exhaust would probably have an effect on the development of the attached vortices, although data showing such effects are not available.

Based on the available data showing the effects of swirl on jet characteristics for jets without crossflow, it appears that swirl may be an important parameter for determining jet-induced surface pressures for a jet in a crossflow. Results have shown that the manner in which swirl is introduced into the jet and the temperature and density gradients in the jet affect turbulence levels in the jet, which in turn affect jet spreading and entrainment. It is recommended that experimental studies for jets in a crossflow attempt to duplicate as nearly as possible the anticipated full-scale jet exhaust swirl characteristics to insure proper modeling of the jet interference effects.

Turbulence

Turbulence intensity data for jets in a crossflow are presented in references 16 and 24. Figure 38 from reference 24 shows the axial distribution of turbulence intensity along the jet centerline and in the front and back mixing regions for a wide range of jet velocity ratios. In this figure, the quantity ξ is defined as the distance along the jet axis multiplied by the ratio of the free-jet potential core length ($R = \infty$) to the potential core length for the given velocity ratio. The turbulence intensity inside the jet increases by a factor $(1 + 1/R)$ as compared to the turbulent intensity of the same jet without a crossflow. Data in reference 16 exhibits similar trends; that is, turbulence intensity increases as jet velocity

ratio decreases. In both references, the potential core length decreases as the jet velocity ratio decreases.

Data could not be found showing the effect of turbulence intensity on jet characteristics or surface pressures for jets in a crossflow. Turbulence level information is not provided by any of the references containing surface pressure data (refs. 1-13).

Effects on jet characteristics due to turbulence level can be inferred from some of the data previously discussed in this report; specifically, data showing effects of jet dynamic pressure decay rates and swirl. While turbulence is not the main parameter of interest in these experimental studies, the effects due to decay rate and swirl are very likely similar to those due to turbulence.

For a given jet velocity ratio, the data of reference 23 show that introduction of swirl in a jet will result in a shortening of the potential core length and an increase in the jet centerline velocity decay rate. Jet spreading rate also increases. Jets with the greatest amount of turbulence intensity have the most effect on these jet characteristics. Data from references 10 and 12 indicate that jet dynamic pressure decay rate has a substantial effect on the jet-induced loading on an adjacent surface. An increase in turbulence intensity, which results in a more rapid jet decay rate, should produce effects similar to those shown in references 10 and 12 and discussed in this report. It is difficult to assess the level of effects of turbulence intensity on jet-induced loading, however, since the amount of change in turbulence level required to produce a reasonably large change in jet decay rate, and consequently in other jet quantities, is not known. Jets from reference 23 which produce the greatest decay rate and spreading

rate changes have a turbulence intensity at the centerline of 6 percent at the exit and 16 percent at a station 5 jet diameters from the jet exit. The nonswirled jet has turbulence intensities of 1 percent and 7 percent, respectively. Similar differences in turbulence intensity may be required to produce large changes in jet decay rate for the jet in a crossflow.

Separation of turbulence level from other parameters influencing jet-induced surface pressures and loadings may not be possible for engines utilized by full scale V/STOL configurations. That is, changes in turbulence level may occur as a result of other jet parameter changes. The data from reference 23 exemplify this point, since introduction of swirl into the jet increased the turbulence level. In this case, the increased turbulence due to swirl was one of the mechanisms for producing changes in the jet spreading and decay rates. The same situation may be true for engines which utilize solid centerbodies. Data from reference 12 showed that the presence of a centerbody in a jet causes a more rapid jet decay rate than that experienced by a jet without a plug. The increase in jet decay rate is probably due in part to an increase in turbulence level brought on by the interaction of the jet flow and the centerbody. Variation of turbulence level with jet decay rate (jet centerbody position) would help to verify this.

Temperature and Density

Experimental investigations of jet-induced surface pressures for a jet in a crossflow (refs. 1-13) attempt to obtain jets whose temperature is nearly equal to that of the free stream. Jet exhaust from full scale V/STOL configurations may not have the same temperature, and therefore density, as the free stream. A limited amount of data showing the effects of jet to free-stream density and temperature ratios on jet center-

line trajectories is presented in references 25 through 27. Reference 25 utilized different gases to model effects of jet density, while references 26 and 27 varied jet exit temperature, thereby obtaining changes in jet density.

Reference 25 used Freon-22 (ρ_j/ρ_∞ = 3.7), heated air (ρ_j/ρ_∞ = 1.05), argon (ρ_j/ρ_∞ = 1.4) and helium (ρ_j/ρ_∞ = .13) as the working substances of the jet. Jet centerline data for q_j/q_∞ = 125 indicate that the helium jet penetrated the free stream the least and the Freon jet penetrated the most. Data presented for three different positions downstream of the jet (x_j/D = 2.5, 5 and 10), differences in penetration (z_j) were of the order of 1.5 jet exit diameters. Differences between the centerlines obtained using heated air and argon jets, whose densities are very nearly the same, were very small.

Reference 26 utilized jets with jet exit temperature ratios (T_j/T_∞) of 1.0 and 2.0 (ρ_j/ρ_∞ not reported) and reference 27 utilized heated jets with jet exit temperature differences (T_j-T_∞) of 75°F (ρ_j/ρ_∞ = .877) and 320° (ρ_j/ρ_∞ = .622). The free-stream temperature was not reported in either reference. Centerline data obtained for q_j/q_∞ = 15.3 and 59.6 (ref. 27) shows very little effect due to jet to free-stream density and temperature ratios. Data from reference 26 for q_j/q_∞ = 64 shows less penetration into the free stream for the hot jet; however, data is very limited and direct comparisons of centerlines is possible at only one position along the centerline.

The above data indicate that for a given jet dynamic pressure ratio, differences in centerline position due to moderate jet to free-stream density ratios ($.5 < \rho_j/\rho_\infty < 1.5$) are of the same order as differences in centerline positions from different experimental investigations. Centerlines

obtained using jets with the same temperature as that of the free stream should be considered accurate for full scale configurations, within the accuracy of the flat plate approximation.

Boundary Layer

An effect to which little attention has been paid is that of the plate boundary layer thickness. Surface pressure distributions from reference 2 for R = 8 showing effects due to plate boundary layer thickness are shown in figure 39. The largest effects are for the region closest to, and to the side and behind the jet. Variation of boundary layer thickness, which is shown to cause substantial differences in surface pressures in the region near the jet, could explain differences in pressures between different sets of data (see fig. 18, for example). Further parametric studies of boundary layer thickness effects must be carried out before such conclusions can be drawn.

CONCLUSIONS

A systematic evaluation of available data to assess the importance of real jet effects on jet-induced loadings on adjacent surfaces for a jet in a crossflow has been made. Four major "real jet" characteristics were investigated: jet exit velocity profile, jet exit and free-stream Mach number combination, swirl and turbulence. In addition, information on jet density/temperature effects and surface boundary layer effects is also presented.

A nonuniform jet exit velocity profile was found in many cases to have a pronounced effect on jet-induced lift and moments

as compared to that of uniform exit profile jets. Attempts to correlate surface pressure and force and moment data using the equivalent idealized jet concept (ref. 13) were unsuccessful.

Attempts to model jet exit velocity profile effects were made using the prediction method of references 14 and 15 in conjunction with available jet centerline trajectory and centerline dynamic pressure decay data. Comparisons of measured and predicted (without correlation factors) plate pressures in the region ahead of the jet for two jet velocity ratios were generally good. Additional information on jet spreading and entrainment and more detailed centerline data in the region near the jet are needed to improve the potential flow model. The correlation factors presently used by the prediction method were generally found to overcorrect results obtained using the potential flow model. It appears that different correlation factors, possibly based on jet centerline decay rate, would have to be obtained for jets with nonuniform velocity profile.

Correlation factors based on jet exit Mach number could not be developed due to inconsistencies in trends exhibited by the available data. In general, the effects of jet exit Mach number on jet-induced loads were found to be of the same order as differences caused by scatter between different sets of data. It does not appear that Mach number (at least for subsonic jets) is an important parameter.

Data from acoustical studies on swirl in jets exhausting into queiscent air were used to infer effects on surface pressure distributions. The available data indicate that swirl enhances turbulent mixing, increases jet expansion and entrainment, and causes a more rapid decay of jet centerline velocities. Also, the manner in which swirl is introduced into the jet was found to vary the effect on the aforementioned jet quantities. Since these changes in jet characteristics individually both increase

and decrease surface pressures and loads, it is not possible to infer the net effect of introducing swirl.

Turbulence level data were not obtained in any of the references containing surface pressure data (refs. 1-13). Available data from other studies show an increase in turbulence level with decreasing jet velocity ratio. General trends exhibited by data from the jet decay rate and swirl studies were used to infer effects due to turbulence level, since an increase in turbulent mixing (increased turbulence level) affects jet decay rate, as well as other jet characteristics. However, data showing the amount of change in turbulence level necessary to effect appreciable changes in jet decay rate and other jet characteristics for jets in a crossflow are presently not available.

A limited amount of jet centerline data showing jet density/temperature effects indicated little effect for moderate jet exit to free-stream density ratios ($.5 < \rho_j/\rho_\infty < 1.5$). Plate boundary layer thickness was found to affect surface pressure, especially in the region near the jet. Such effects could explain differences in surface pressures between different sets of data obtained for the same jet velocity ratio.

RECOMMENDATIONS

A reasonable amount of surface pressure data are available for jets exhausting from a flat plate into a crossflow. For the most part, the objective of these tests was to obtain a data base of "clean" jet flows to permit development of mathematical models and predictive methods. From the standpoint of full scale V/STOL applications, the data base is deficient in two respects. First, the flow conditions for each experiment

were not sufficiently well documented, probably because the importance of some parameters was not recognized. Second, there is not enough systematic investigation of the "real jet" characteristics that are present and important in full scale applications. It seems sensible to do additional work both in small and large scale, and the recommendations follow this approach.

The small scale work ought to continue to serve the purpose of aiding modelers in developing predictive methods. For flat plates, there is probably sufficient data for single "clean" jets for a range of initial inclination angles. The primary need is for additional systematic investigation of "real jet" effects. From this study, the variables that appear most important to consider are nonuniform exit velocity profile, swirl, and turbulence. The state for single jets issuing from bodies is much less developed. The need here is for single "clean" jets on long cylinders, with jet-to-body diameter ratio as an additional parameter, and single "real" jets, again using exit profile, swirl, and turbulence as the most important parameters. Finally, if there is an indicated need from the full scale concept work, multiple jets with jet-jet interaction could be examined.

Because of the purpose of the small scale work, it is vital that any experiments be well planned and executed. The jet needs to be designed to produce the proper range of characteristics in a controllable fashion. The flow needs to be completely documented in terms of jet exit mean velocity profile, decay of centerline velocity, centerline location, entrainment, swirl, and turbulence level. The surface should have sufficient pressure taps to define the variations, particularly near the jet, and ideally should be laid out in rays and arcs of taps rather than a Cartesian system. Documentation

needs to be complete, with tabulated data, so modelers can most easily make use of the data.

The opportunity for large scale data is present in the tests of real, near-full-size configurations that are done primarily to obtain overall force and moment characteristics. Because of the size, complexity, and cost of these tests, it clearly is not practical to fully document the jet wake and surface pressures as in small scale tests. However, there is some minimum amount of data that ought to be considered for every large scale test. This would include some surface pressures in the region of the jet. The upstream ray ($\beta = 0°$) is useful because of small viscous effects, and the downstream ray ($\beta = 180°$) because of maximum effects. Perhaps two other rays at $\beta = 60°$ and $120°$ would be useful. Fewer rays with small radial increments are preferred to more rays with larger radial increments. As a minimum, the jet exit mean velocity profile and turbulence level should be measured, including both axial and swirl components. At the very least, these data would serve to document the important characteristics of real full-scale jets.

Other data sources could include another fixed rake in the jet wake perhaps 2 jet diameters from the exit, smoke to visualize the wake boundary, a thermal image for a hot wake to locate the wake boundary, or laser velocimeter measurements. As a matter of priority in the latter, a description of the velocities in the vertical plane of symmetry of the jet (if there is one) would serve to obtain centerline locations and velocity decay, which are important in modeling.

REFERENCES

1. Vogler, R. D.: Surface Pressure Distributions Induced on A Flat Plate by a Cold Air Jet Issuing Perpendicularly from the Plate and Normal to a Low-Speed Free-Stream Flow. NASA TN D-1629, Mar. 1963.

2. Bradbury, L. J. S. and Wood, M. N.: The Static Pressure Distribution Around a Circular Jet Exhausting Normally from a Plane Wall Into an Airstream. Aeronaut. Res. Council C. P. No. 882, Aug. 1965.

3. Ousterhout, D. S.: An Experimental Investigation of a Cold Jet Emitting from a Body of Revolution Into a Subsonic Free Stream. NASA CR-2089, Aug. 1972.

4. Fearn, R. L. and Weston, R. P.: Induced Pressure Distribution of a Jet in a Crossflow. NASA TN D-7916, June 1975.

5. Soullier, A.: Testing at Sl.MA for Basic Investigations on Jet Interactions: Distributions of Pressure Around the Jet Orifice. NASA TT F-14066, Jan. 1972.

6. Fricke, L. B., Wooler, P. T., and Ziegler, H.: A Wind Tunnel Investigation of Jets Exhausting Into a Crossflow. AFFDL-TR-70-154, Vol. I - Test Description and Data Analysis, Vol. II - Additional Data for the One-Jet Configuration, Dec. 1970.

7. Mosher, D. K.: An Experimental Investigation of a Turbulent Jet in a Cross Flow. Georgia Inst. of Tech. Rept. GIT-AER-70-715, Dec. 1970. (Ph.D. Thesis)

8. Taylor, P.: An Investigation of an Inclined Jet in a Crosswind. Aeronaut. Quart., Vol. XXVIII, Part 1, Feb. 1977.

9. Aoyagi, K.: NASA/Ames Research Center, work in preparation.

10. Kuhlman, J. M., Ousterhout, D. S., and Warcup, R. W.: Experimental Investigation of Effect of Jet Decay Rate on Jet-Induced Pressures on a Flat Plate. NASA CR-2979, Apr. 1978.

11. Schwendemann, M. F.: A Wind Tunnel Investigation of Stratified Jets and Closely Spaced Jets Exhausting into a Crossflow. Northrop Aircraft Division, Rept. NOR 73-98, May 1973.

12. Kuhlman, J. M., Ousterhout, D. S., and Warcup, R. W.: Experimental Investigation of Effects of Jet Decay Rate on Jet-Induced Pressures on a Flat Plate: Tabulated Data. NASA CR-158990, Nov. 1978.

13. Ziegler, H. and Wooler, P. T.: Analysis of Stratified and Closely Spaced Jets Exhausting into a Crossflow. NASA CR-132297, Nov. 1973.

14. Perkins, S. C., Jr. and Mendenhall, M. R.: A Correlation Method to Predict the Surface Pressure Distribution on an Infinite Plate from which a Jet is Issuing. NASA CR-152,160, May 1978.

15. Perkins, S. C., Jr. and Mendenhall, M. R.: A Correlation Method to Predict the Surface Pressure Distribution on an Infinite Plate or a Body of Revolution from which a Jet is Issuing. NASA CR-152,345, May 1980.

16. Keffer, J. F. and Baines, W. D.: The Round Turbulent Jet in a Cross-Wind. J. Fluid Mech., Vol. 15, Part 4, Apr. 1963, pp. 481-497.

17. Margason, R. J.: The Path of a Jet Directed at Large Angles to a Subsonic Free Stream. NASA TN D-4919, Nov. 1968.

18. Baines, W. D.: Discussion of Diffusion of Submerged Jets by Albertson, M. L., et al. Trans. ASCE, Vol. 115, Dec. 1948, pp. 677-684.

19. Lau, J. C.: Mach Number and Temperature Effects on Jets. AIAA Journal, Vol. 18, No. 6, June 1980, pp. 609-610.

20. Schwartz, I. R.: Swirling-Flow Jet Noise Suppressors for Aircraft Engines. AIAA Paper No. 76-508, July 1976.

21. Schwartz, I. R.: Jet Noise Suppression by Swirling the Jet Flow. Progress in Astronautics and Aeronautics, Aeroacoustics, Jet and Combustion Noise, Duct Acoustics, Vol. 37, edited by H. T. Nagamatsu, J. V. O'Keefe, and I. R. Schwartz, AIAA, New York, 1975, pp. 191-205.

22. Schwartz, I. R.: Minimization of Jet and Core Noise of a Turbojet Engine by Swirling the Exhaust Flow. Progress in Astronautics and Aeronautics, Aeroacoustics, Jet and Combustion Noise, Duct Acoustics, Vol. 43, edited by I. R. Schwartz, H. T. Nagamatsu, and W. Strahle, AIAA, New York, 1976, pp. 379-398.

23. Young, A. D. and Rao, K. N.: Same Low Speed Experimental Results on the Effects of Swirl and Velocity Distribution on an Axi-Symmetric Jet. The Aeronautical Quarterly, Vol. XXIX, Part 4, Nov. 1978, pp. 270-284.

24. Camelier, I. and Karamchetti, K.: An Experimental Study of the Structure and Acoustic Field of a Jet in a Cross Stream. Joint Institute for Aeronautics and Acoustics Rept. TR-2, Stanford University, Jan. 1976.

25. Golubev, V. A., Klimkin, V. F. and Makarov, I. S.: Trajectories of Single Jets of Different Densities Propagating in a Deflecting Airstream (translation). Journal of Engineering Physics, Vol. 34, No. 4, Oct. 1978, pp. 395-398.

26. Harms, L.: Experimental Investigation of the Flow Field of a Hot Turbulent Jet with Lateral Flow. Part 2. NASA TT F-15706, Sept. 1973.

27. Kamotani, Y. and Greber, I.: Experiments on a Turbulent Jet in a Crossflow. NASA CR-72893, June 1971.

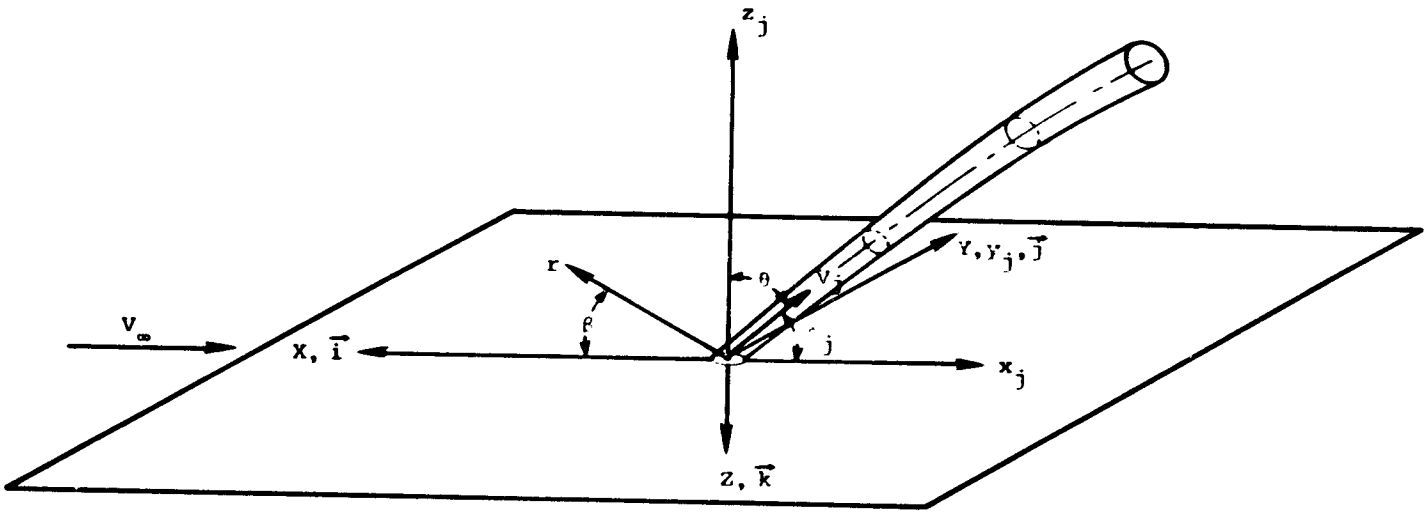

(a) Coordinate systems definition

Figure 1.- Isometric view of a jet issuing from a flat plate into a subsonic crossflow.

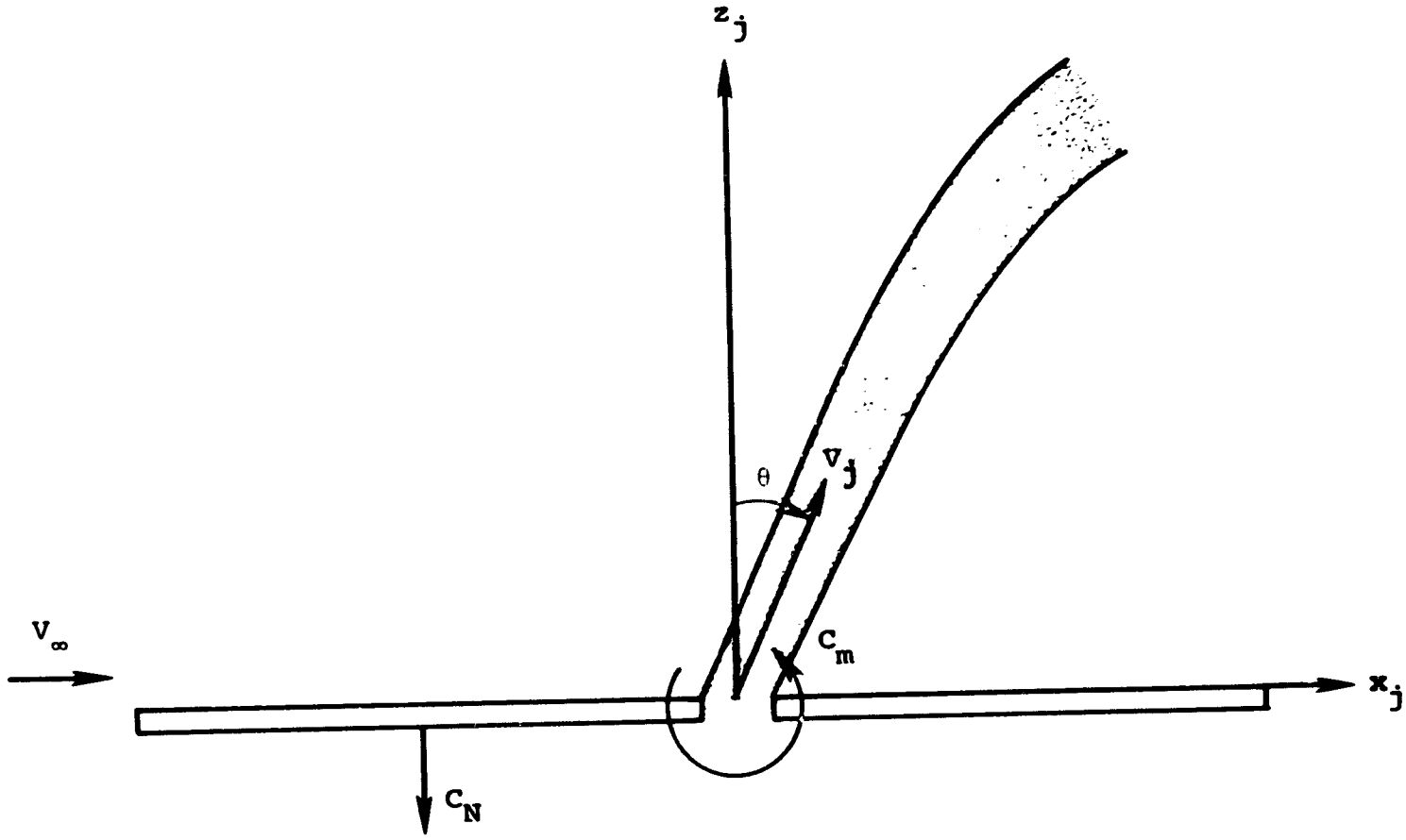

(b) Positive sense of normal force and pitching moment for integrated loads on flat plate.

Figure 1.- Concluded.

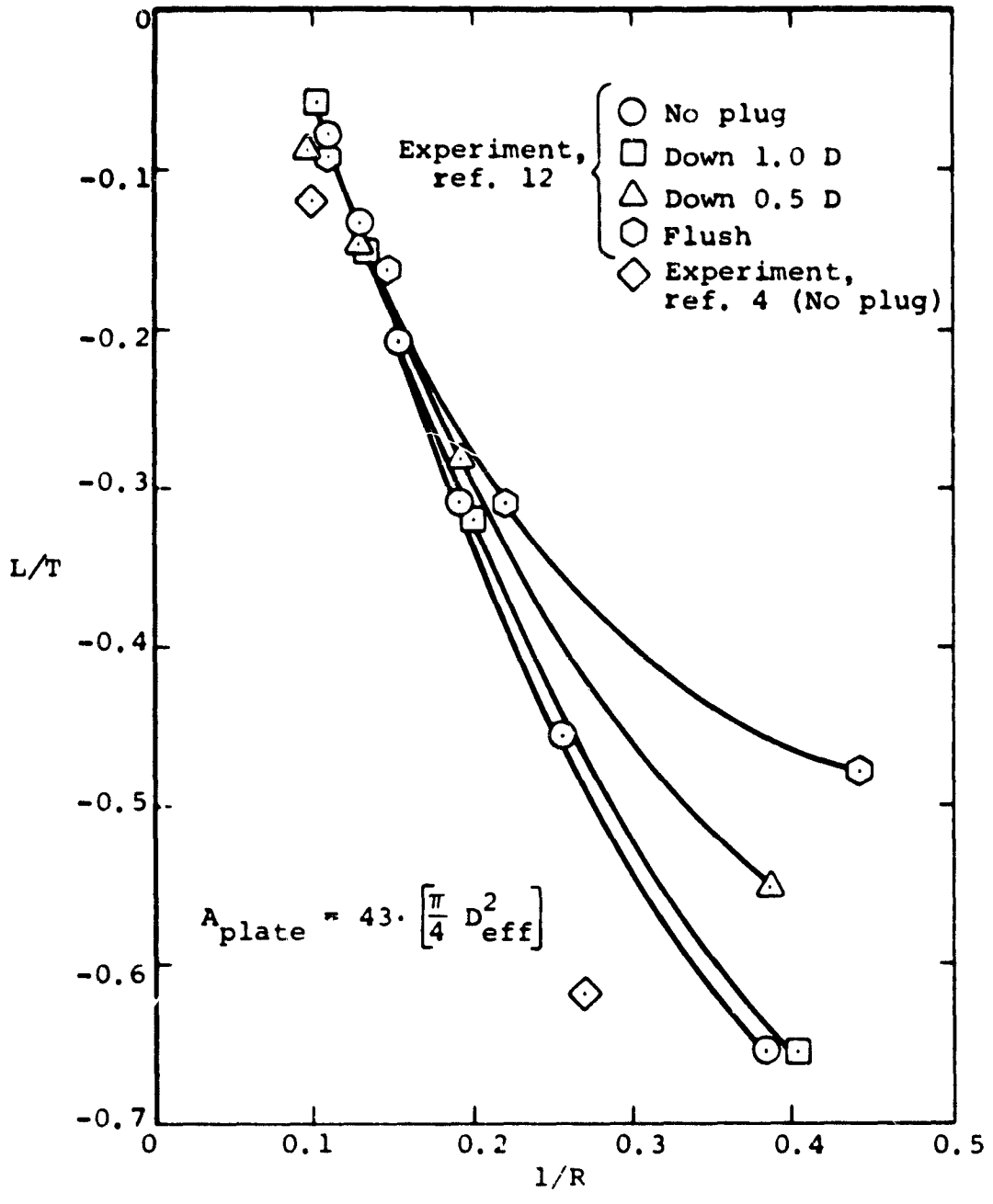

(a) Lift loss

Figure 2.- Integrated lift loss and pitching moment for round ended plug configurations compared with unplugged jets.

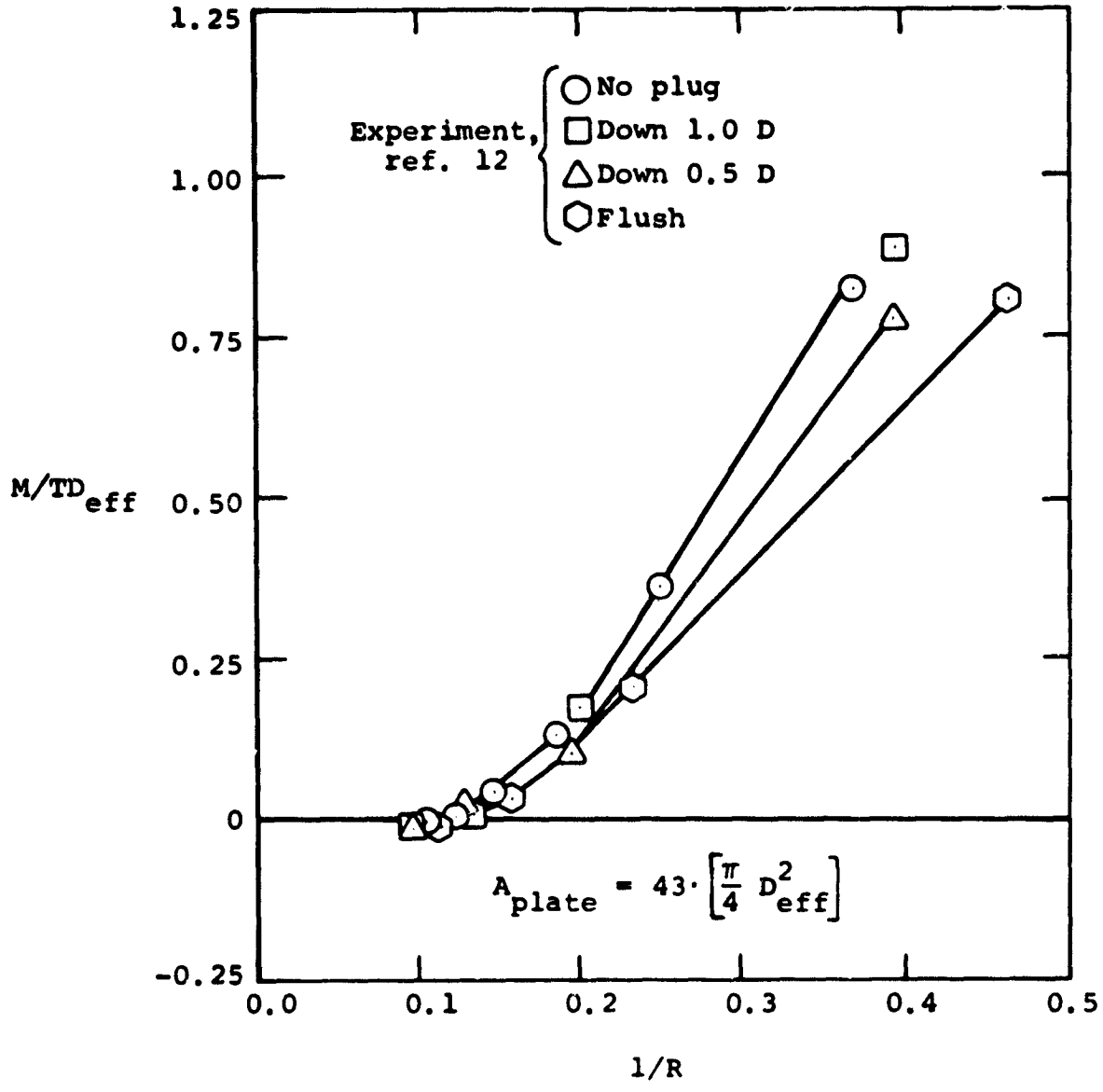

(b) Pitching moment

Figure 2.- Concluded.

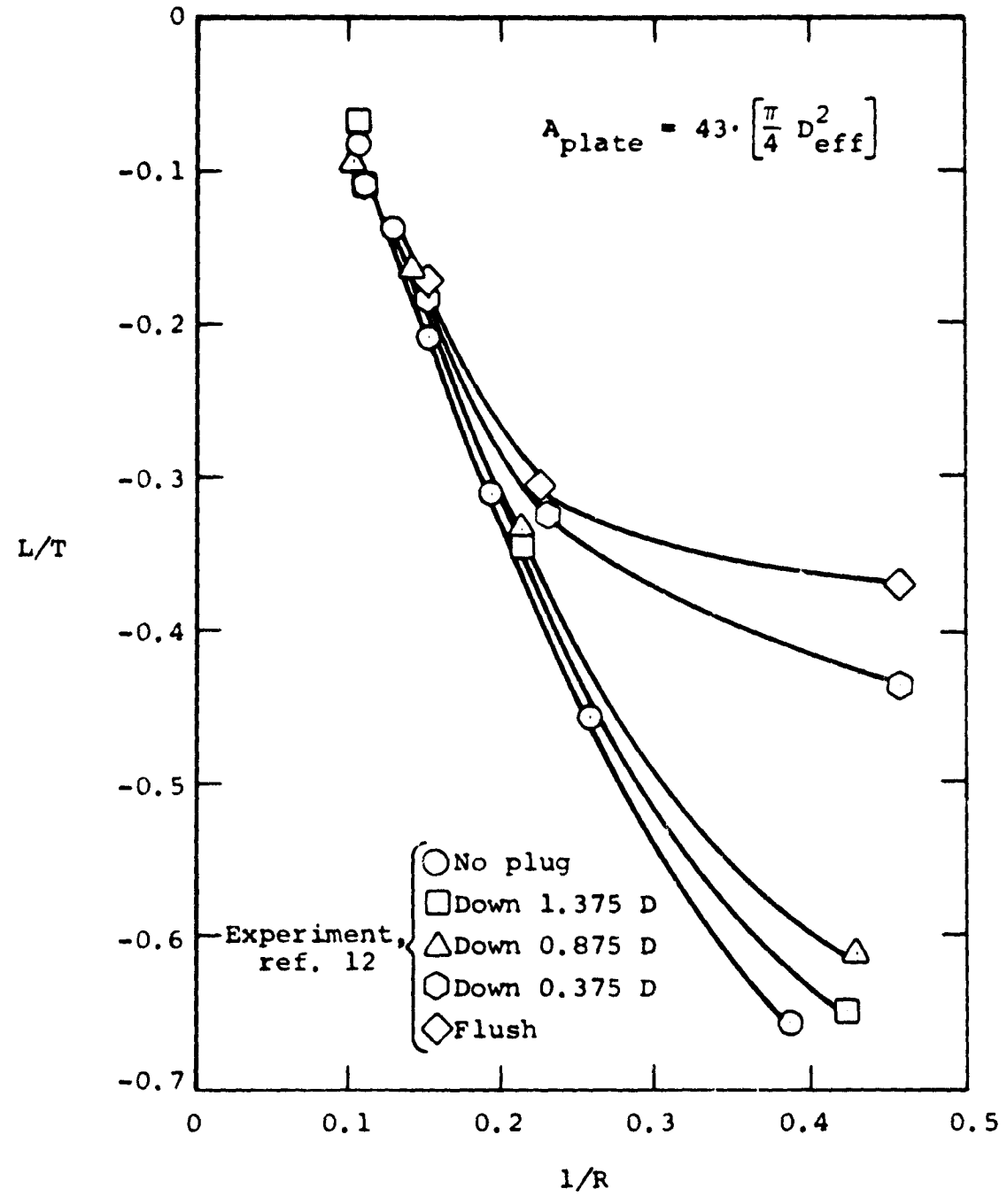

(a) Lift loss

Figure 3.- Integrated lift loss and pitching moment for flat tipped plug configurations compared with unplugged jets.

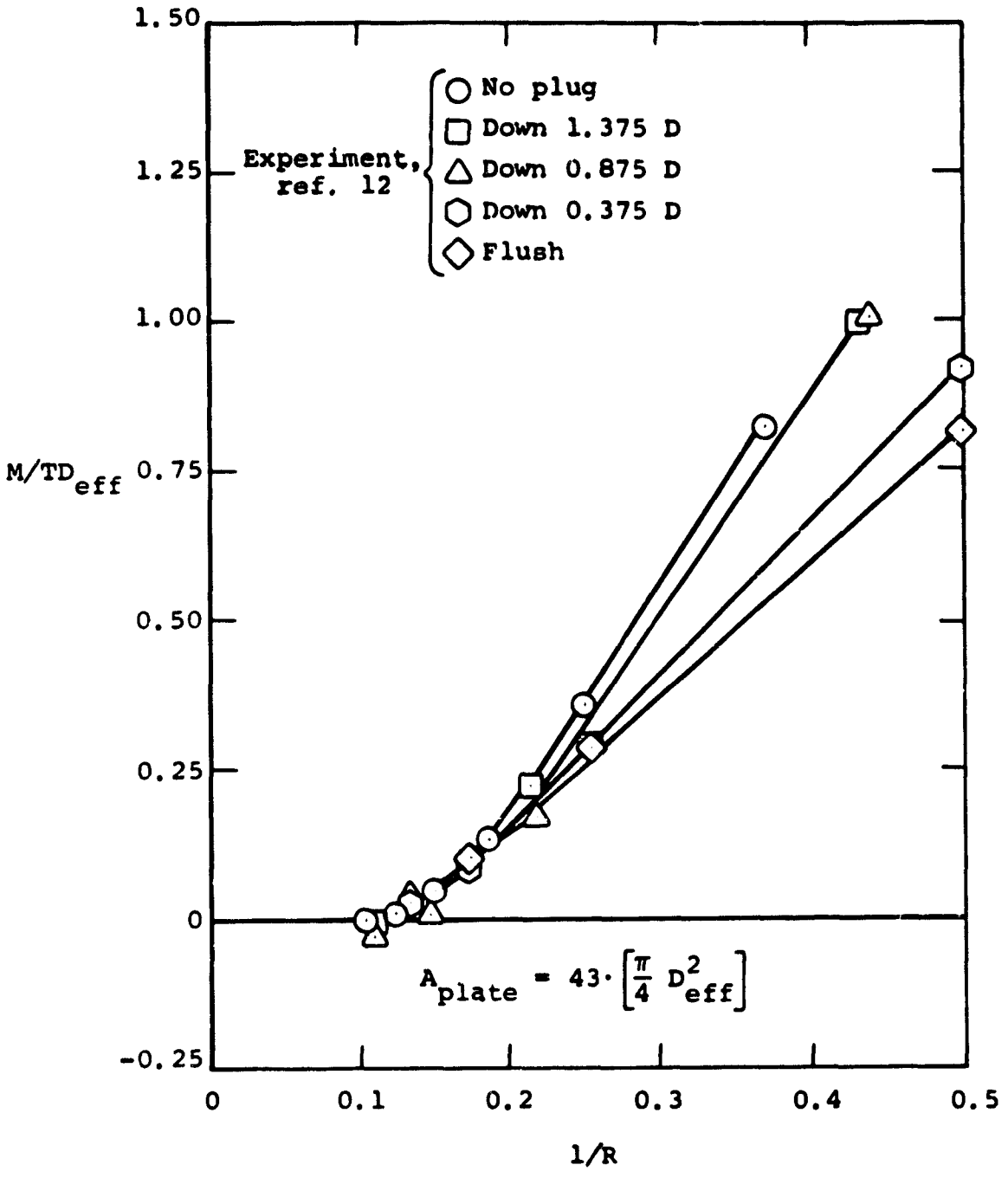

(b) Pitching moment

Figure 3.- Concluded.

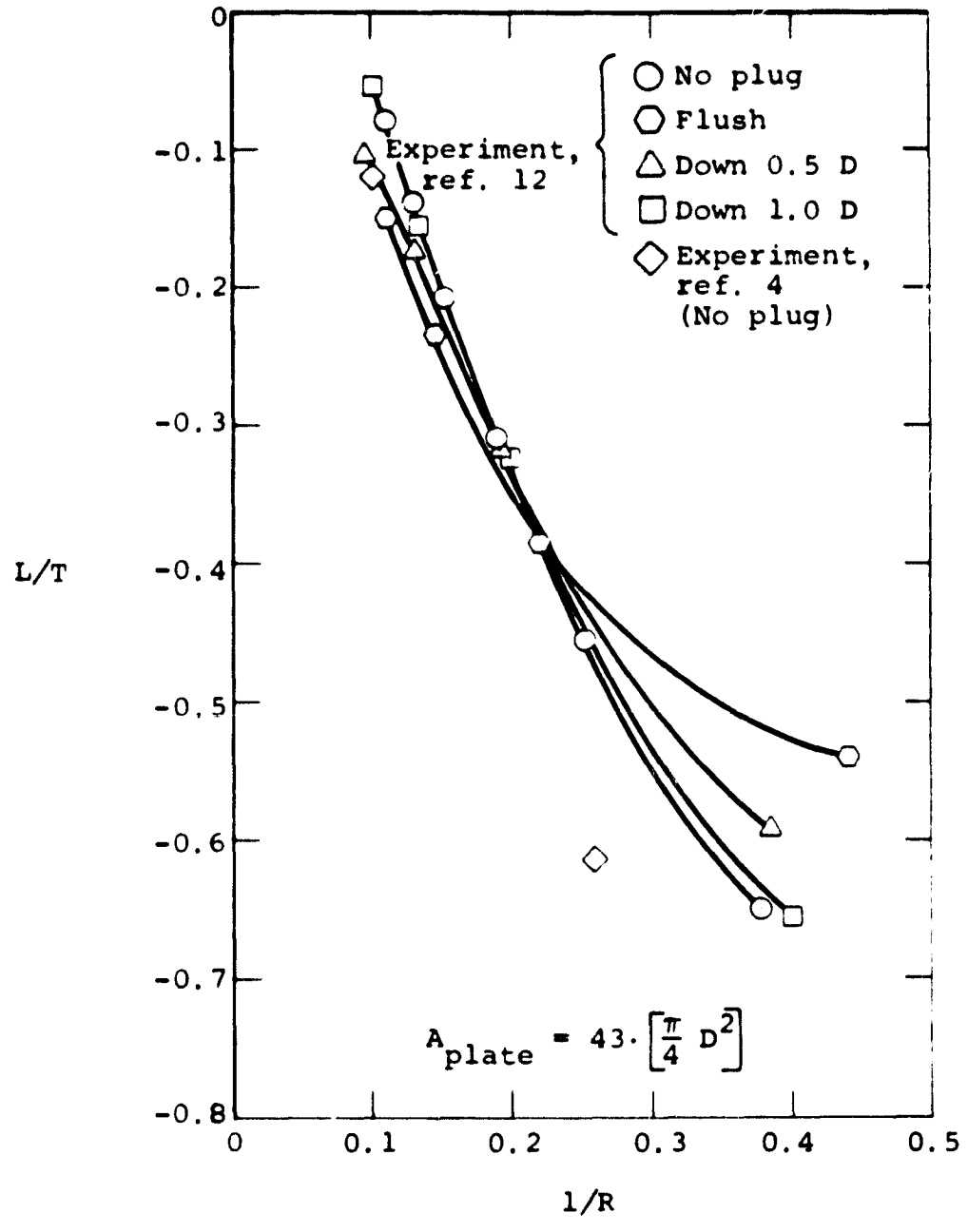

(a) Lift loss

Figure 4.- Integrated lift loss and pitching moment for round ended plug configuration compared with unplugged jets.

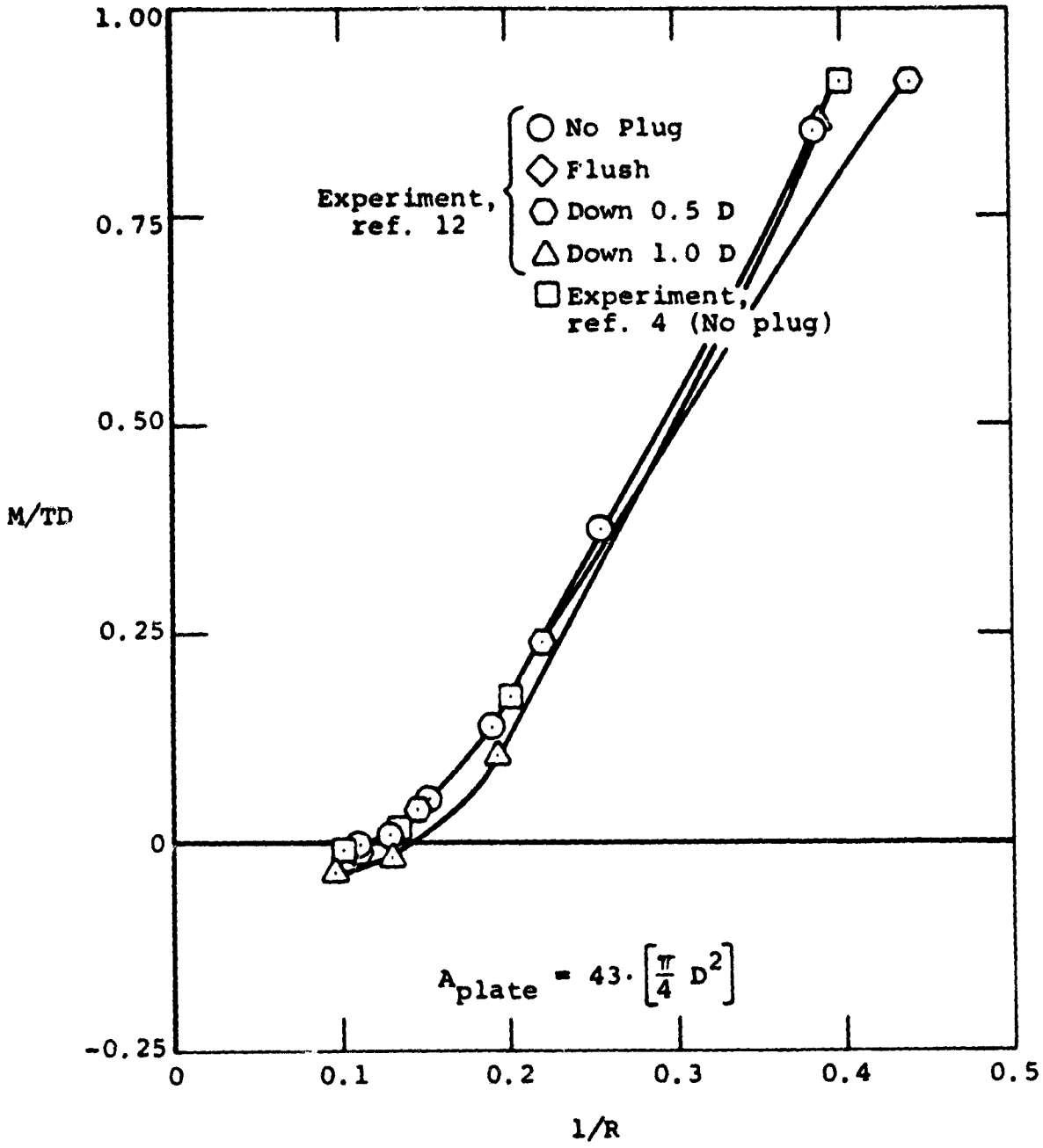

(b) Pitching moment

Figure 4.- Concluded.

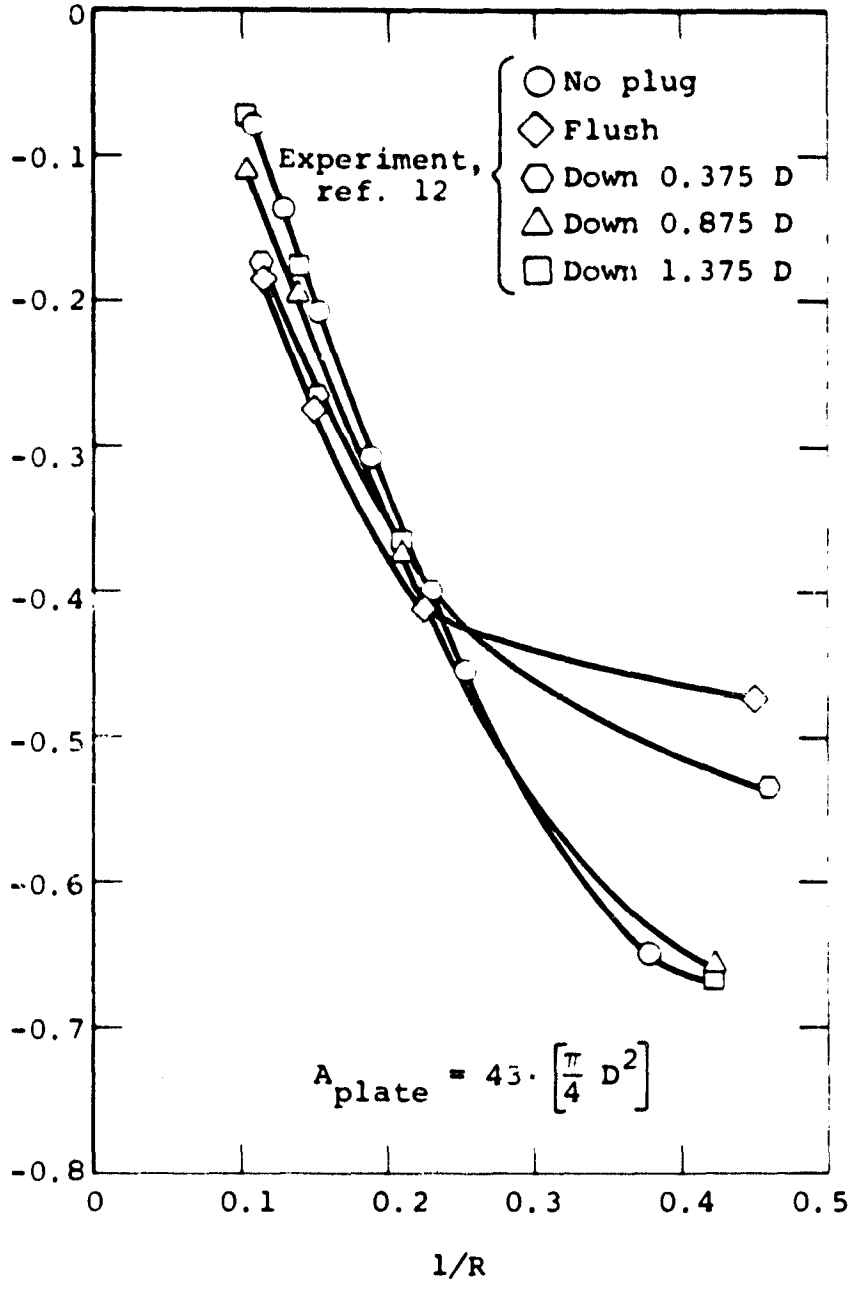

(a) Lift loss

Figure 5.- Integrated lift loss and pitching moment for flat ended plug configuration compared with unplugged jets.

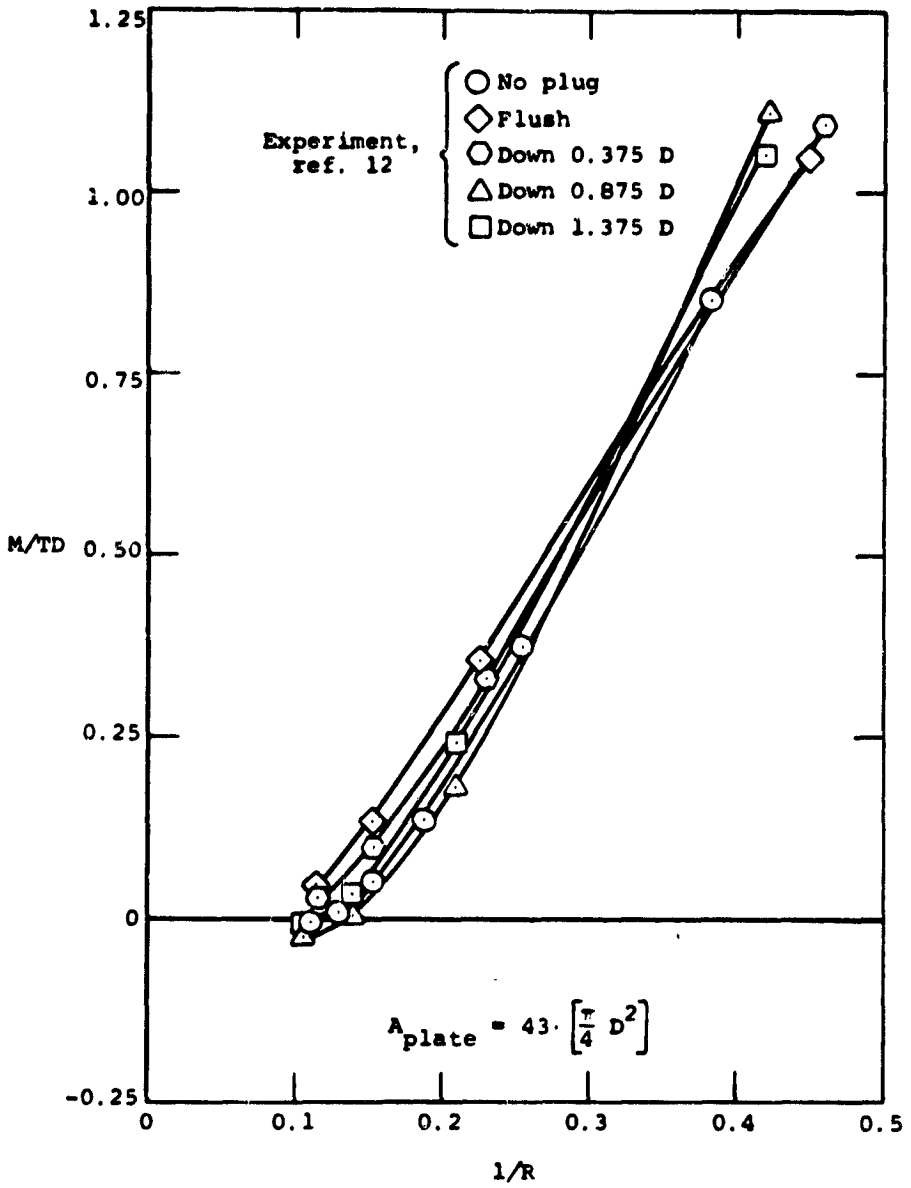

(b) Pitching moment

Figure 5.- Concluded.

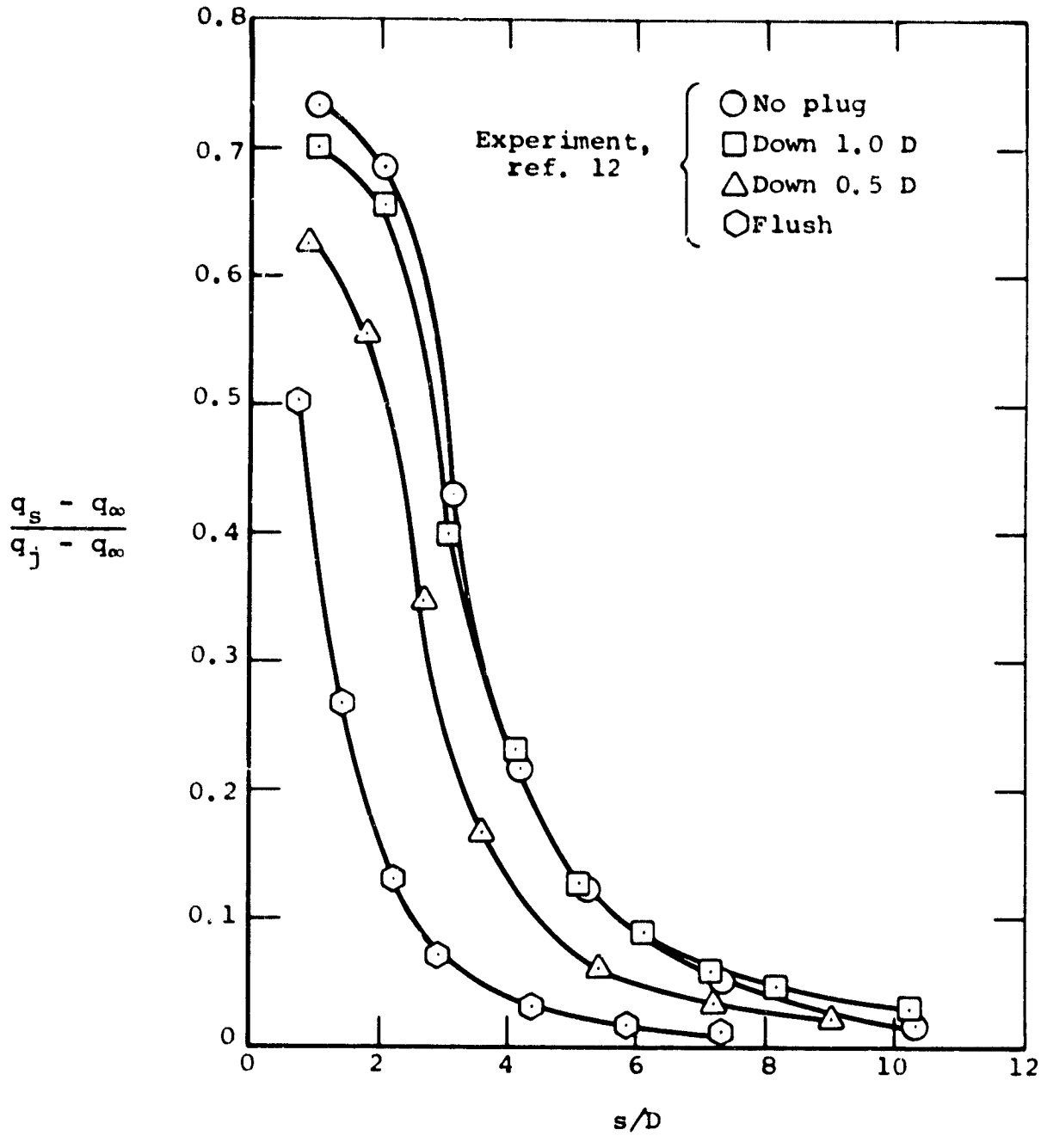

(a) Round plug centerbodies

Figure 6.- Measured dynamic pressure decay along jet centerline for plug and no plug jets, R = 2.5.

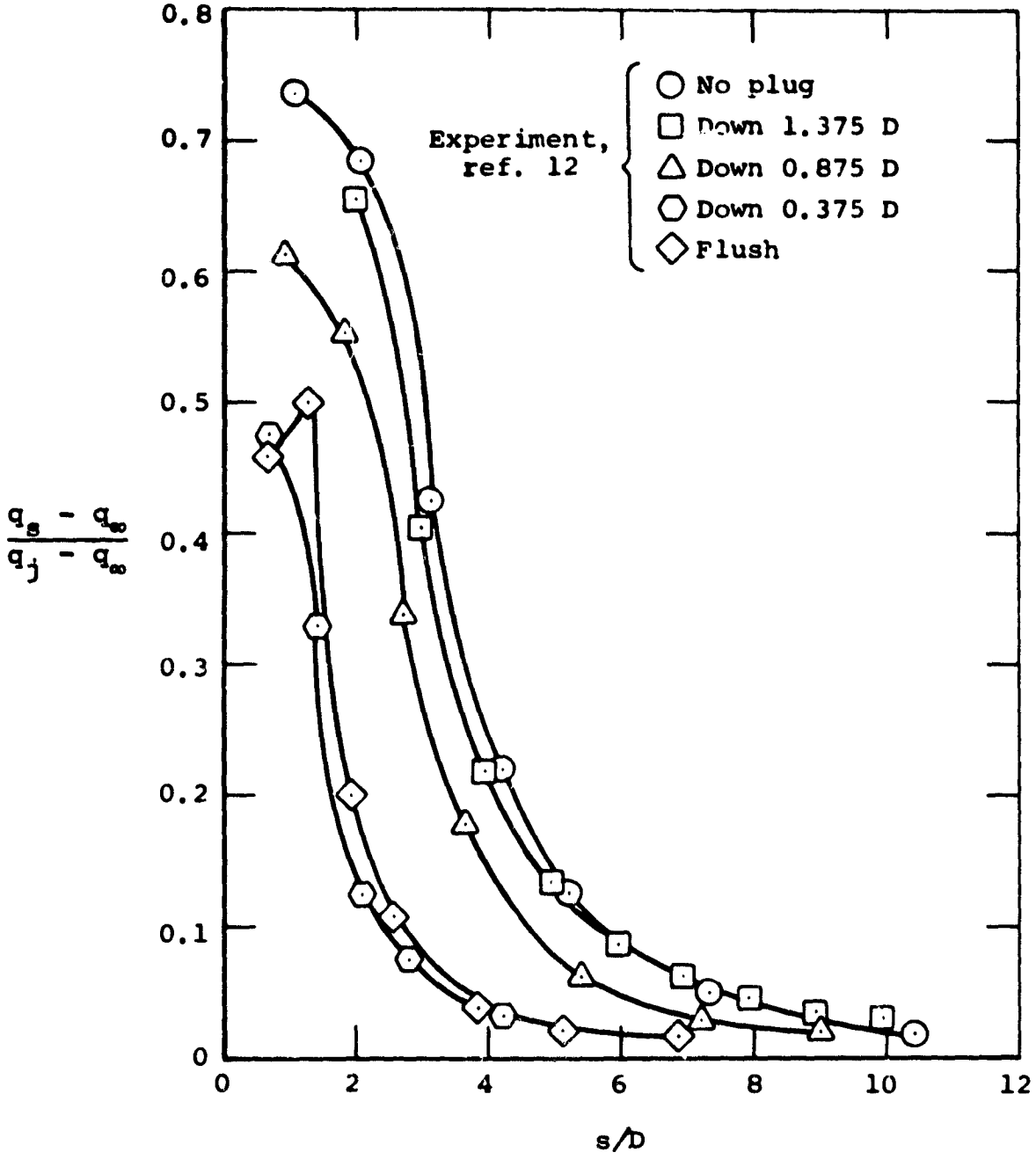

(b) Flat plug centerbodies

Figure 6.- Concluded.

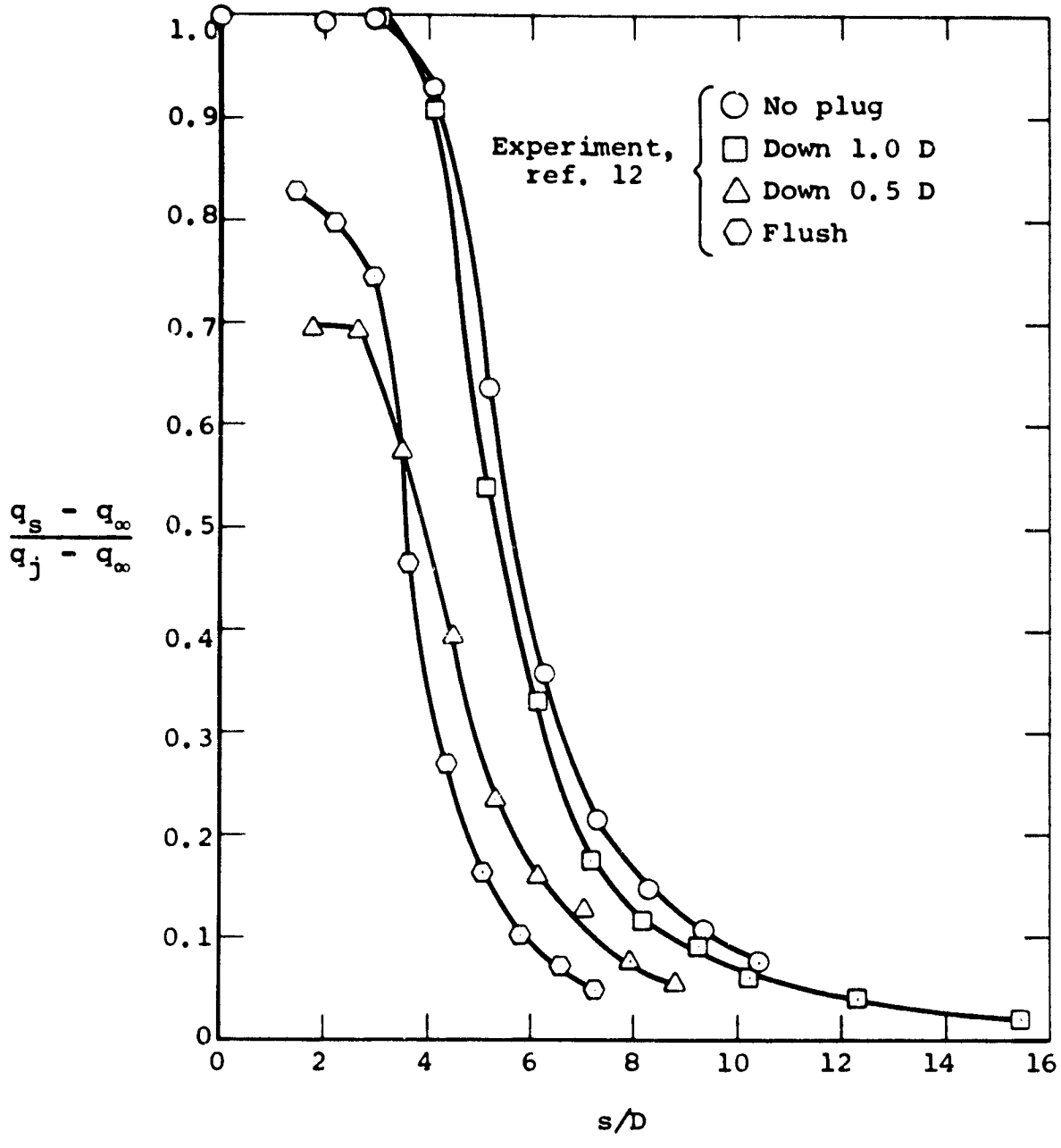

(a) Round tip centerbodies

Figure 7.- Measured dynamic pressure decay along jet centerline for plug and no plug jets, R = 8.

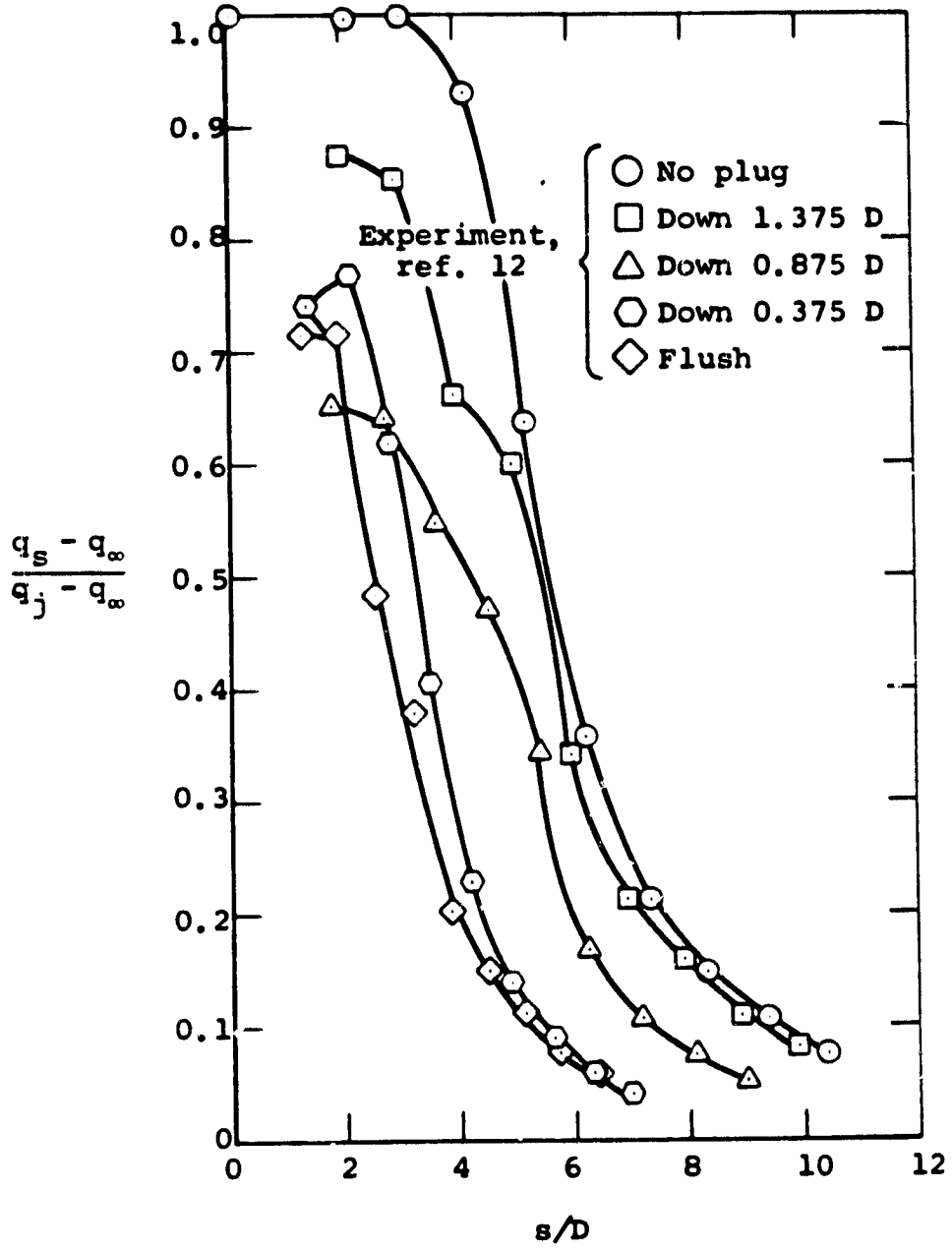

(b) Flat tip centerbodies

Figure 7.- Concluded.

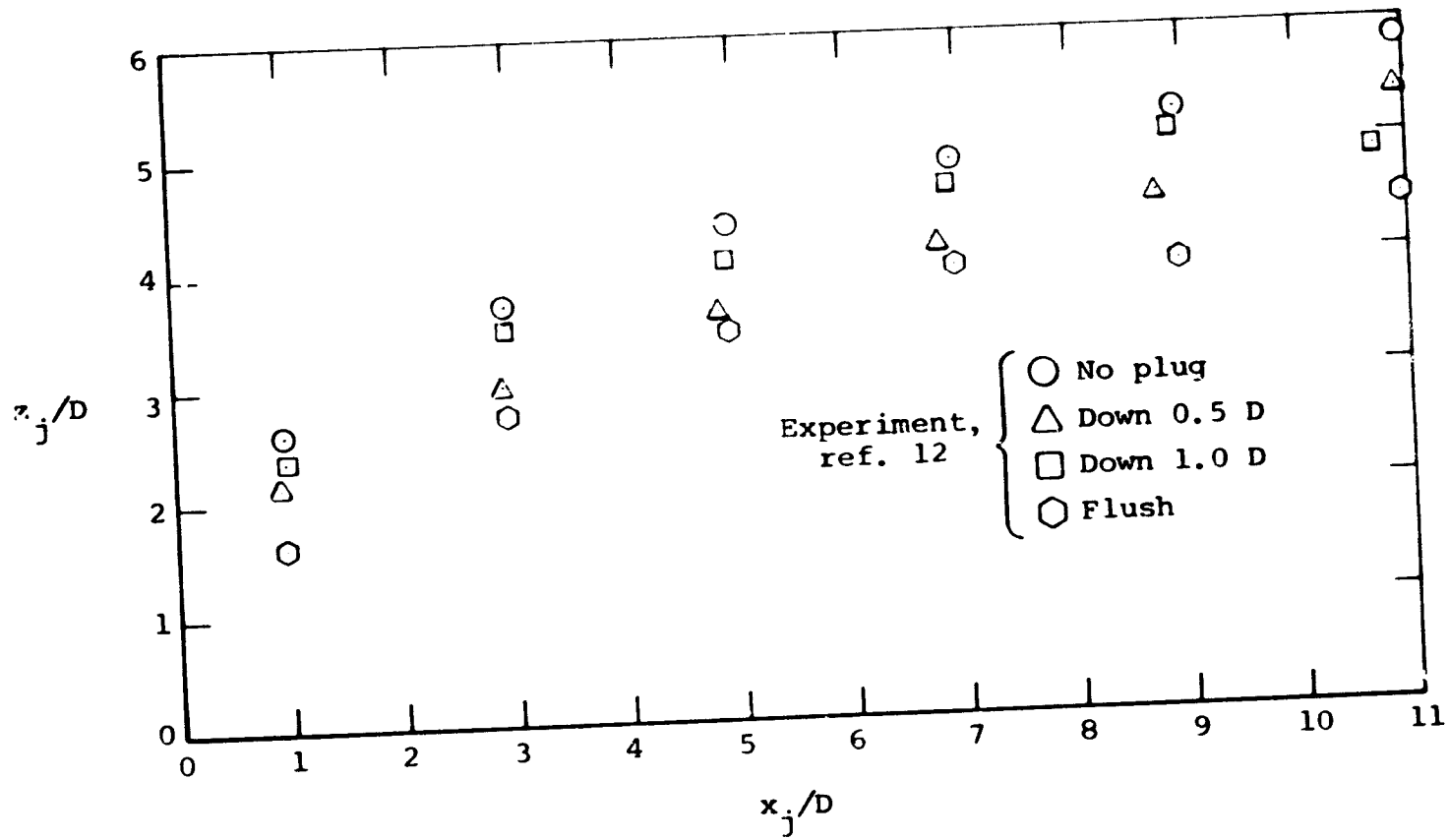

(a) Round plug centerbodies

Figure 8.- Measured jet centerline trajectories for plug and no plug jets, R = 2.5.

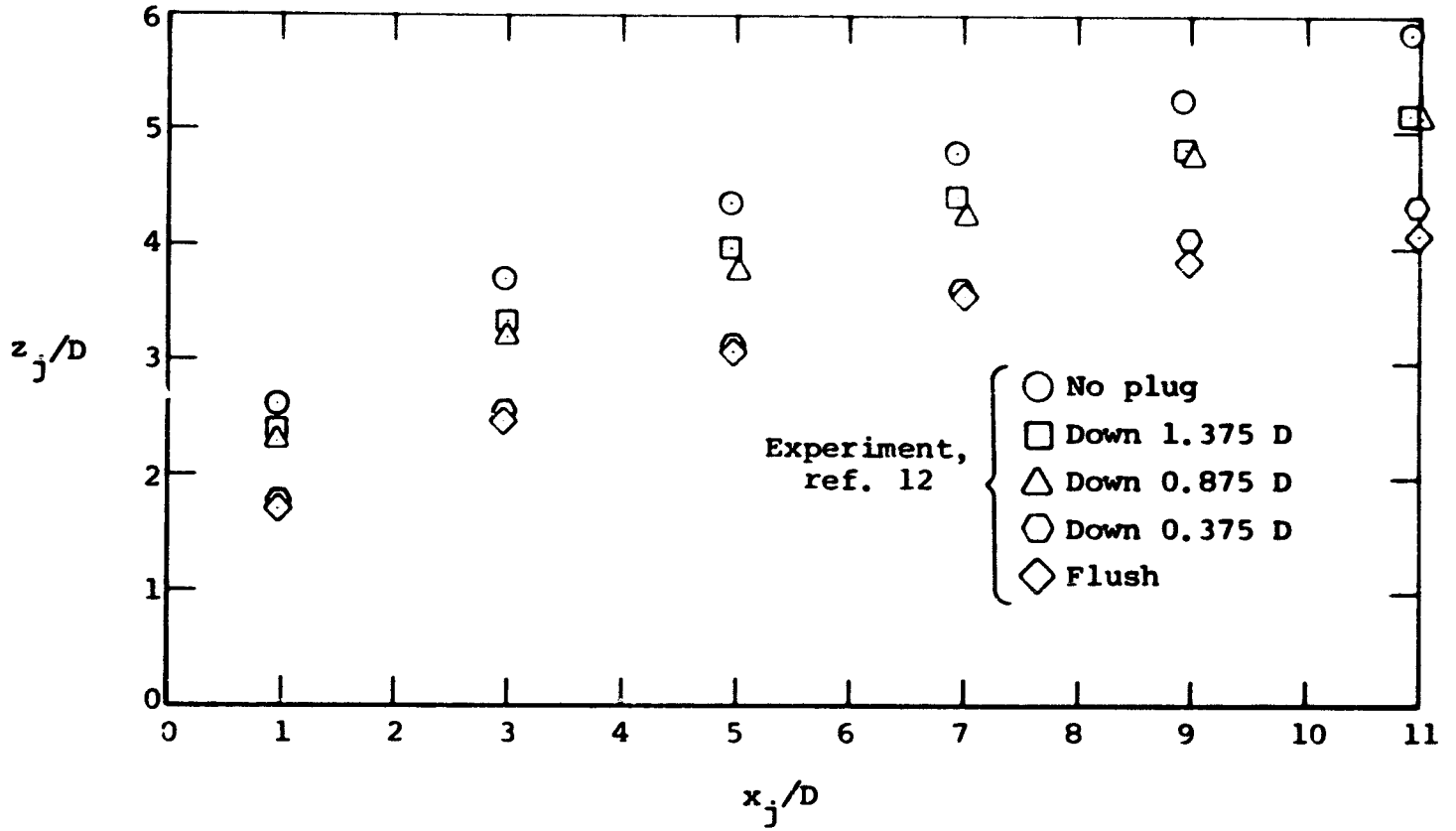

(b) Flat plug centerbodies

Figure 8.- Concluded.

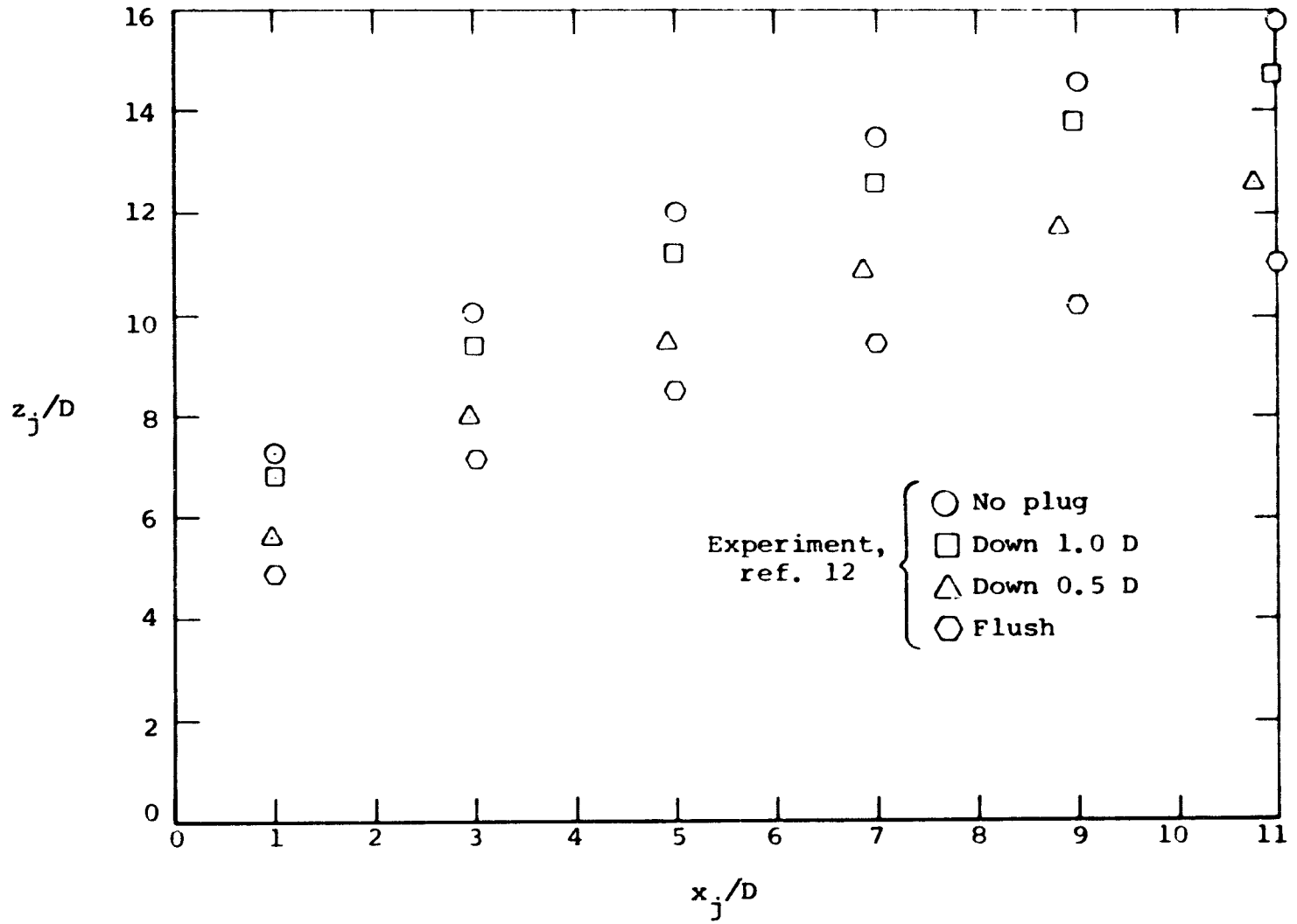

(a) Round plug

Figure 9.- Measured jet centerline trajectories for plug and no plug jets, R = 8.

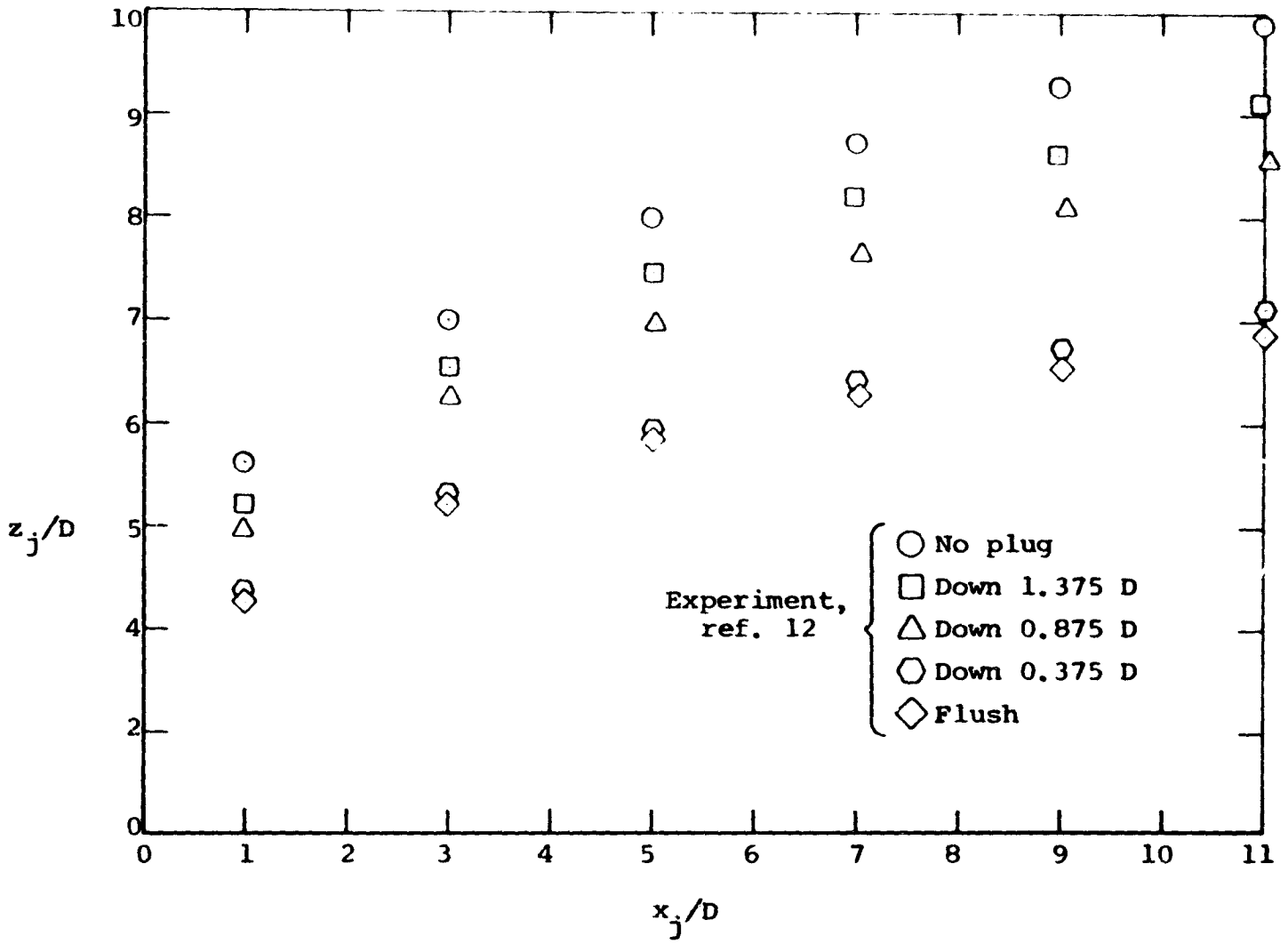

(b) Flat plug centerbodies

Figure 9.- Concluded.

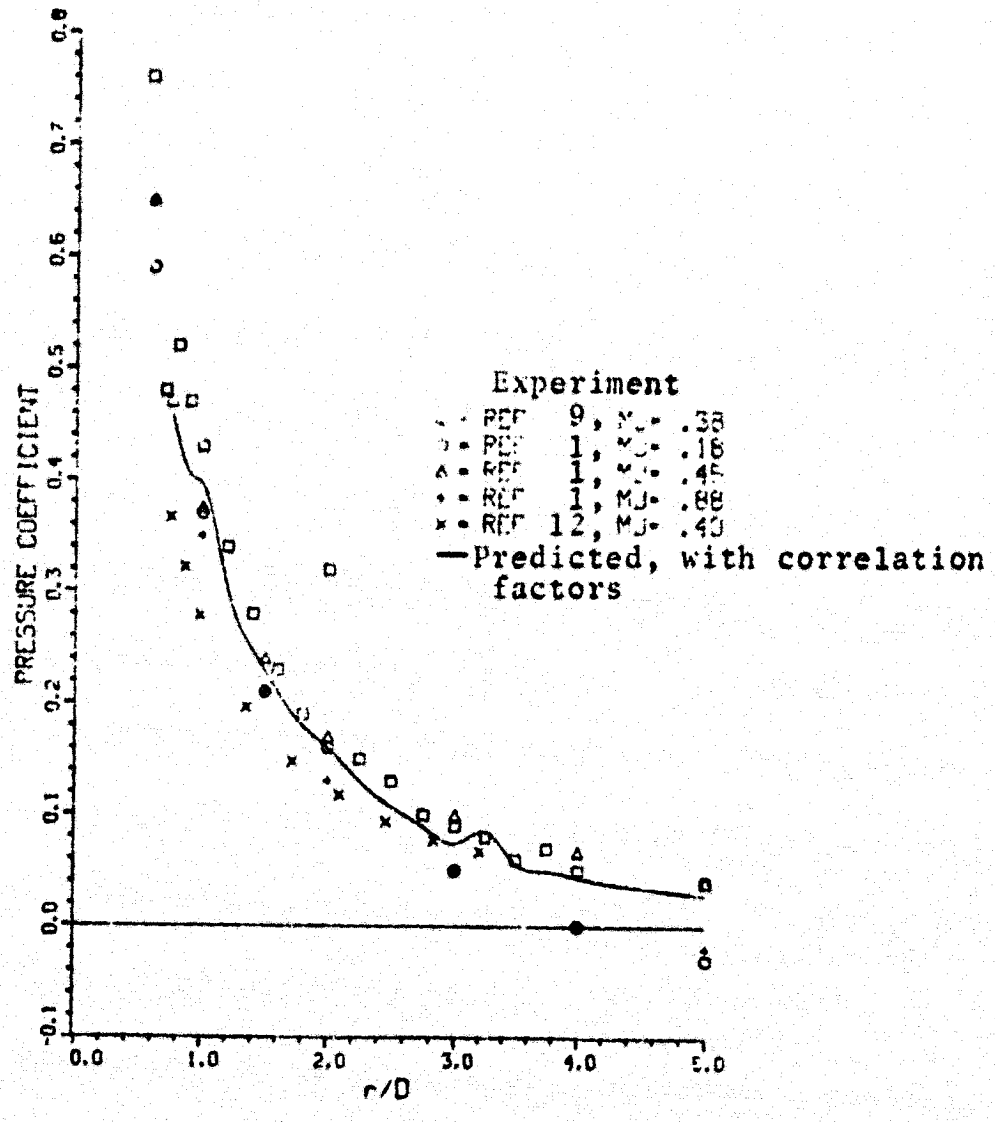

(a) $\beta = 0°$

Figure 10.- Comparison of measured and predicted plate pressure distributions for uniform exit profile jets, R ≈ 2.5.

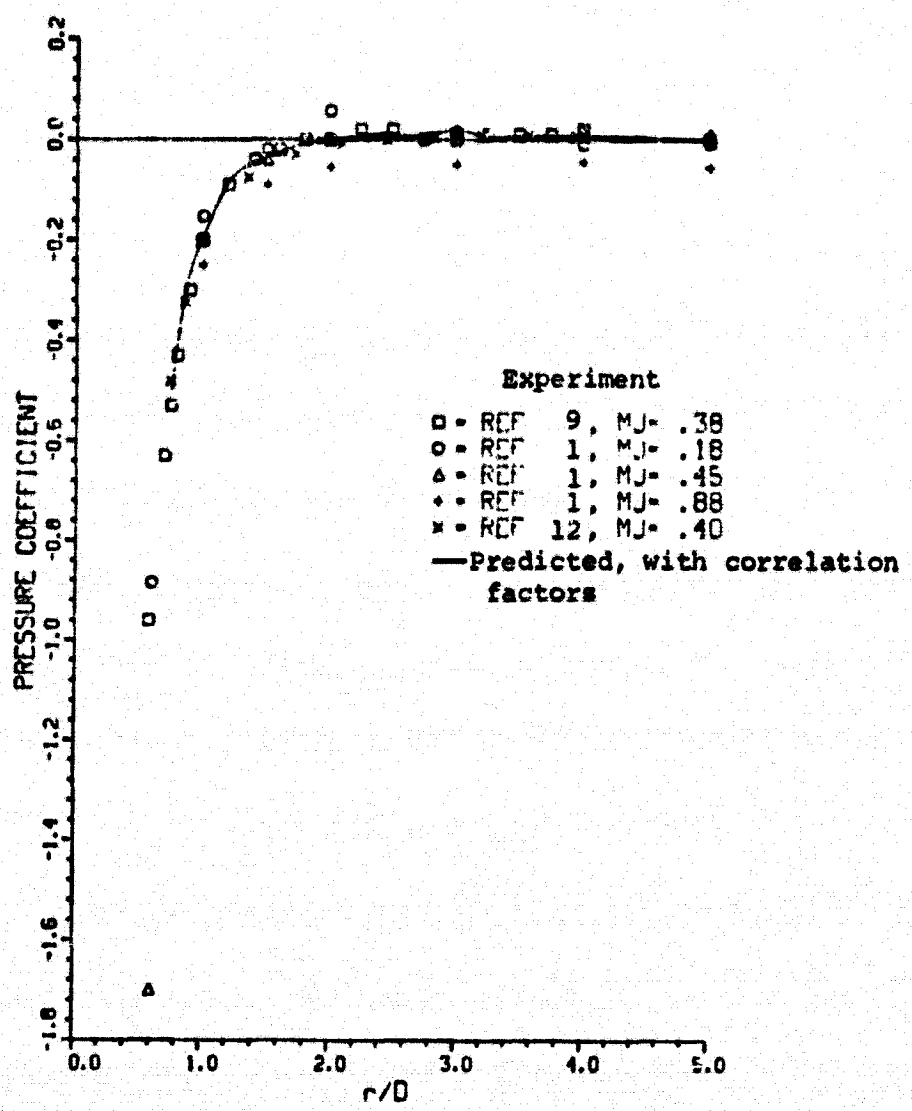

(b) $\beta = 60°$

Figure 10.- Continued.

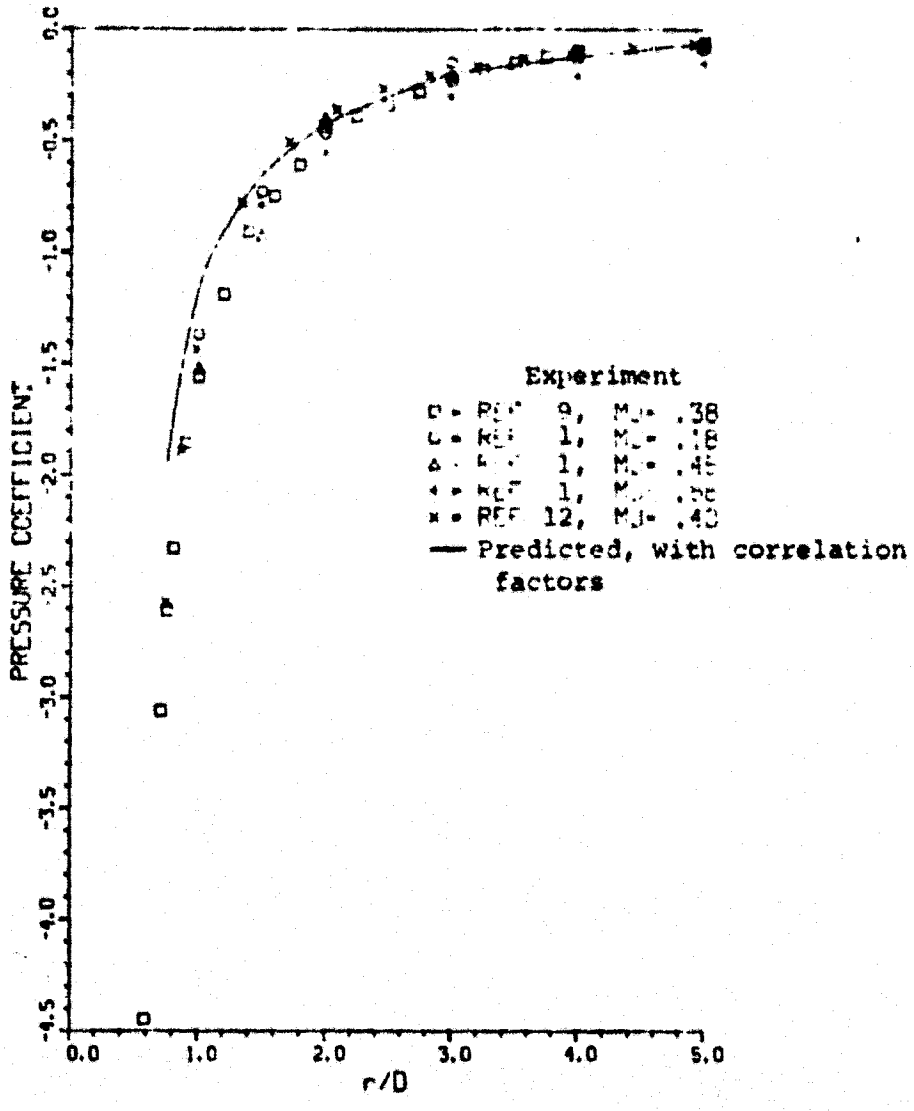

(c) $\beta = 120°$

Figure 10.- Continued.

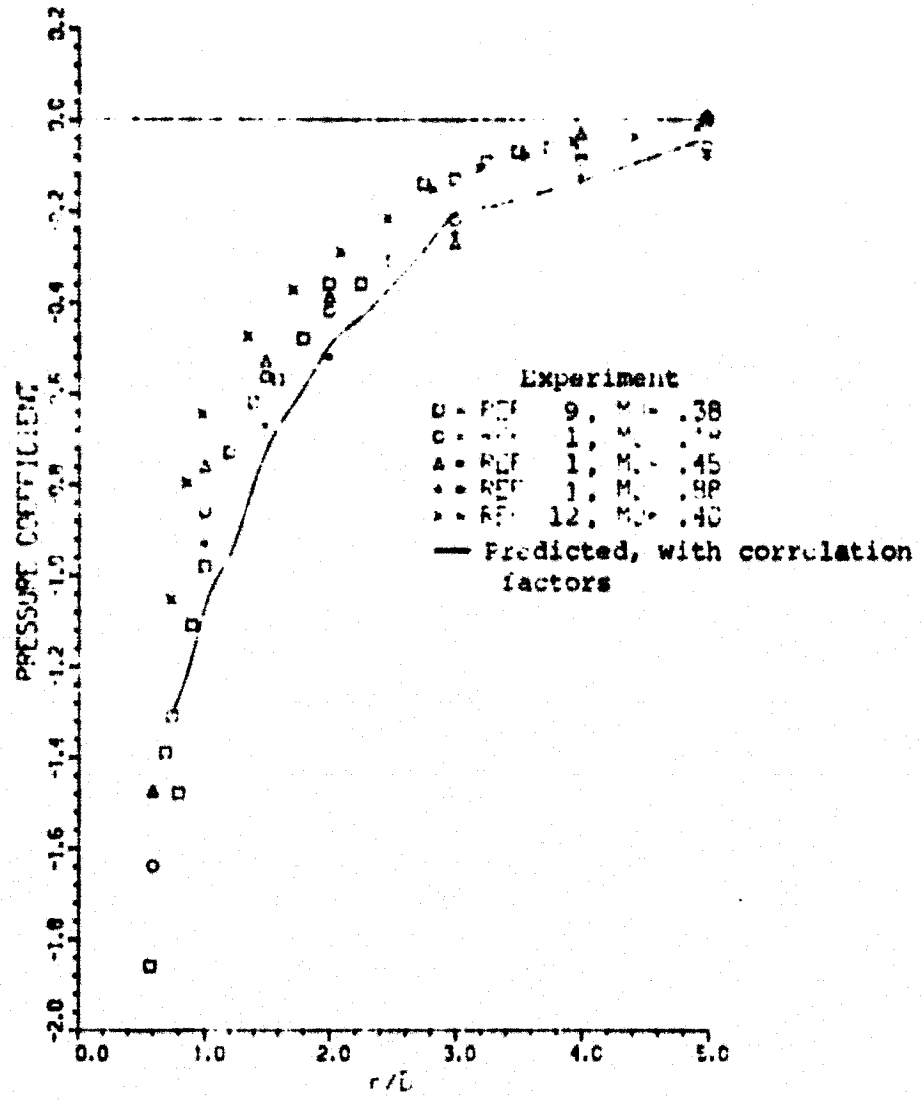

(d) $\beta = 180^{\circ}$

Figure 10.- Concluded.

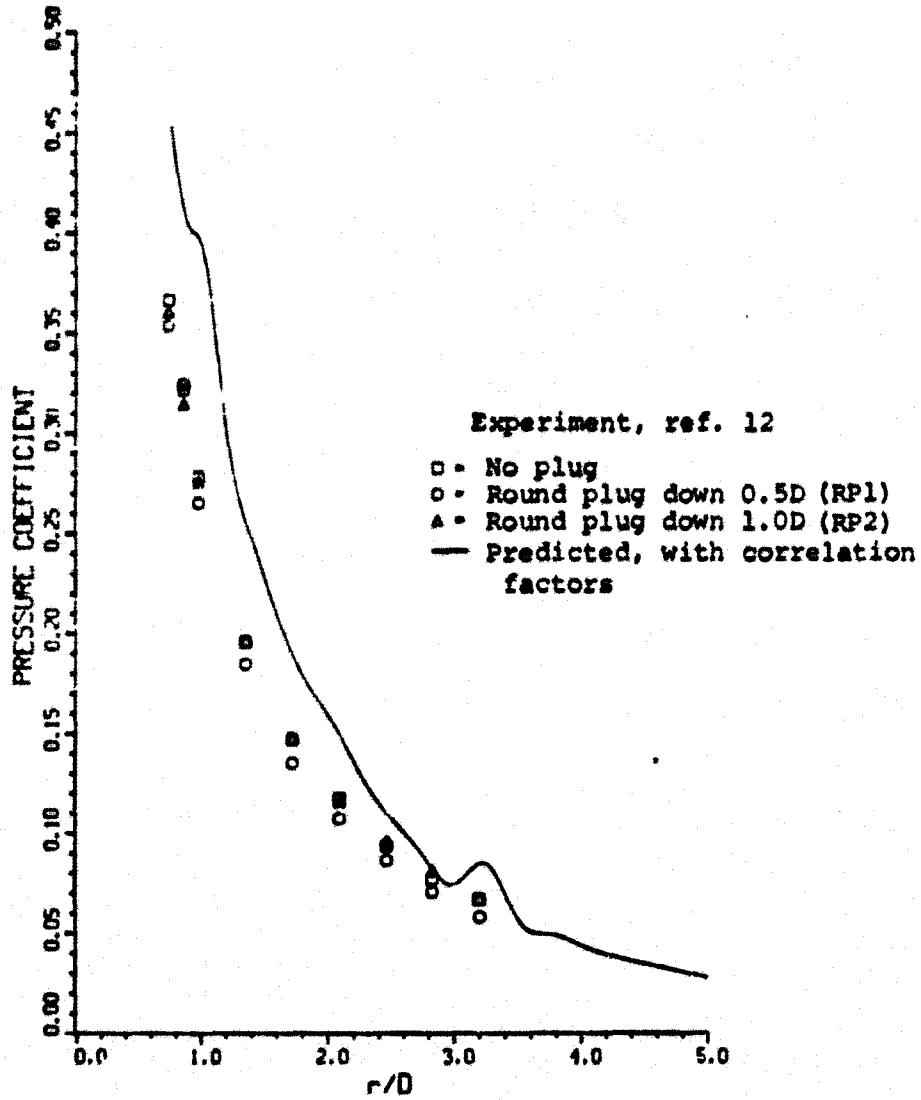

(a) $\beta = 0°$

Figure 11.- Comparison of measured and predicted plate pressure distributions showing effects of nonuniform exit profiles, $R \approx 2.5$.

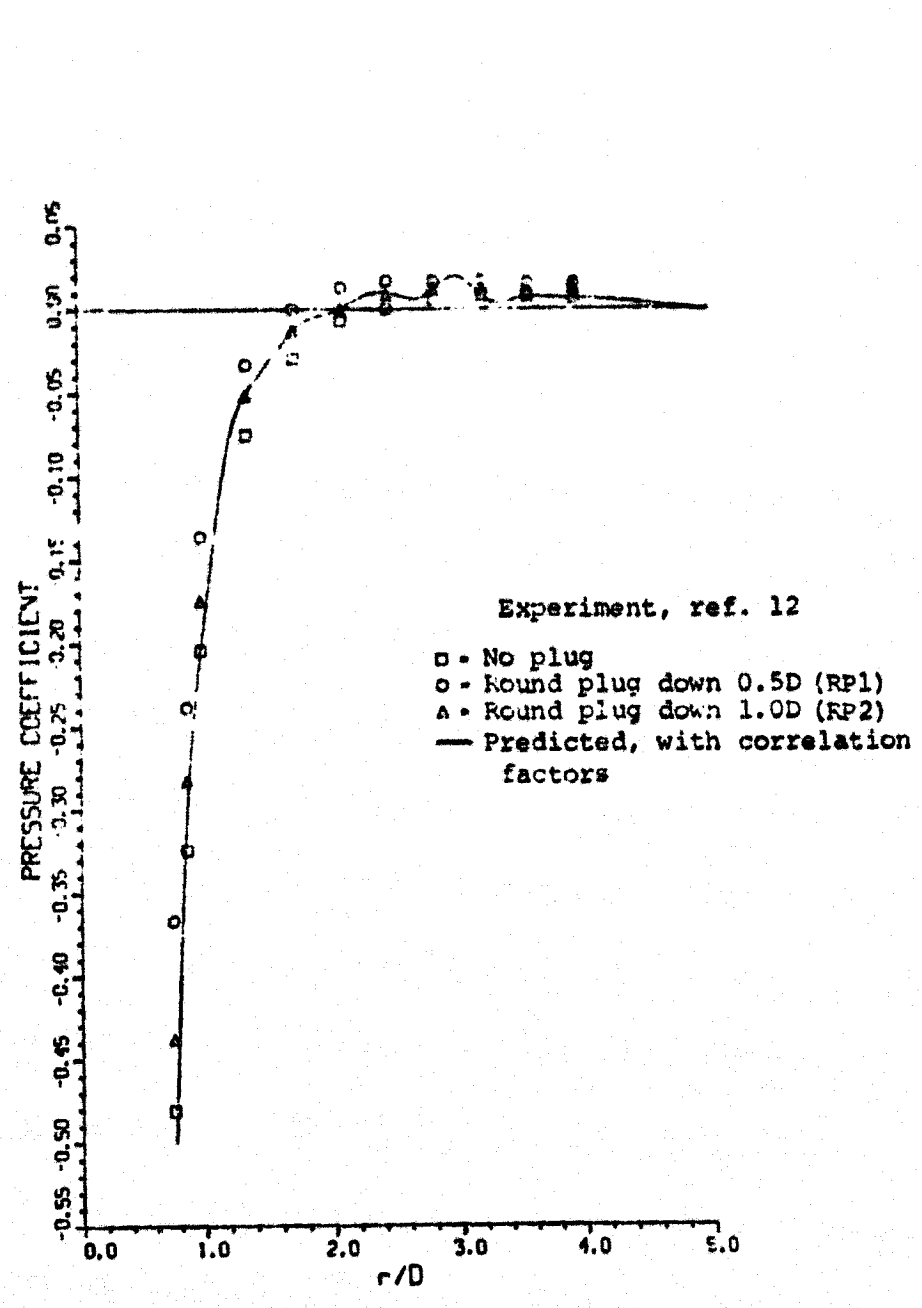

(b) $\beta = 60^{\circ}$

Figure 11.- Continued.

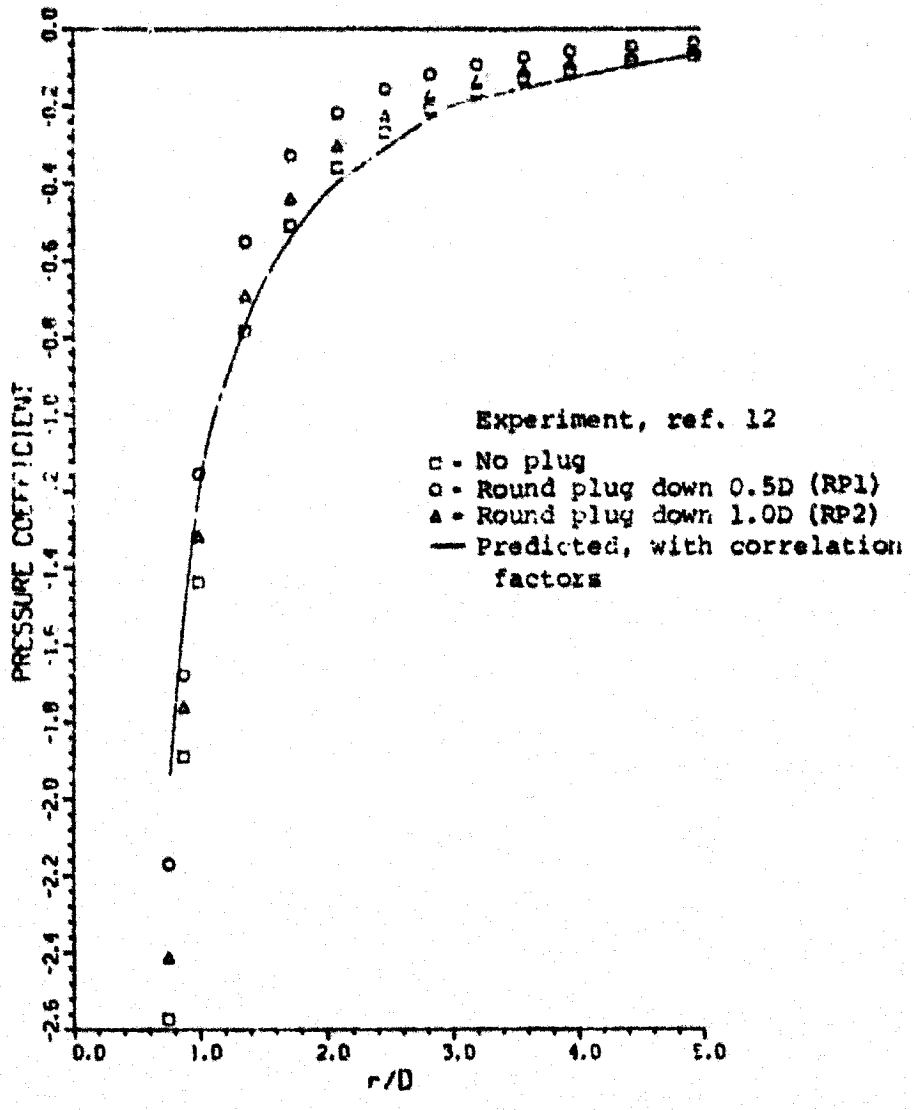

(c) $\beta = 120°$

Figure 11.- Continued.

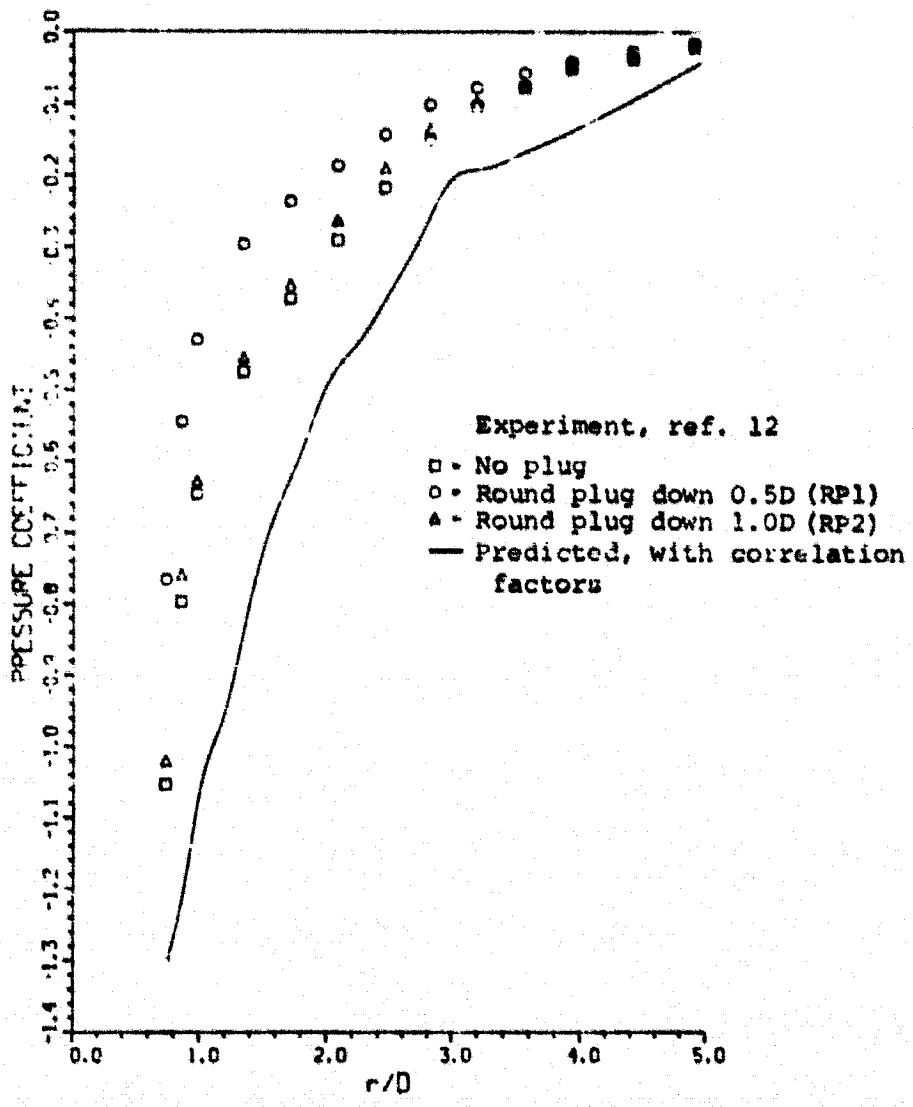

(d) $\beta = 180°$

Figure 11.- Concluded.

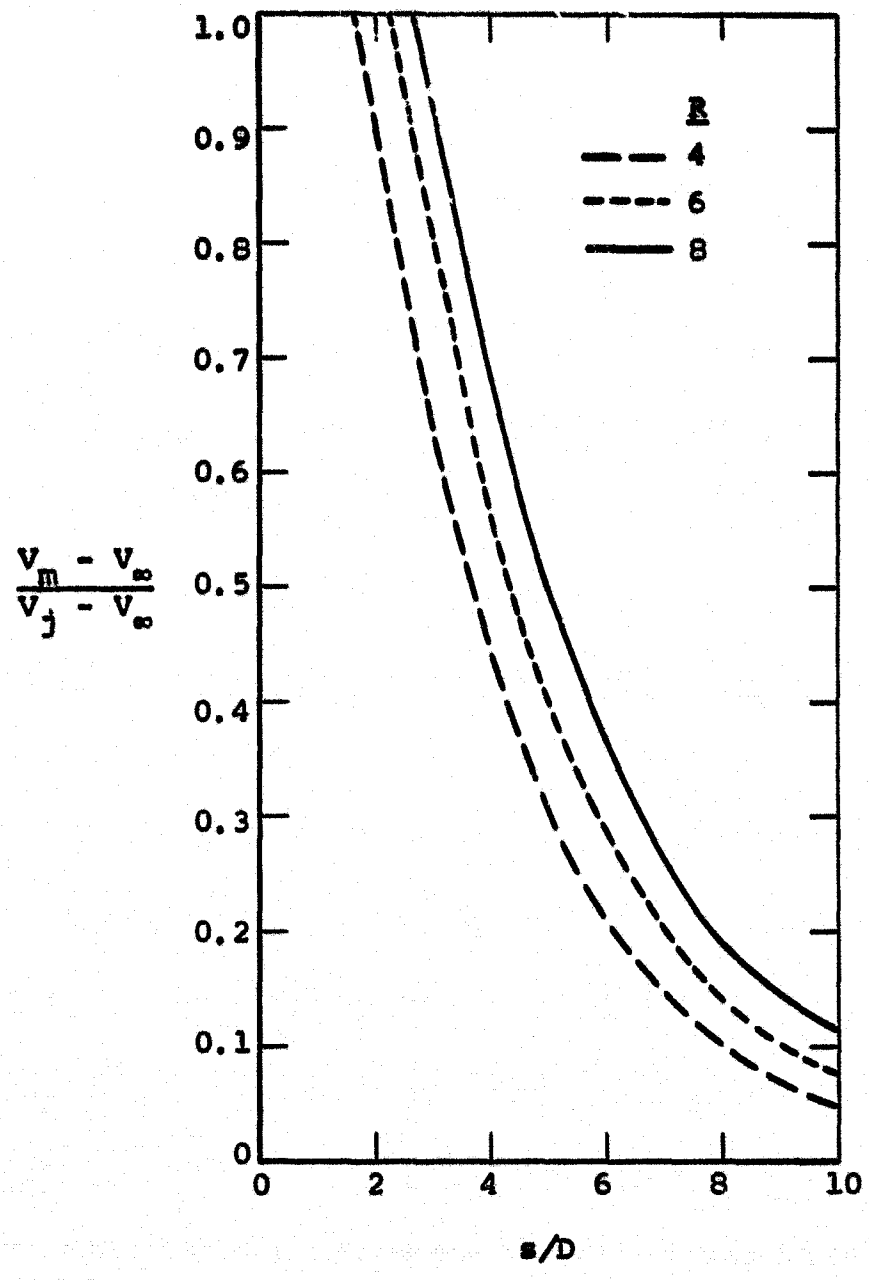

Figure 12.- Jet centerline velocity decay rates for uniform exit profile jets of reference 16.

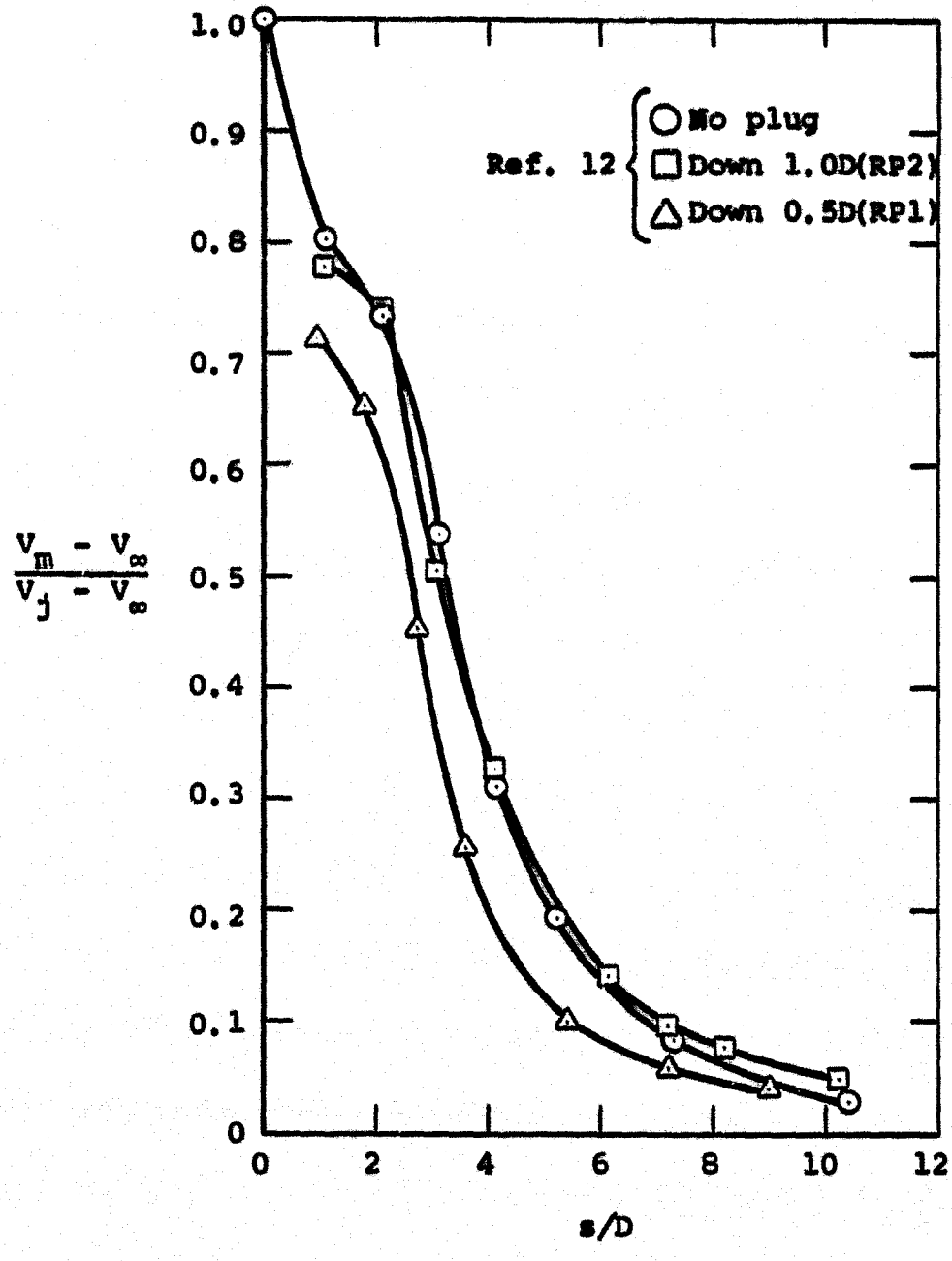

Figure 13.- Jet centerline velocity decay rates for round plug and no plug jets, R = 2.5.

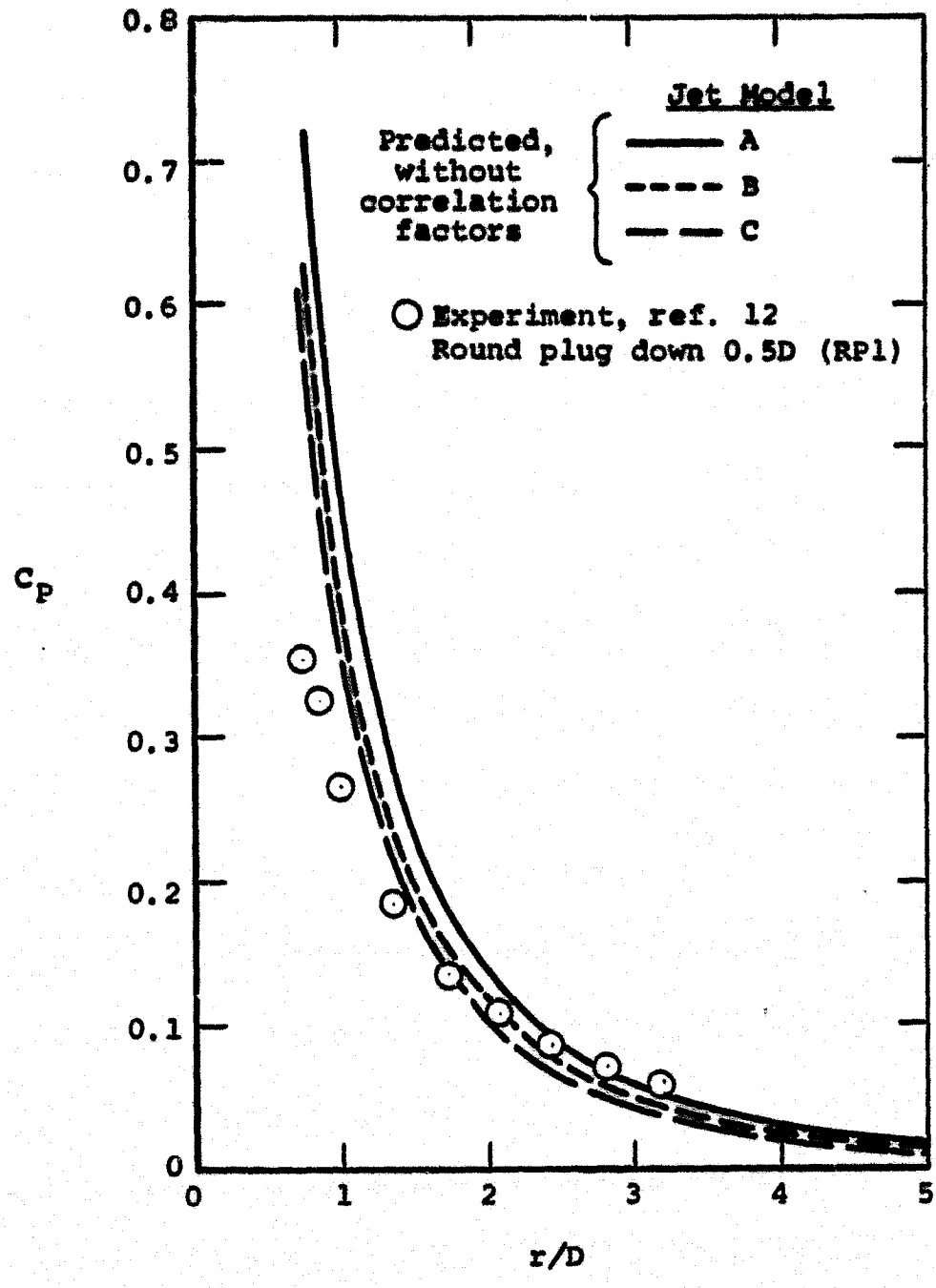

(a) $\beta = 0°$

Figure 14.- Comparison of measured and predicted plate pressure distributions for round plug down 0.5D (RP1) jet, R = 2.59.

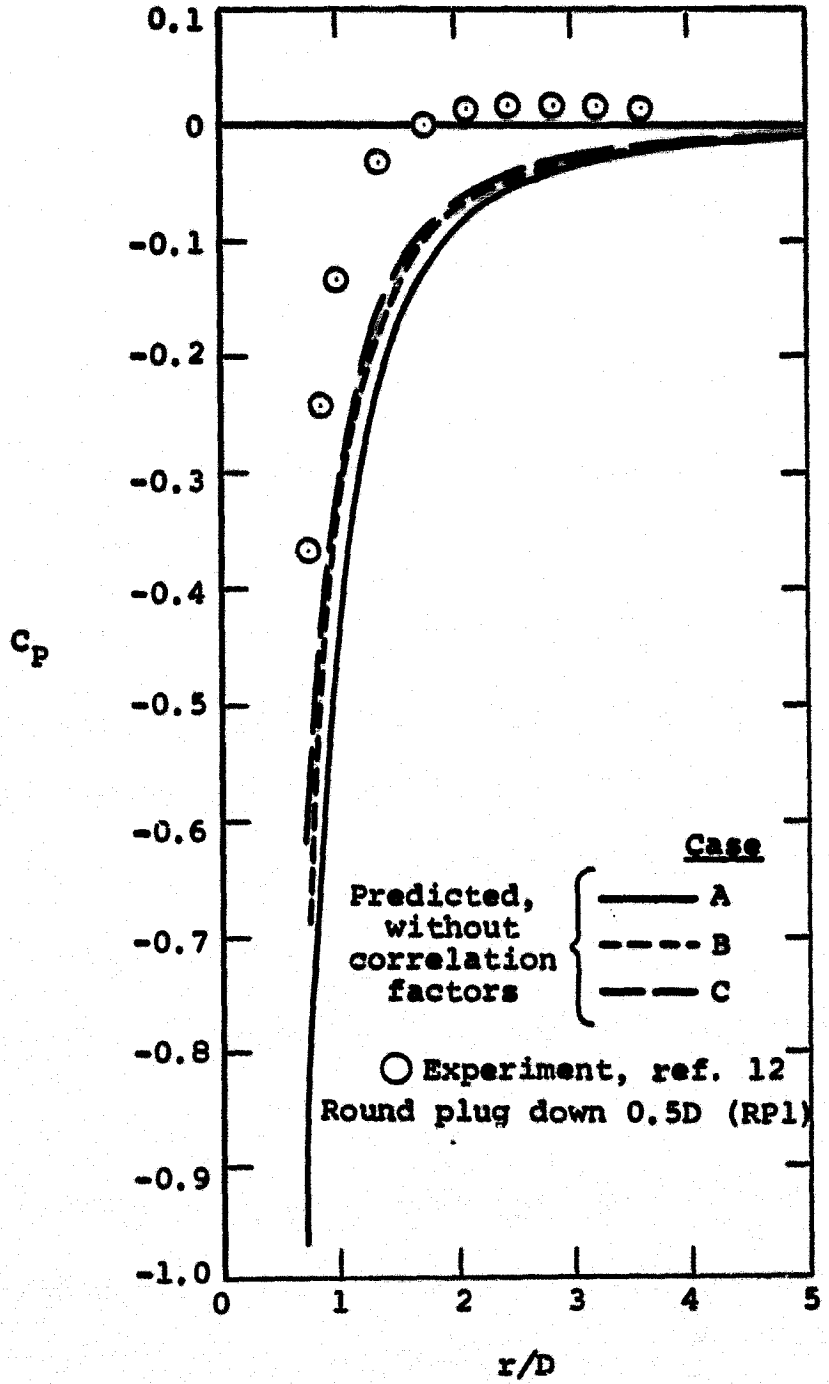

(b) $\beta = 60^{\circ}$

Figure 14.- Concluded.

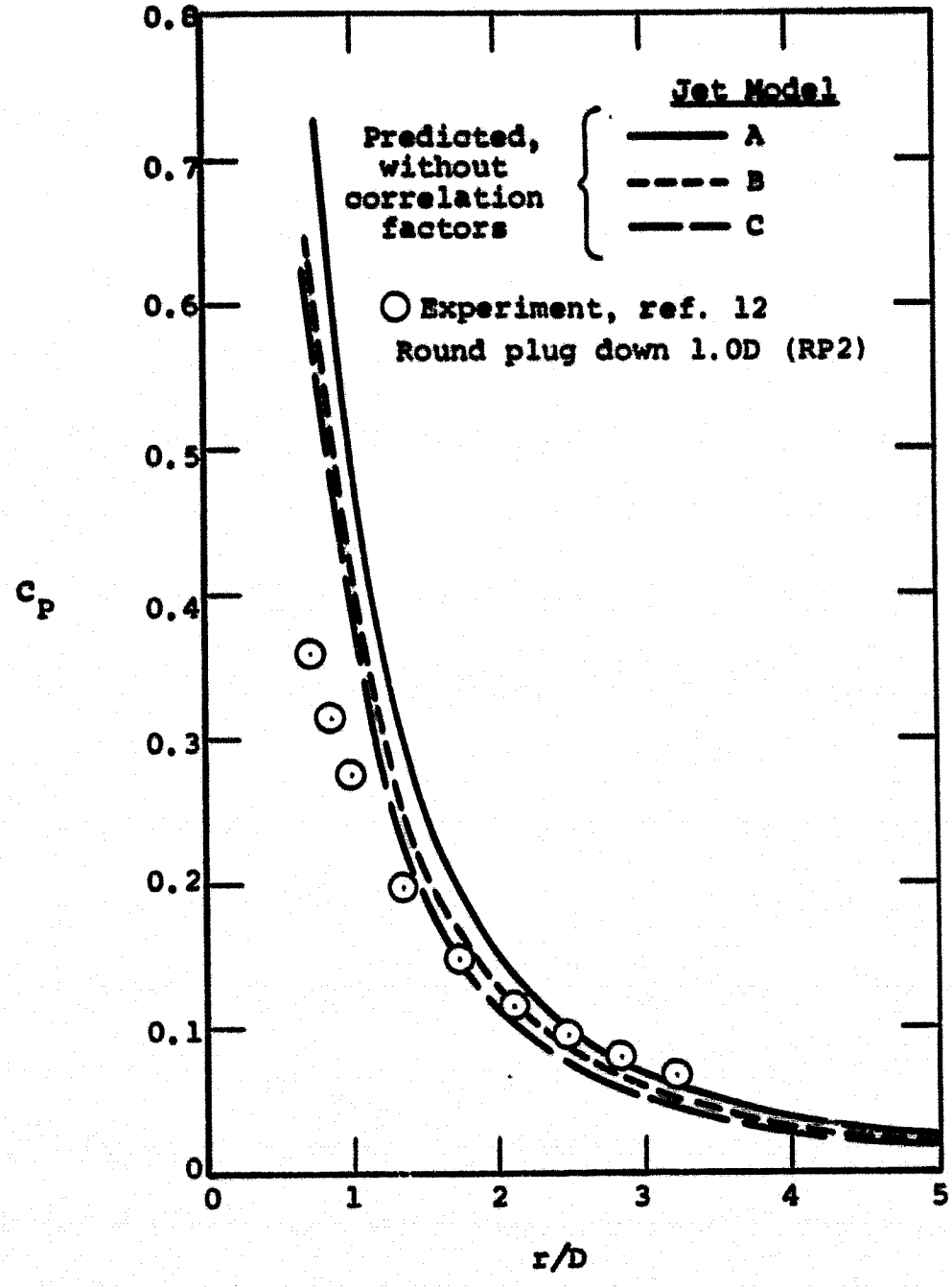

(a) $\beta = 0^\circ$

Figure 15.- Comparison of measured and predicted plate pressure distributions for round plug down 1.0D (RP2) jet, R = 2.5.

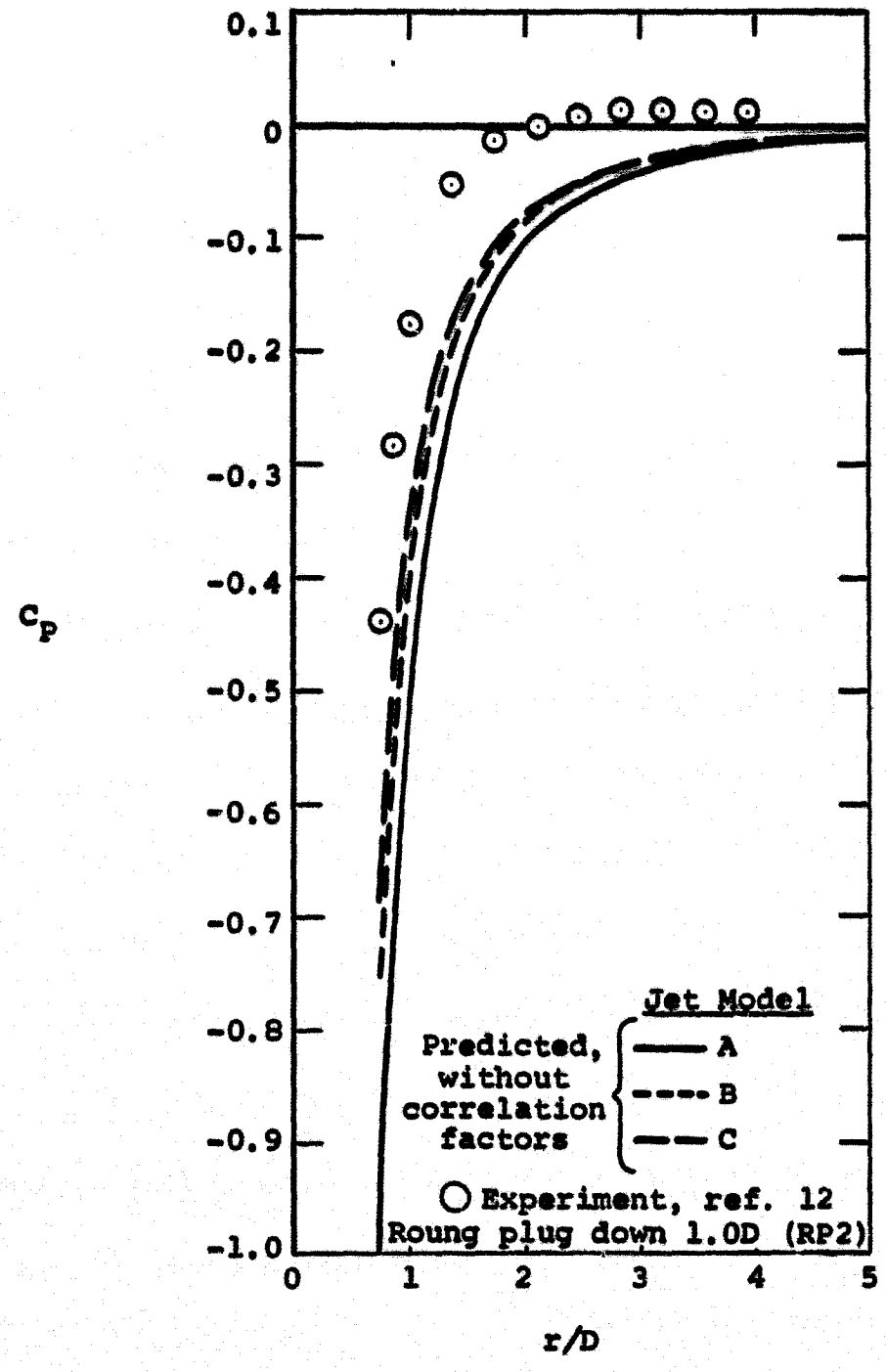

(b) $\beta = 60^\circ$

Figure 15.- Concluded.

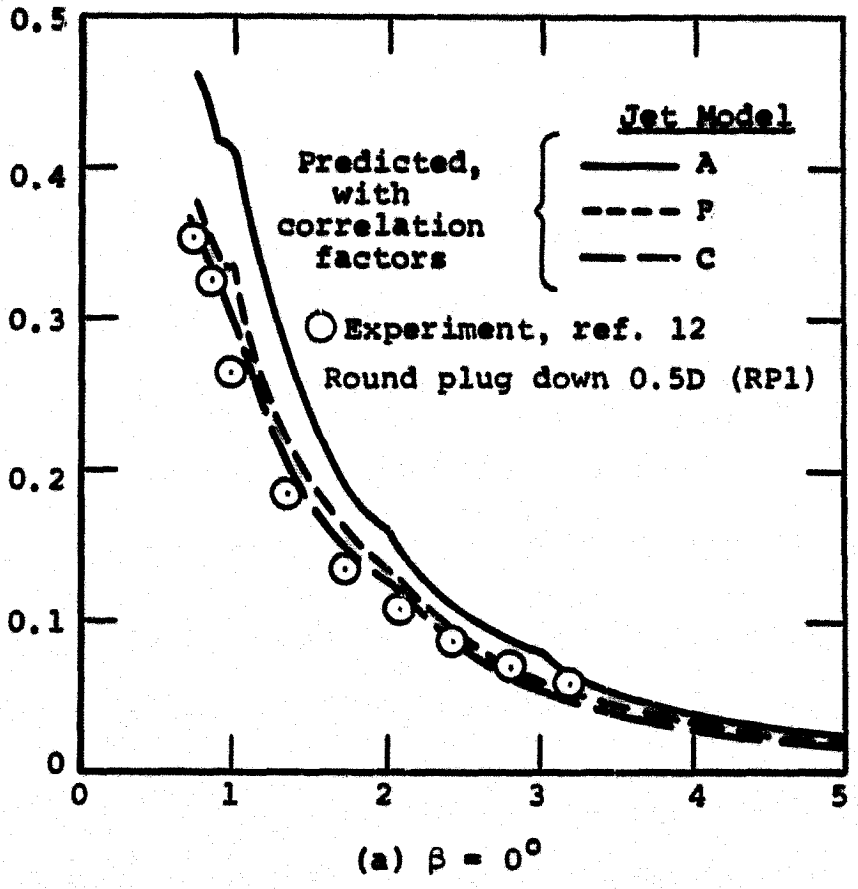

Figure 16.- Comparison of measured and predicted plate pressure distributions for round plug down 0.5D (RP1) jet, R = 2.59.

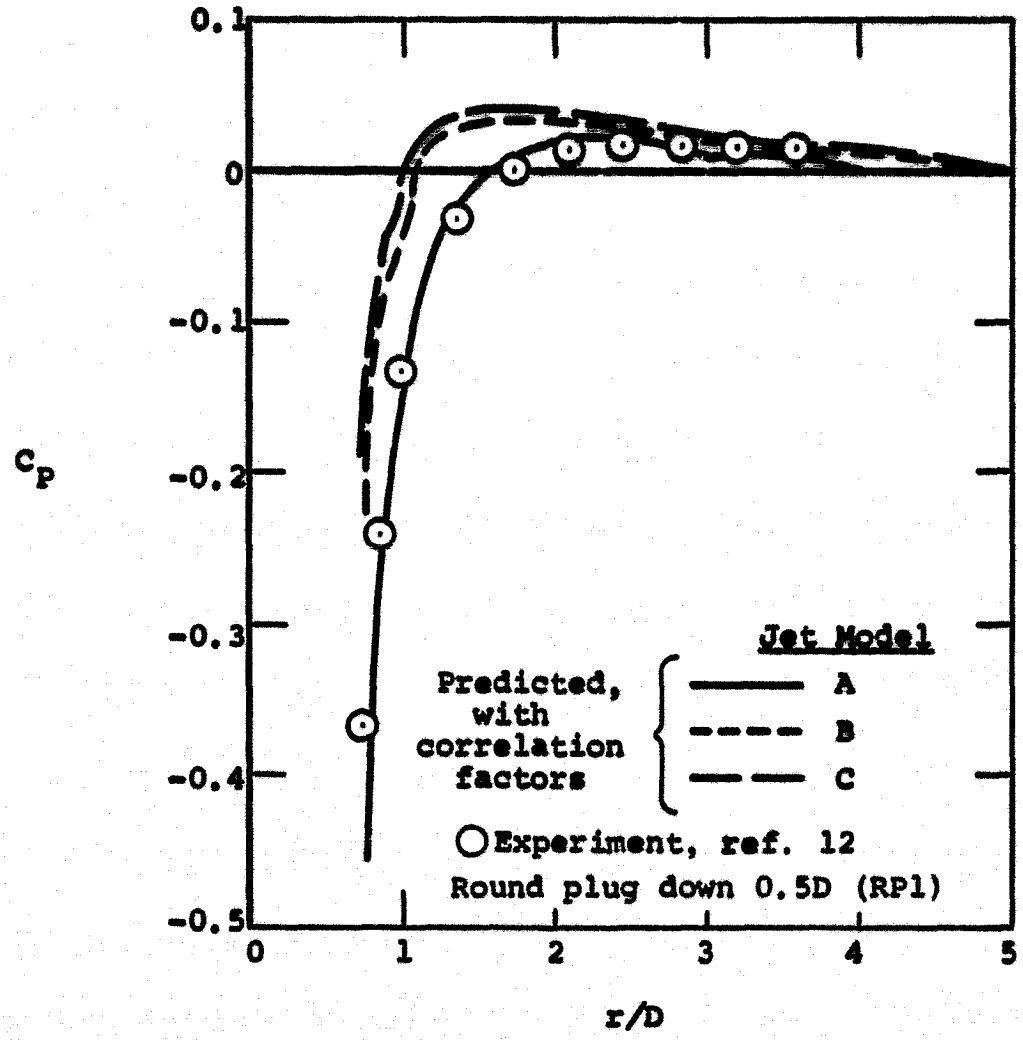

(b) $\beta = 60^\circ$

Figure 16.- Continued.

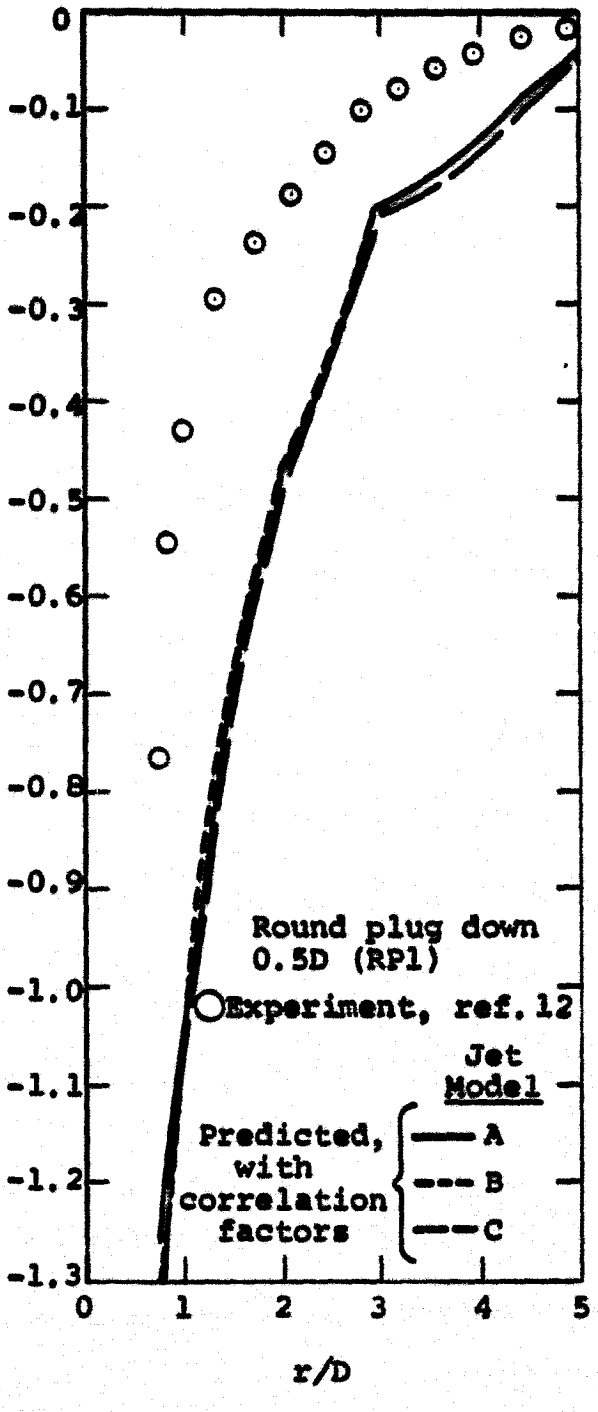

(c) $\beta = 180^{\circ}$

Figure 16.- Concluded.

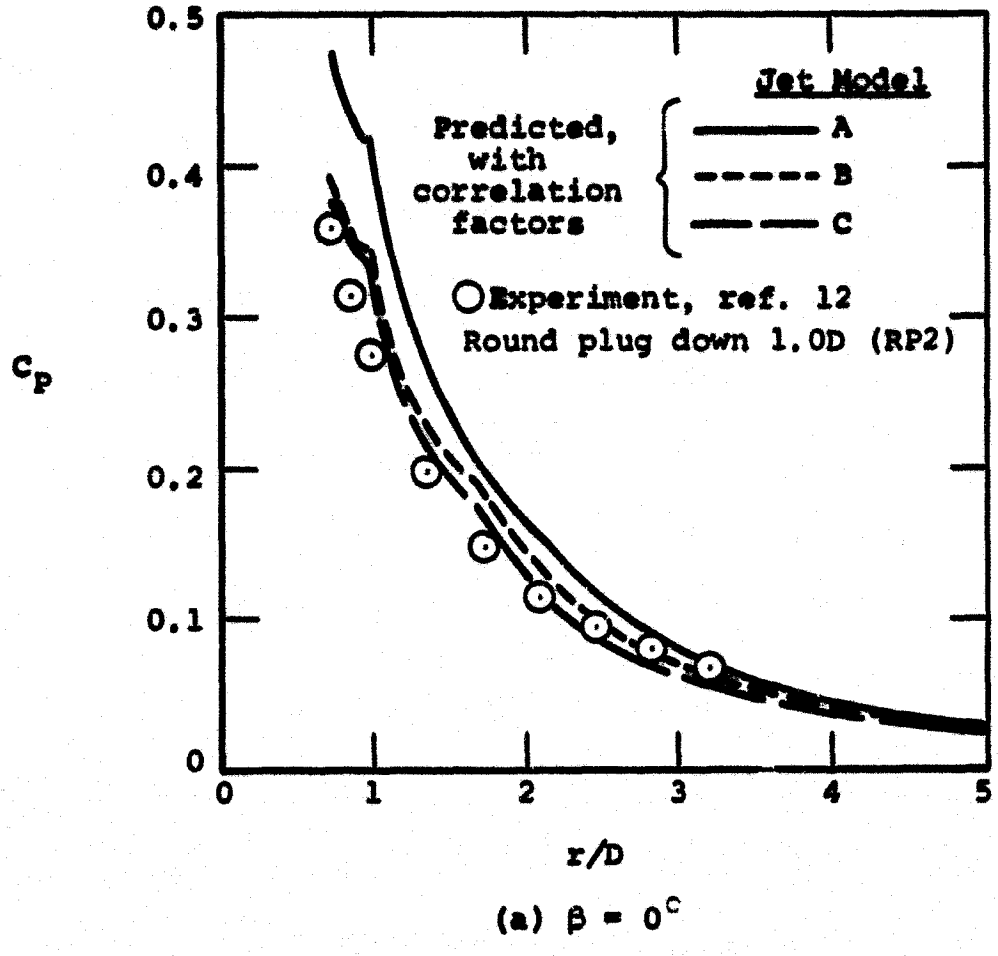

(a) $\beta = 0^c$

Figure 17.- Comparison of measured and predicted plate pressure distributions for round plug down 1.0D (RP2) jet, R = 2.5.

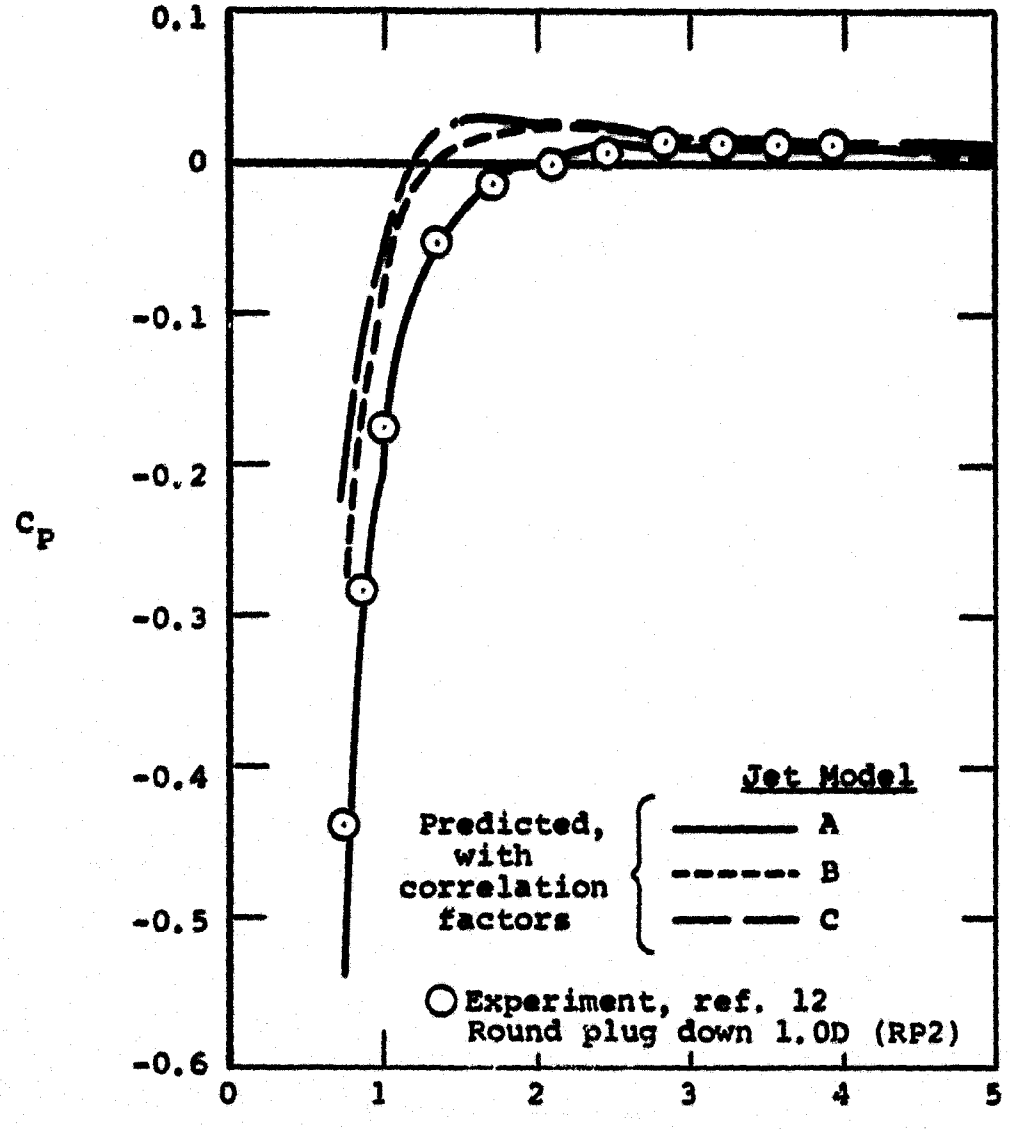

(b) $\beta = 60^{\circ}$

Figure 17.- Continued.

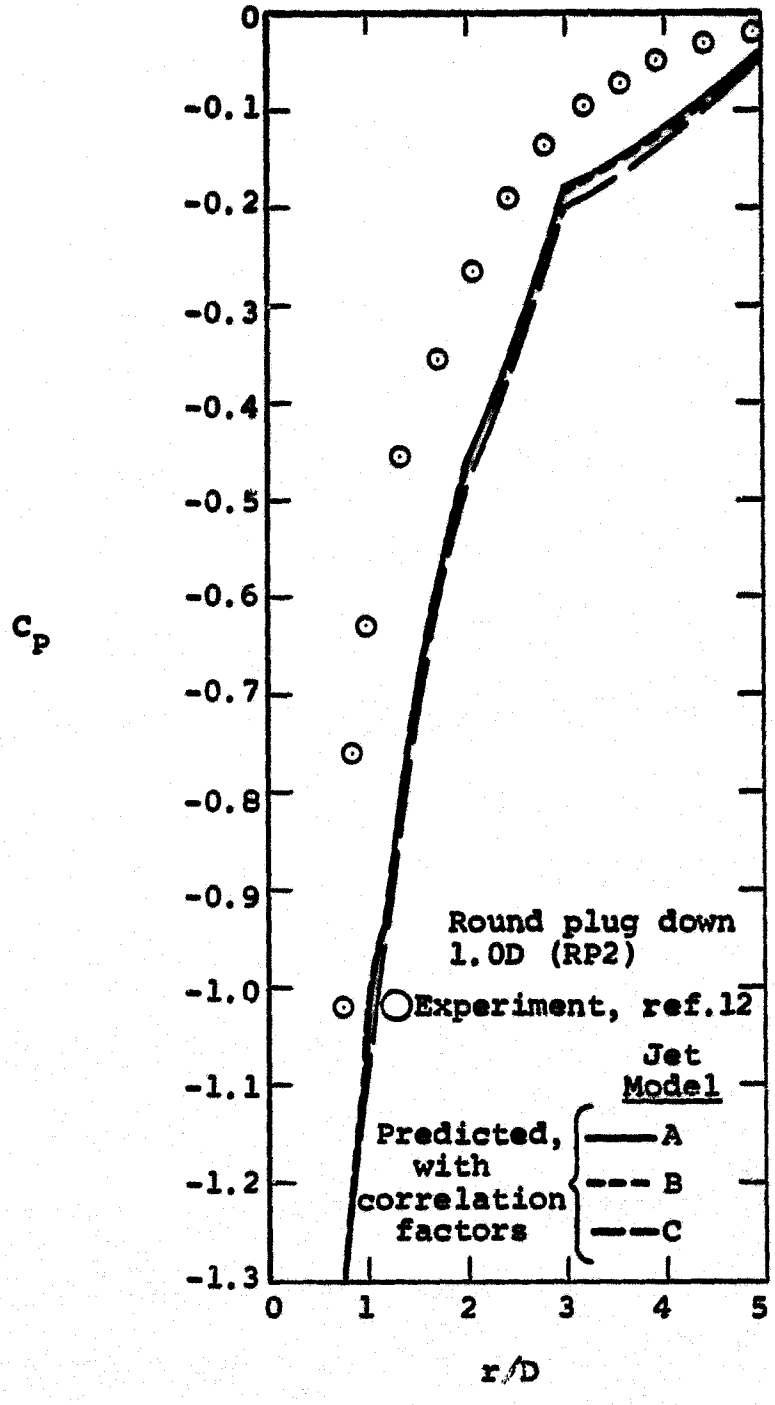

(c) $\beta = 180^{\circ}$

Figure 17.- Concluded.

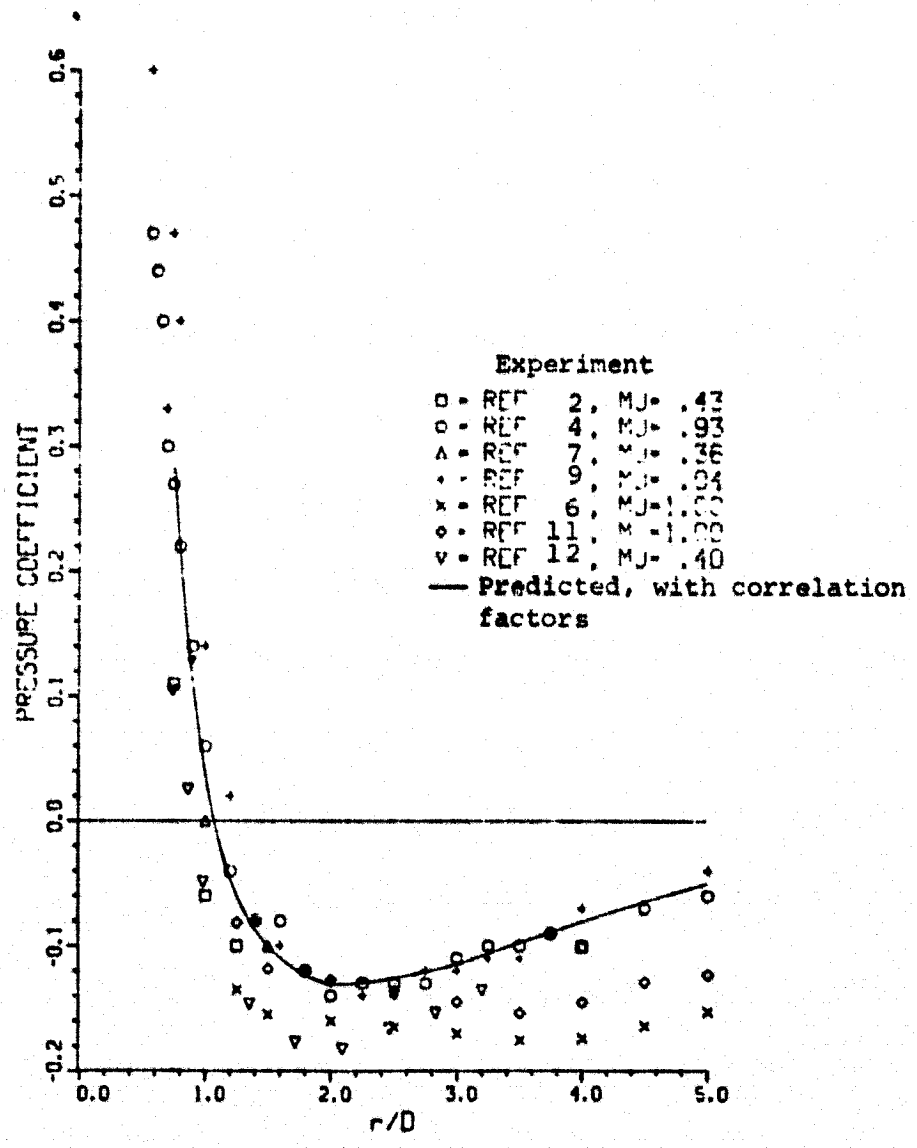

(a) $\beta = 0°$

Figure 18.- Comparison of measured and predicted plate pressure distributions for uniform exit profile jets, R ≈ 8.

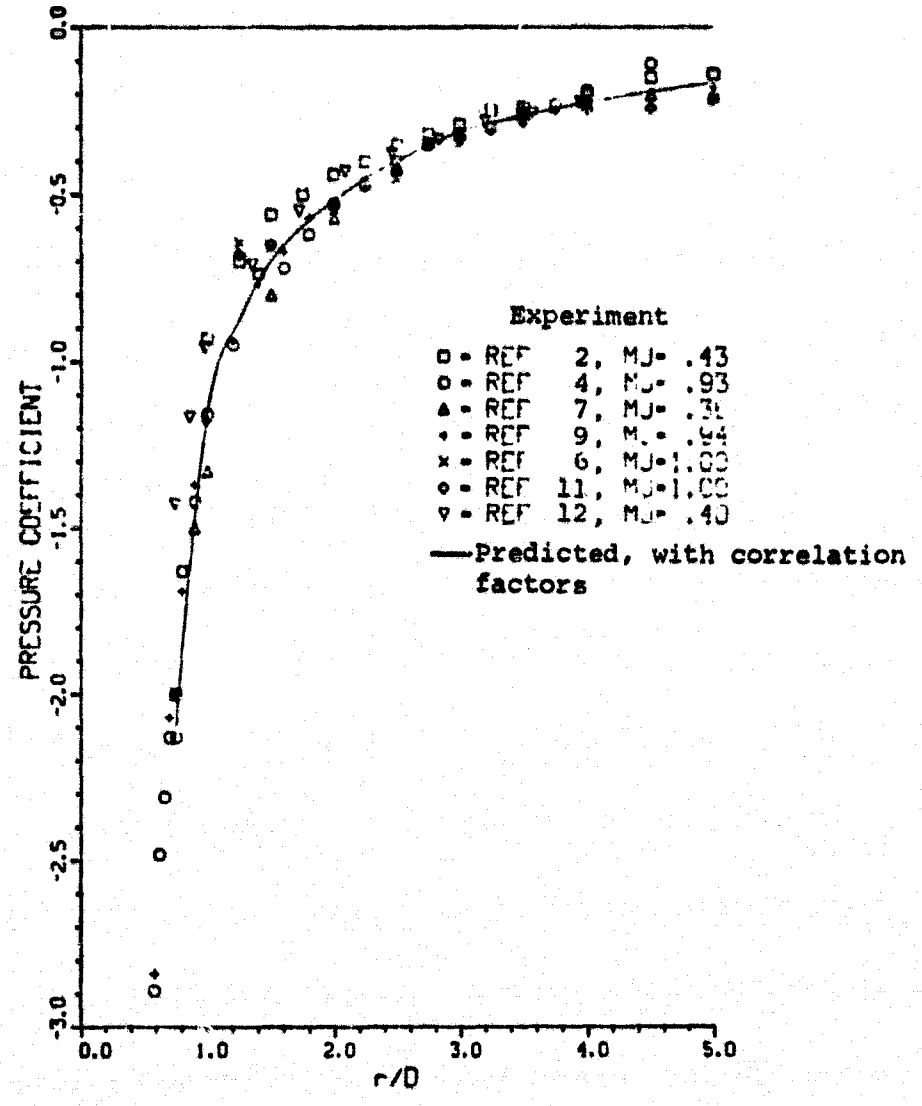

(b) $\beta = 60°$

Figure 18.- Continued.

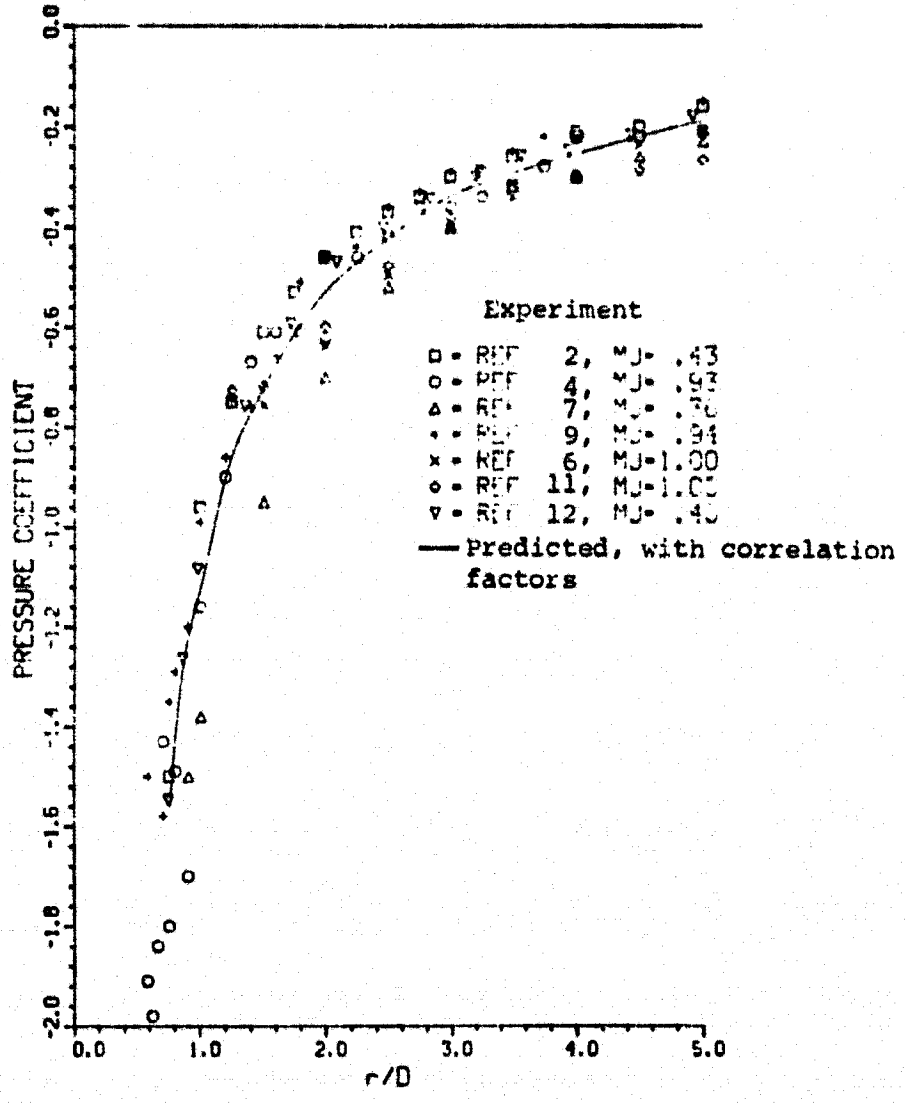

(c) $\beta = 120°$

Figure 18.- Continued.

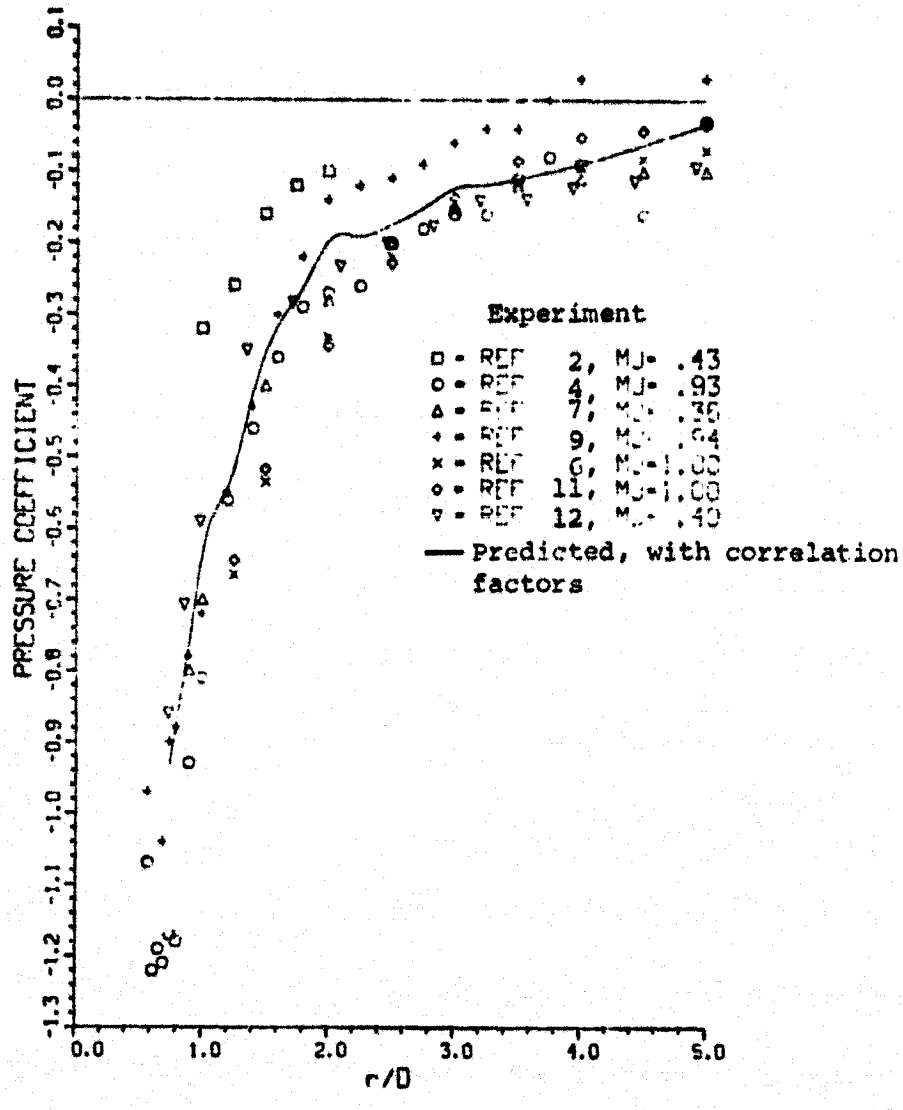

(d) $\beta = 180°$

Figure 18.- Concluded.

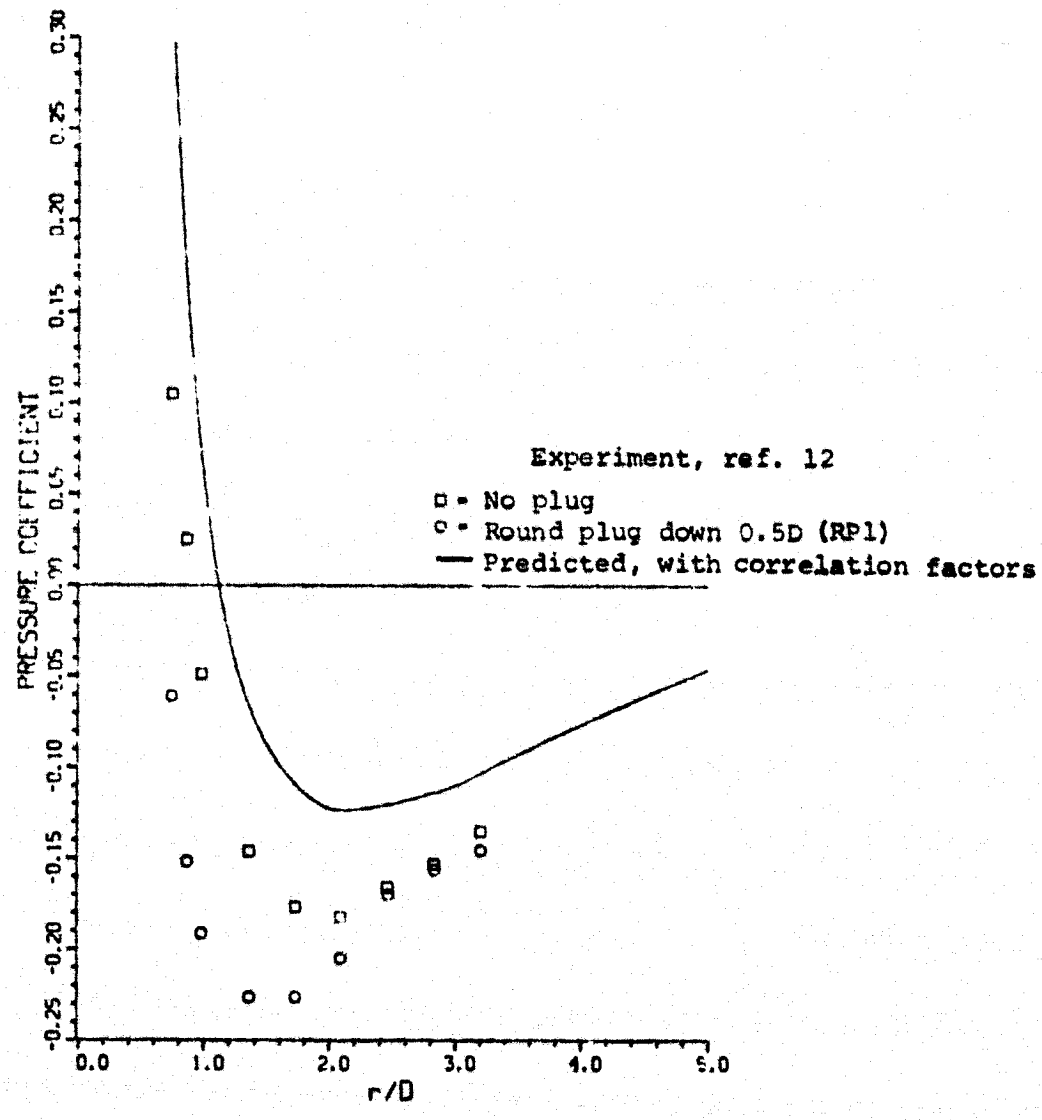

(a) $\beta = 0°$

Figure 19.- Comparison of predicted and measured plate pressure distributions showing effects of nonuniform exit profiles, R = 7.8.

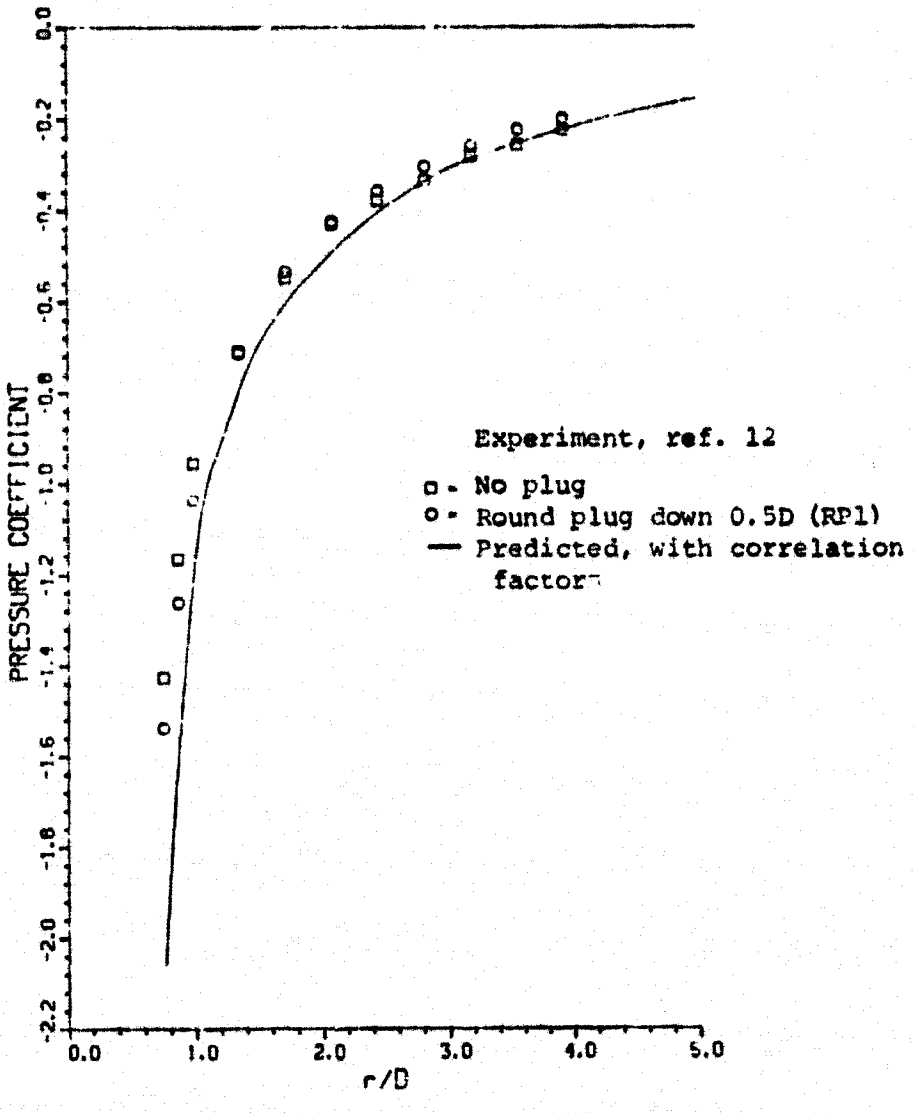

(b) $\beta = 60°$

Figure 19.- Continued.

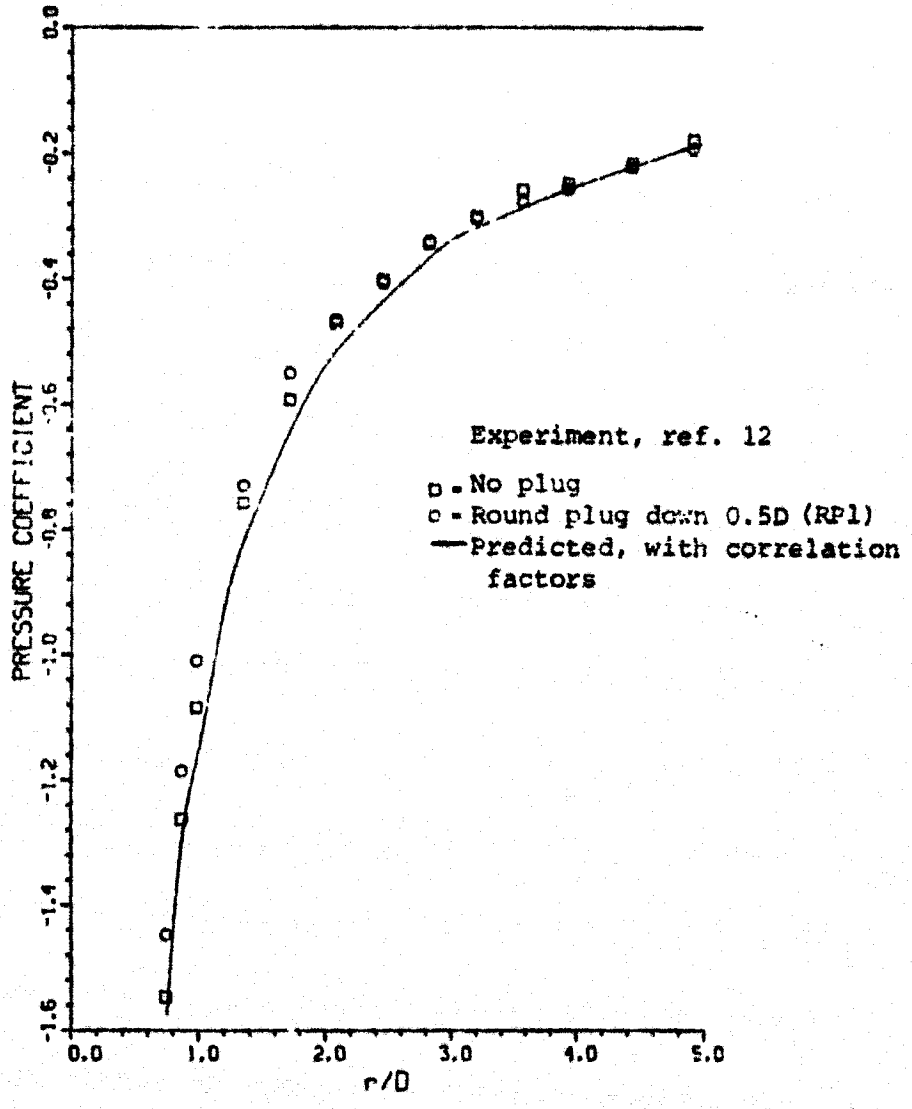

(c) $\beta = 120°$

Figure 19.- Continued.

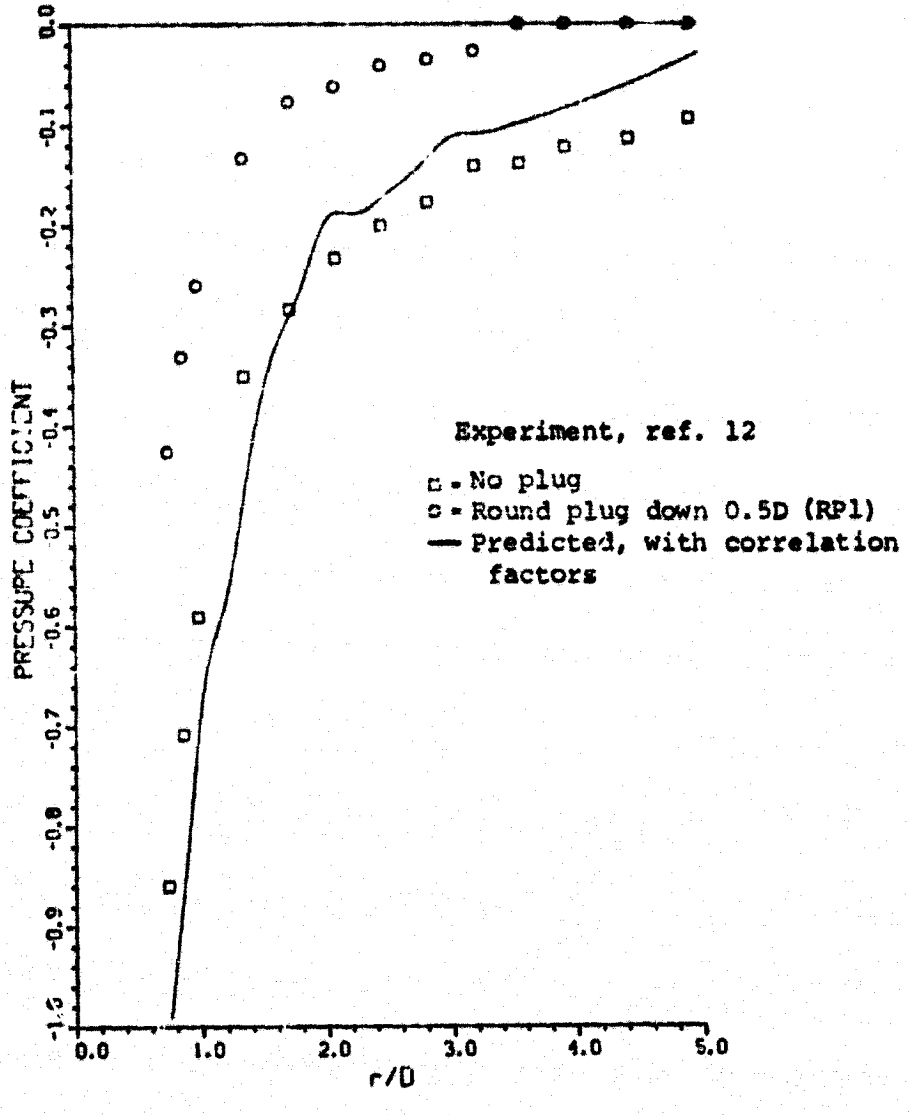

(d) $\beta = 180°$

Figure 19.- Concluded.

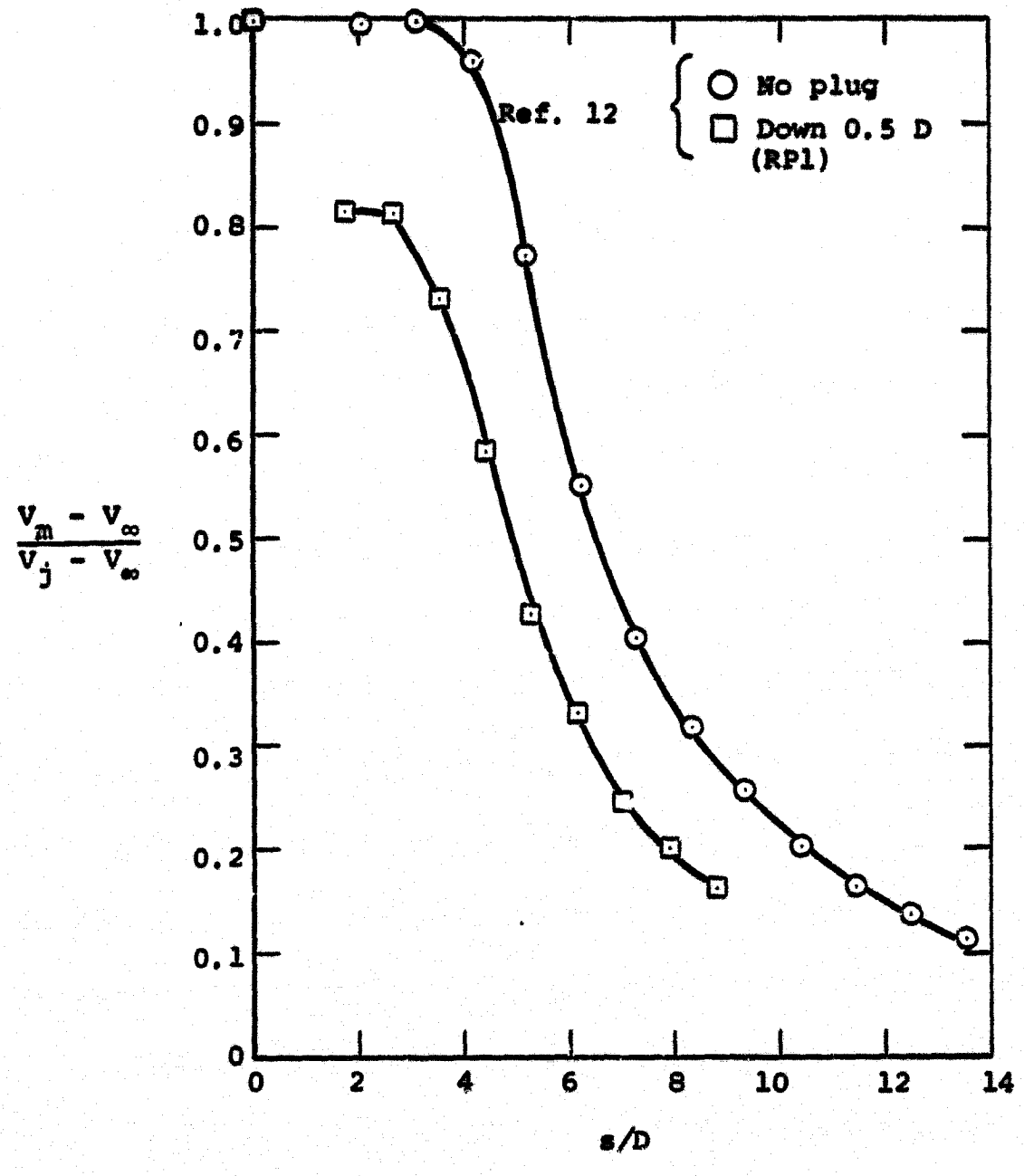

Figure 20.- Jet centerline velocity decay rates for round plug down 0.5D (RP1) and no plug jets, R = 8.

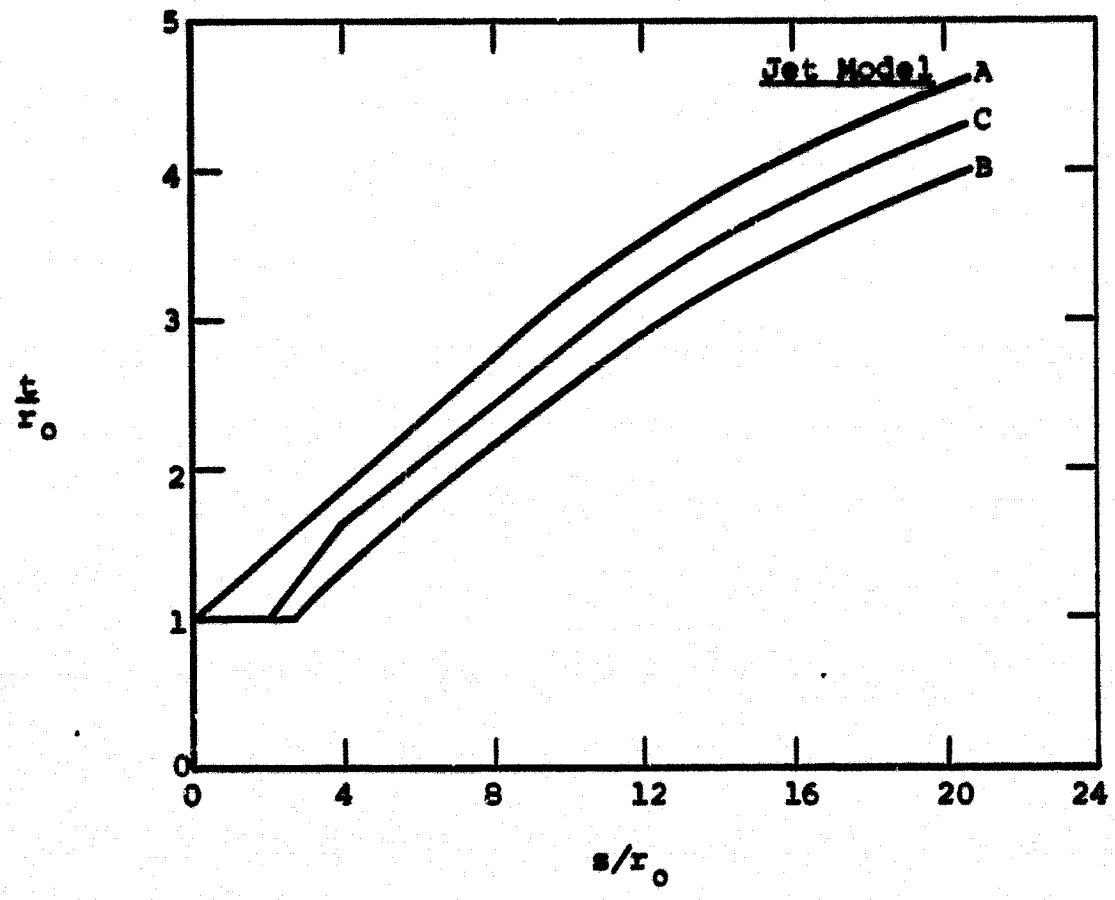

Figure 21.- Jet expansion curves for the round plug down 0.5 D (RP1) jet, R = 7.76.

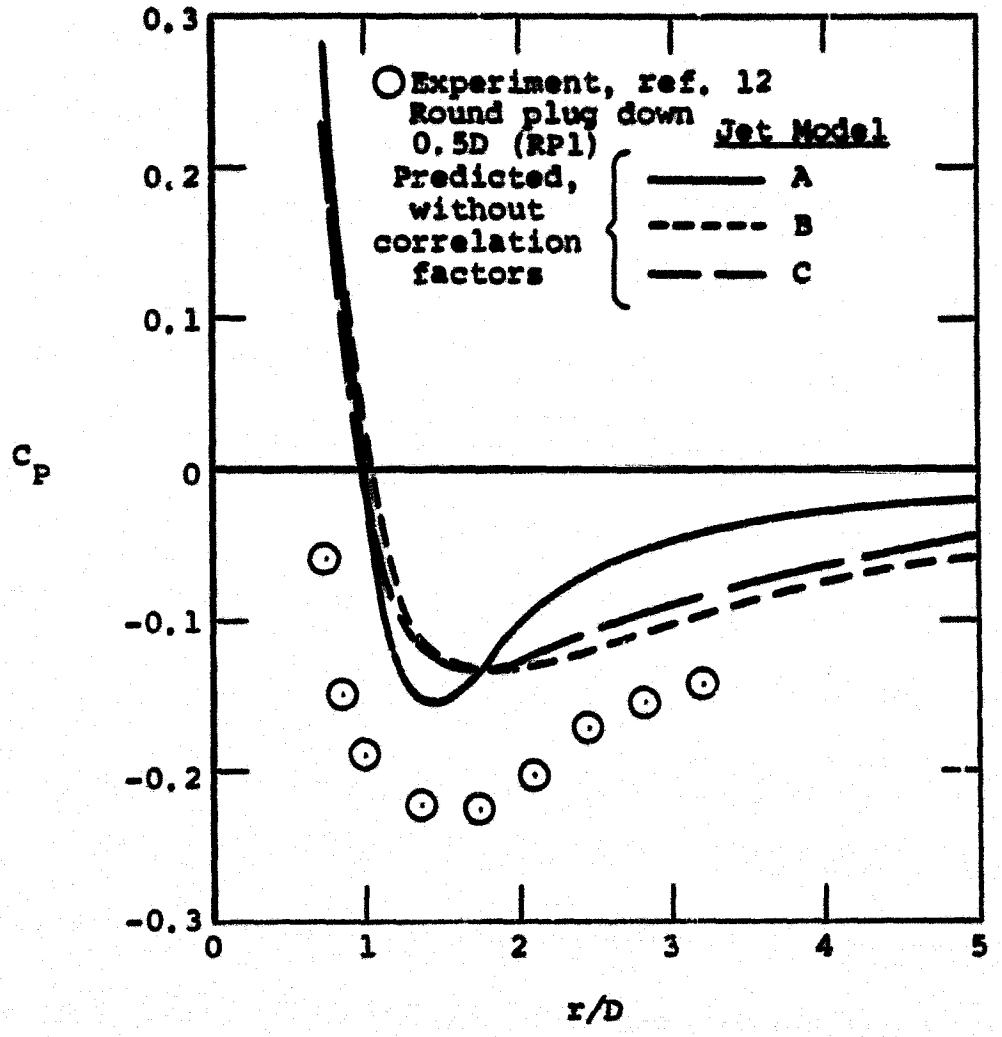

(a) $\beta = 0^\circ$

Figure 22.- Comparison of measured and predicted plate pressure distributions for the round plug down 0.5D (RP1) jet, R = 7.76.

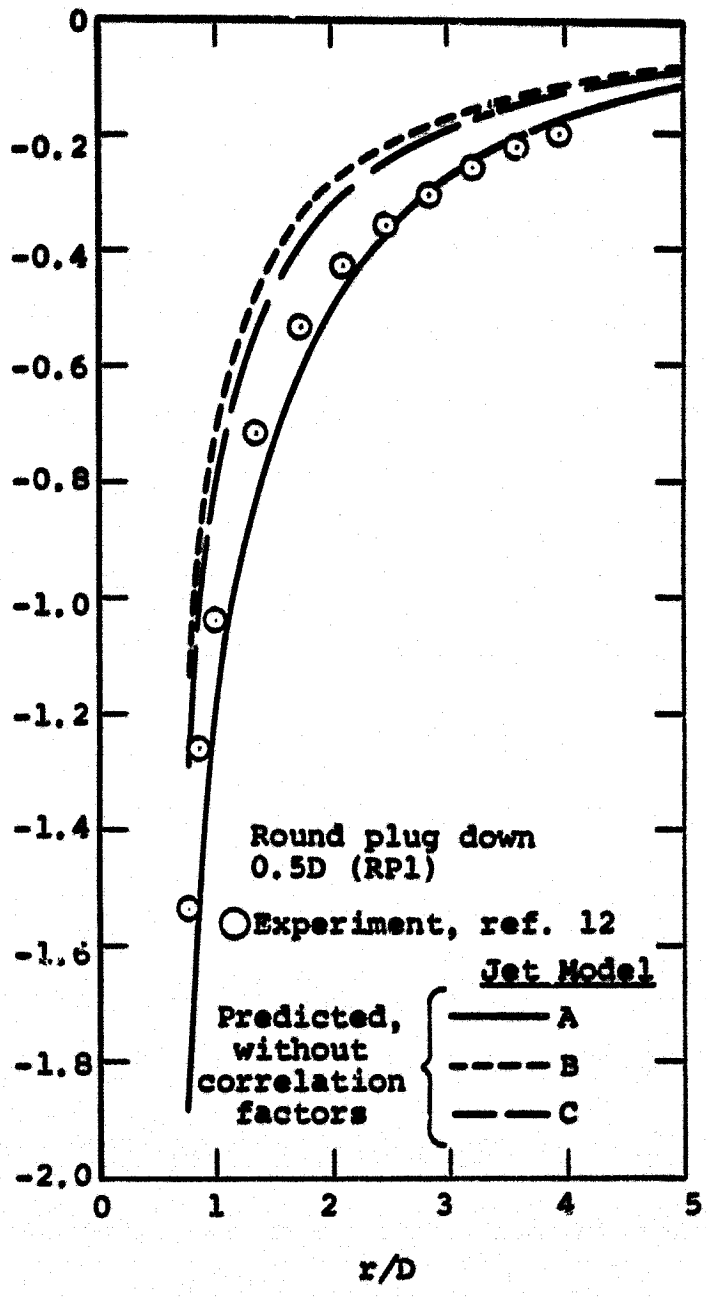

(b) $\beta = 60^{\circ}$

Figure 22.- Continued.

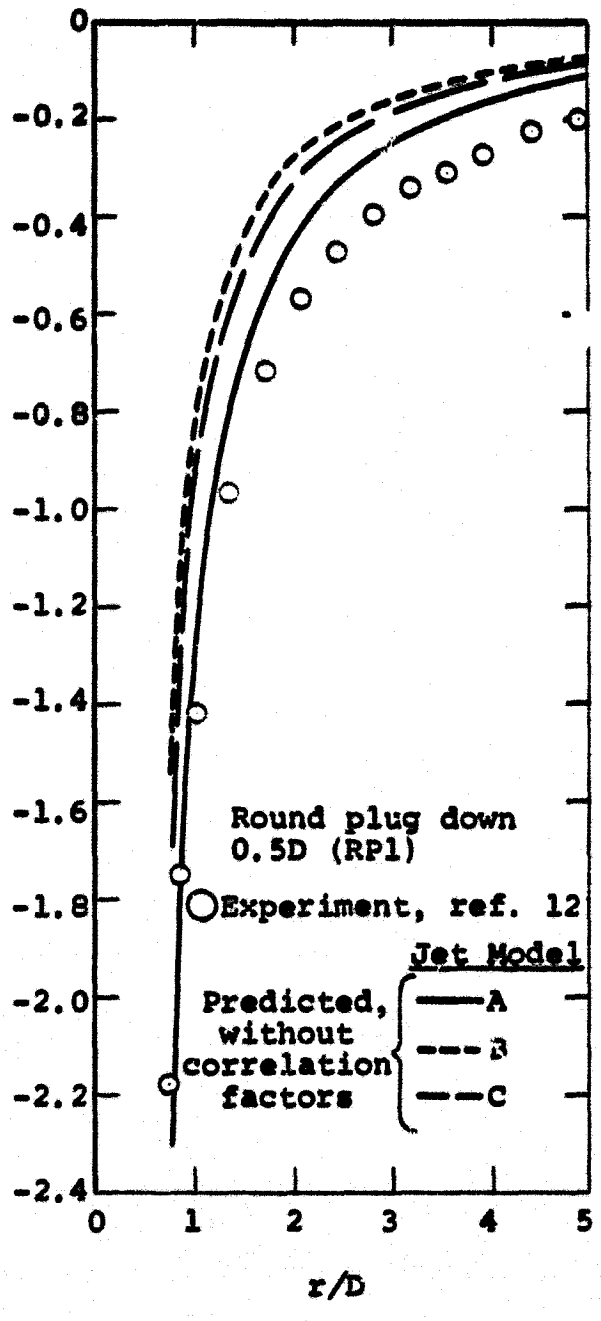

(c) $\beta = 90^\circ$

Figure 22.- Concluded.

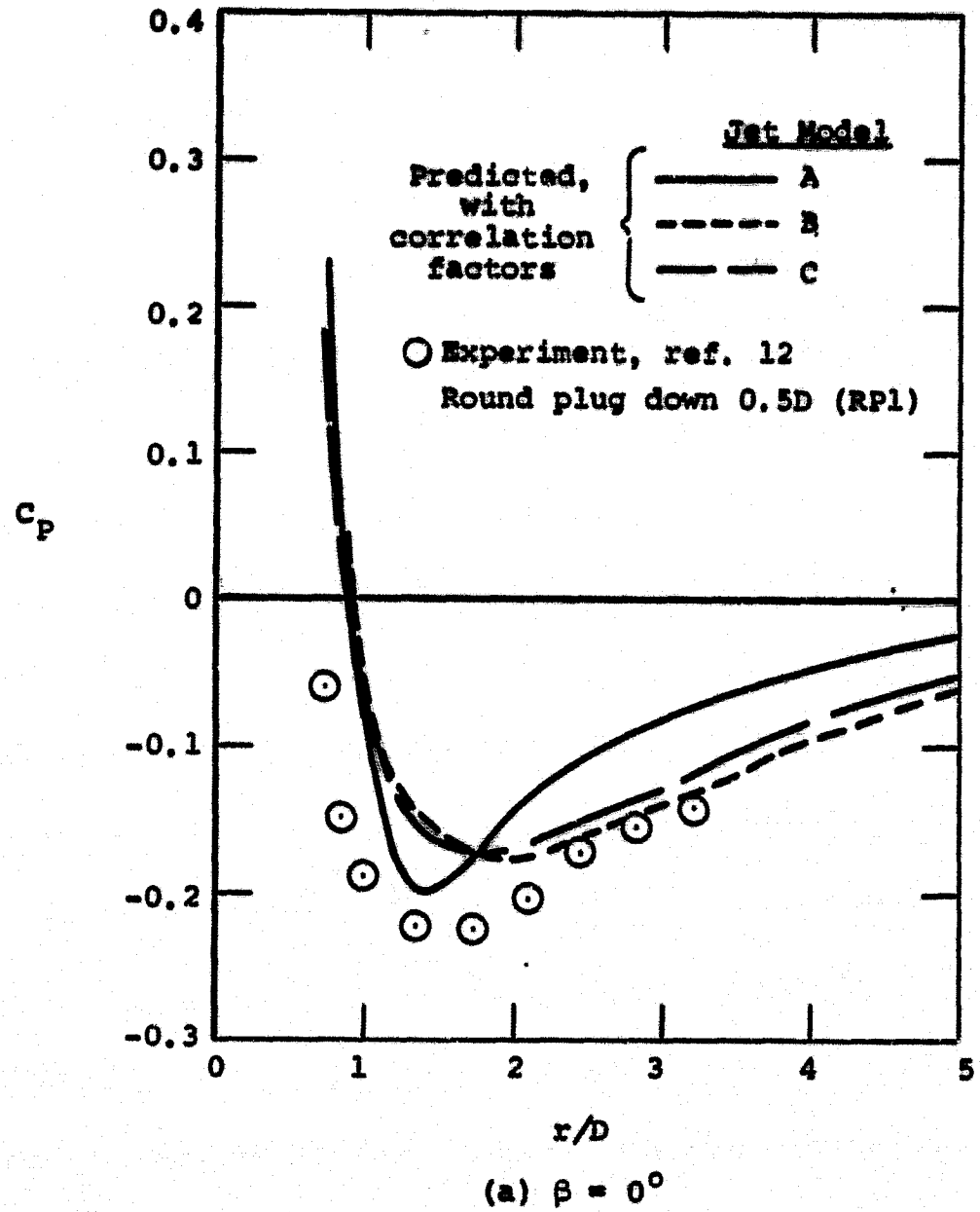

(a) $\beta = 0^\circ$

Figure 23.- Comparison of measured and predicted plate pressure distributions for the round plug down 0.5D (RP1) jet, R = 7.76.

C-2

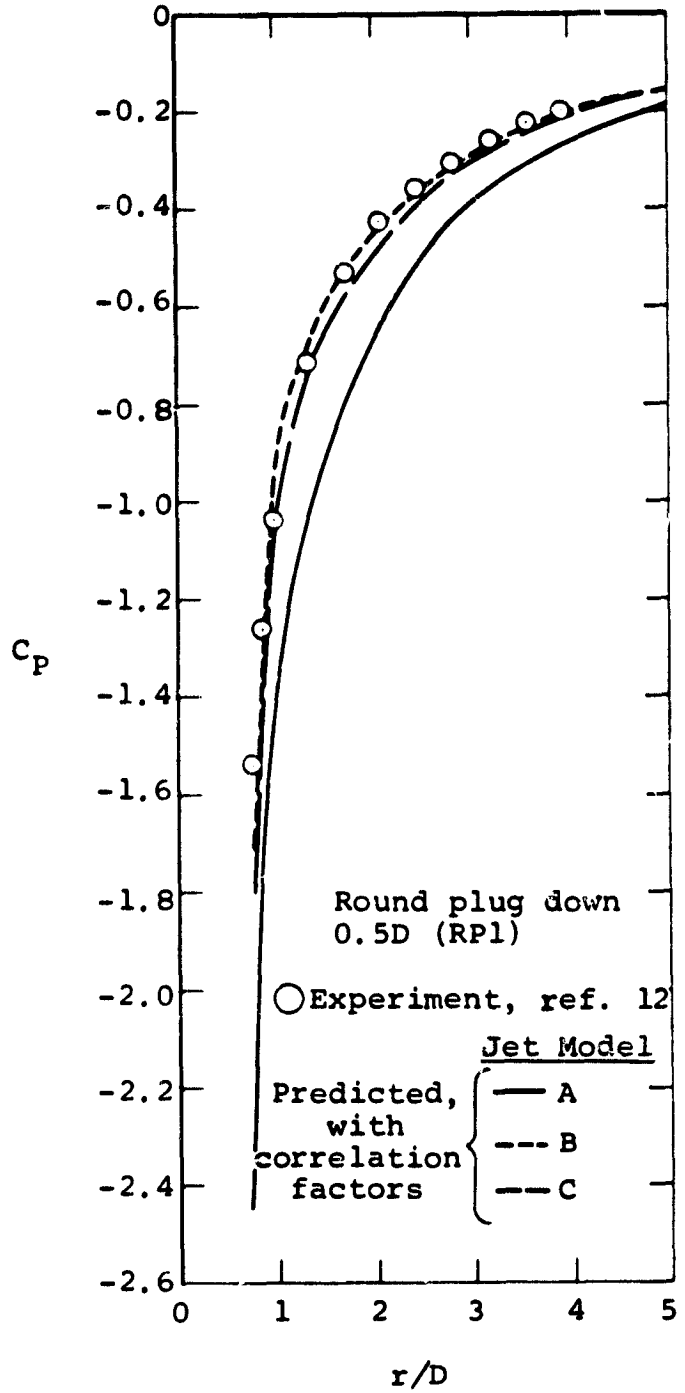

(b) $\beta = 60^\circ$

Figure 23.- Continued.

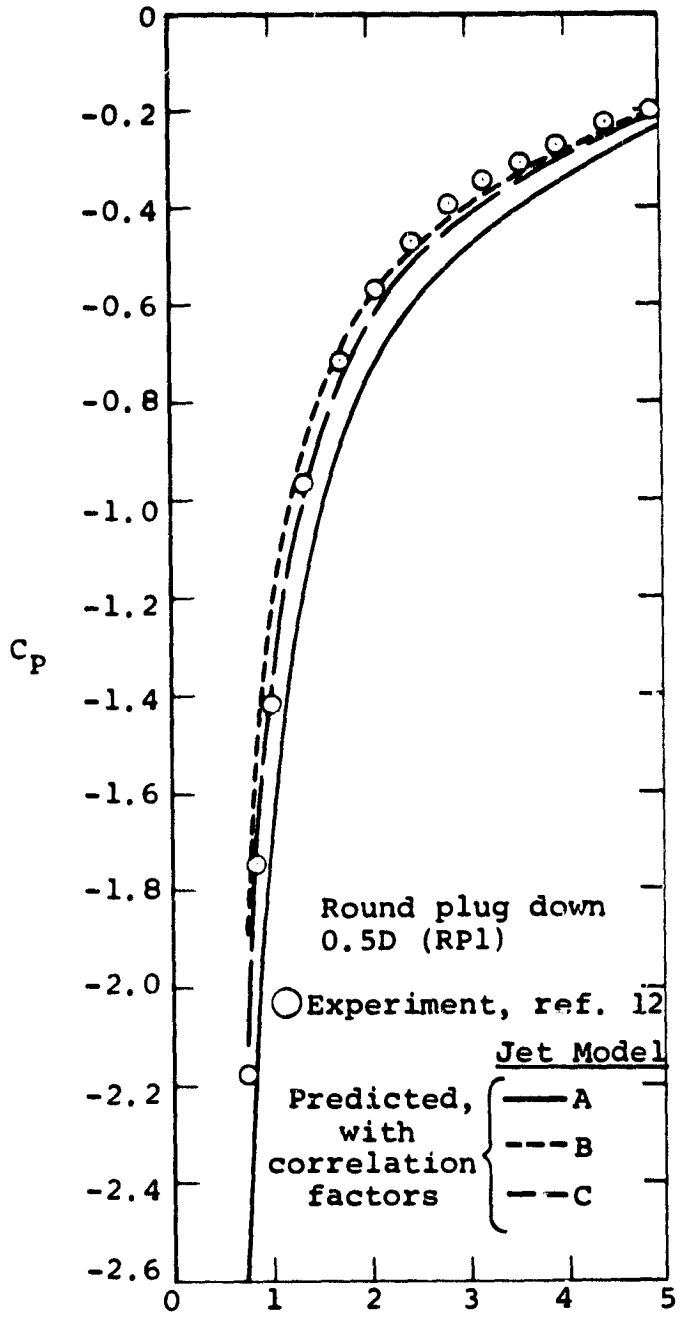

(c) $\beta = 90^\circ$

Figure 23.- Continued.

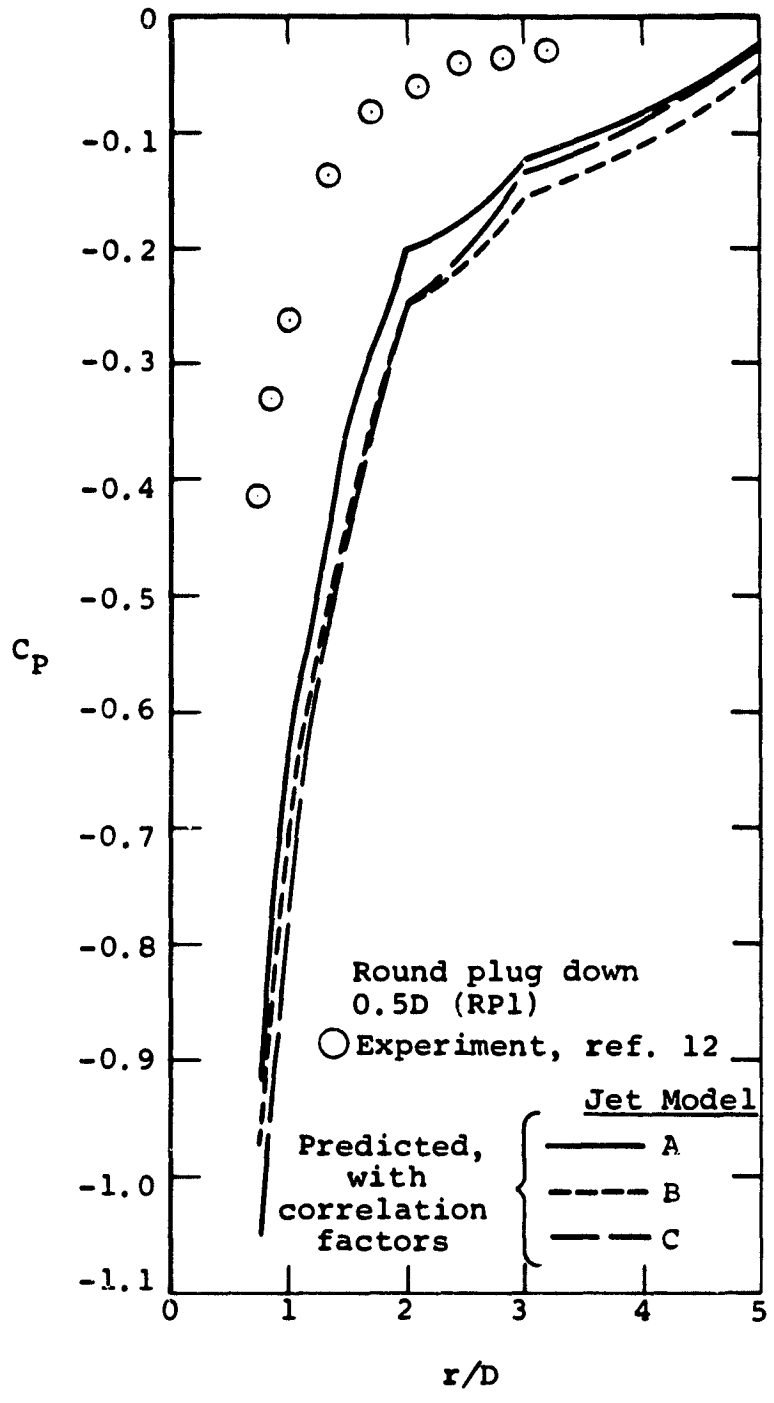

(d) $\beta = 180^{\circ}$

Figure 23.- Concluded.

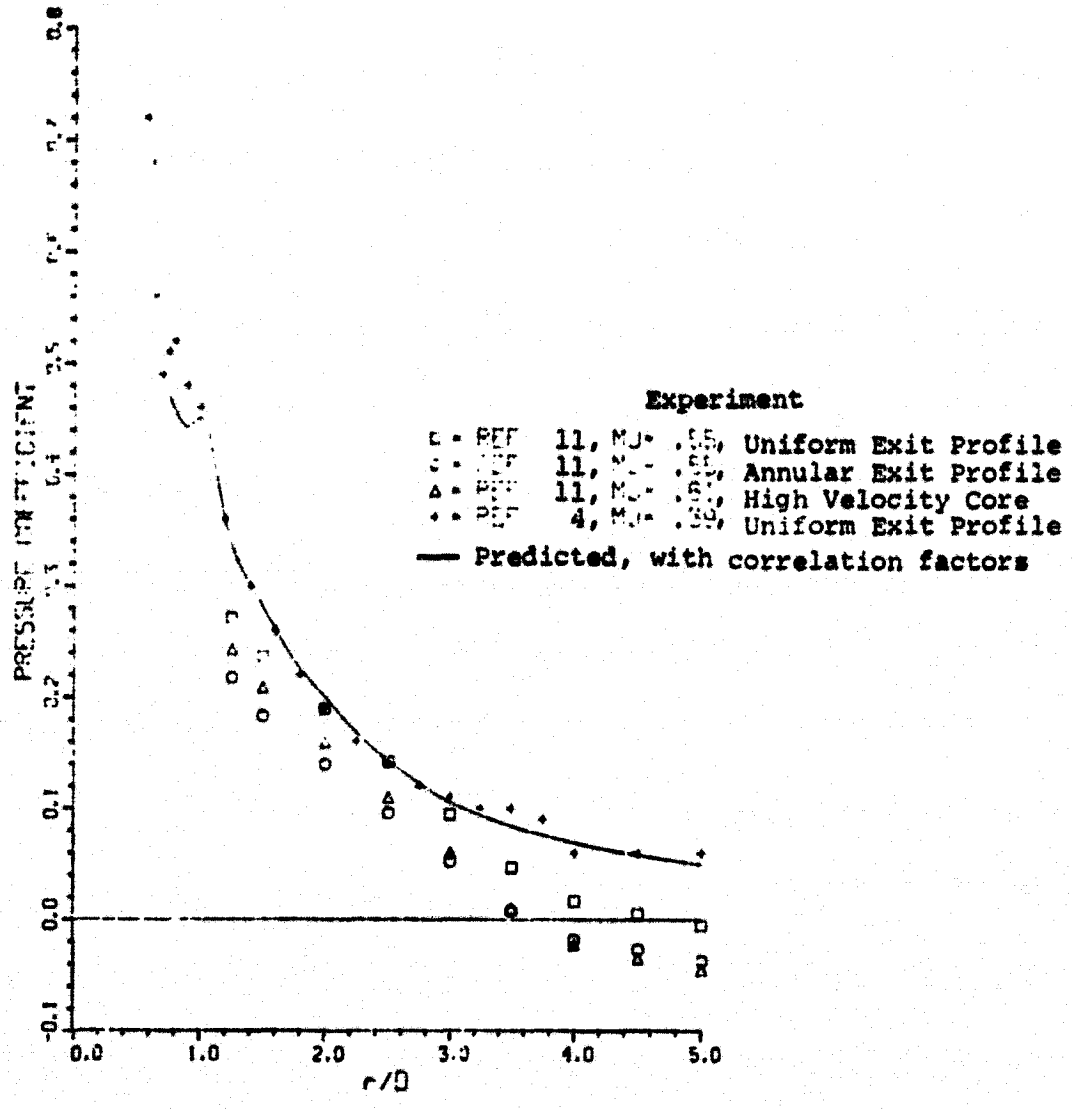

(a) $\beta = 0°$

Figure 24.- Comparison of predicted and measured plate pressure distributions showing effects of nonuniform exit profiles, R = 2.2.

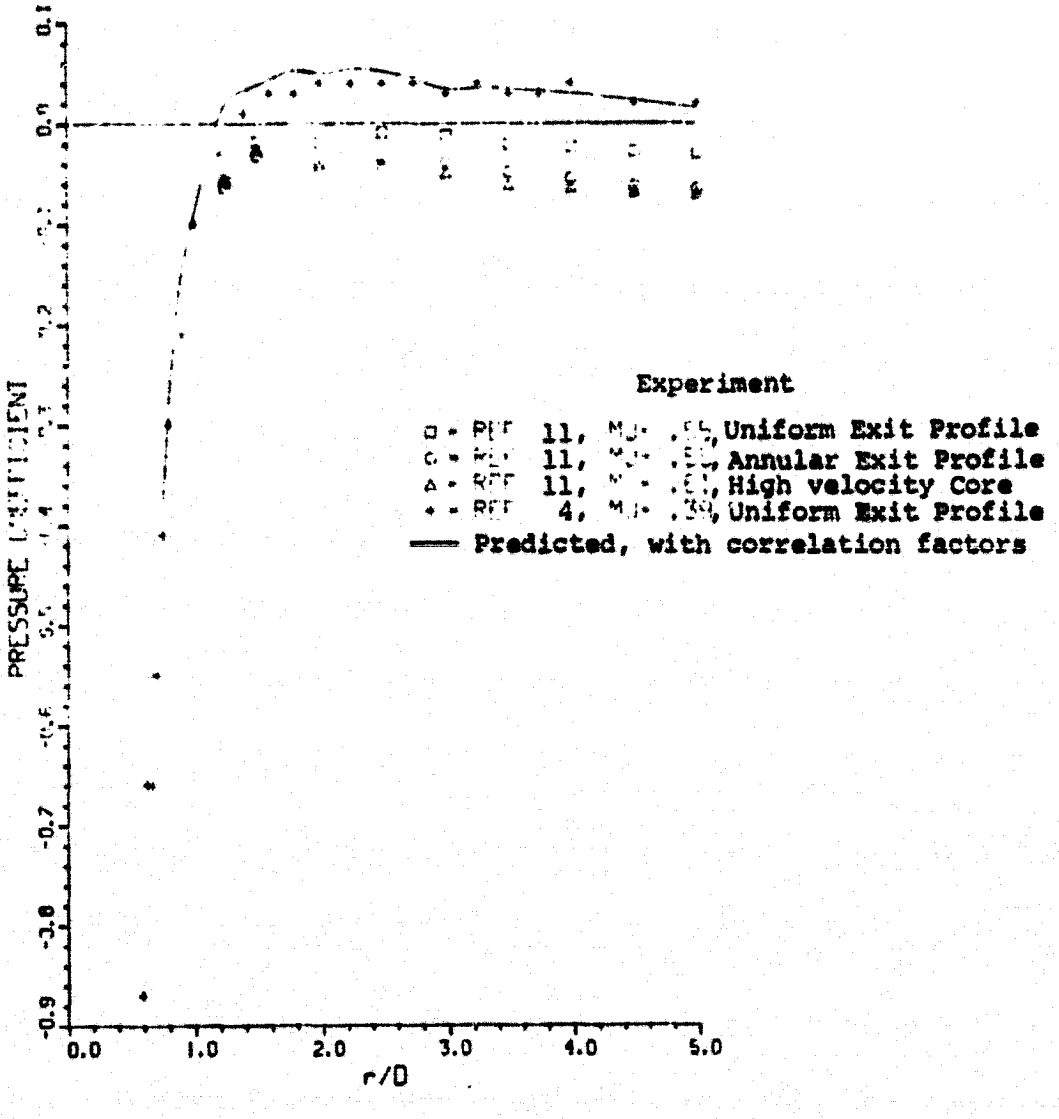

(b) $\beta = 60°$

Figure 24.- Continued.

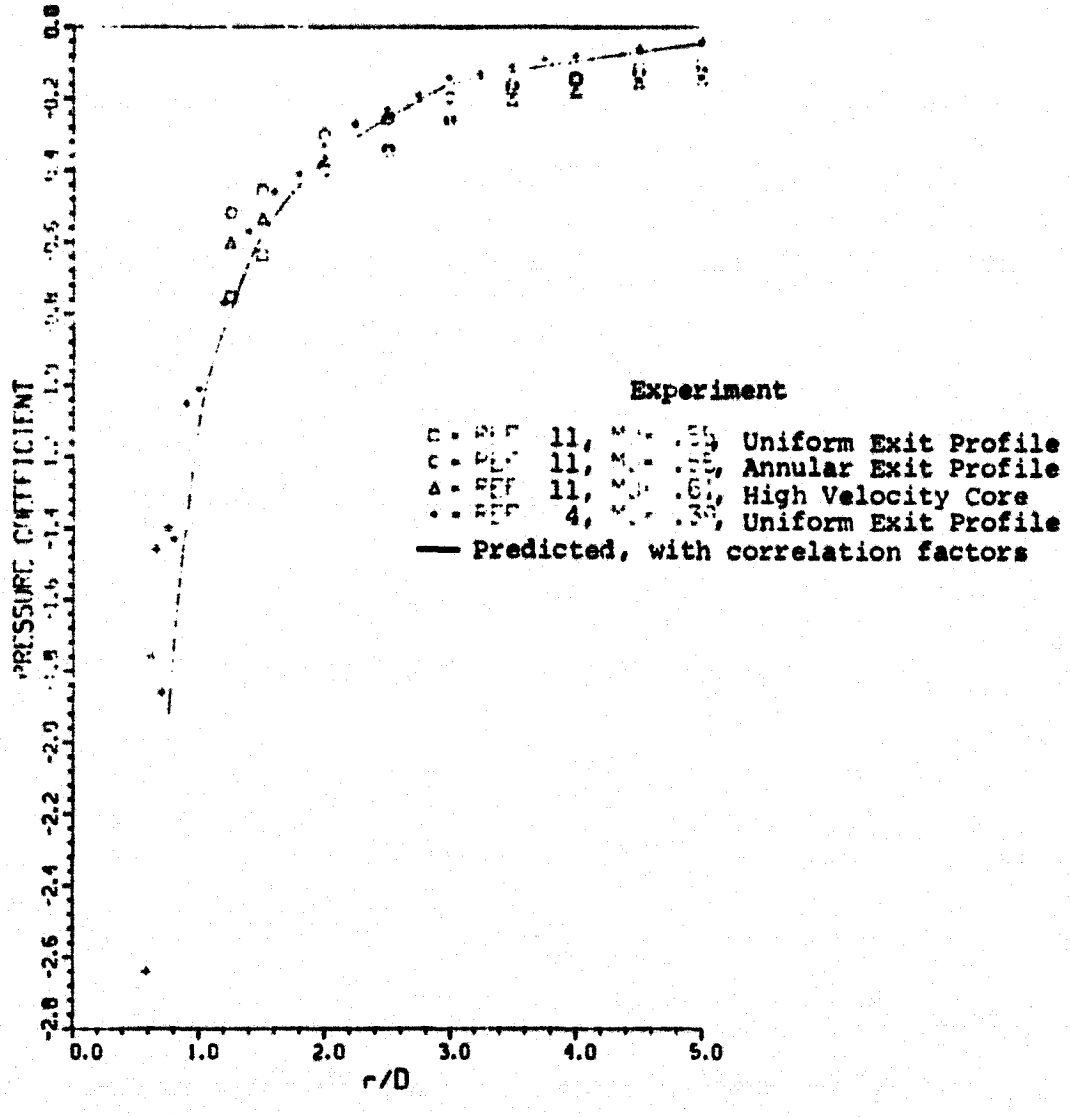

(c) $\beta = 120°$

Figure 24.- Continued.

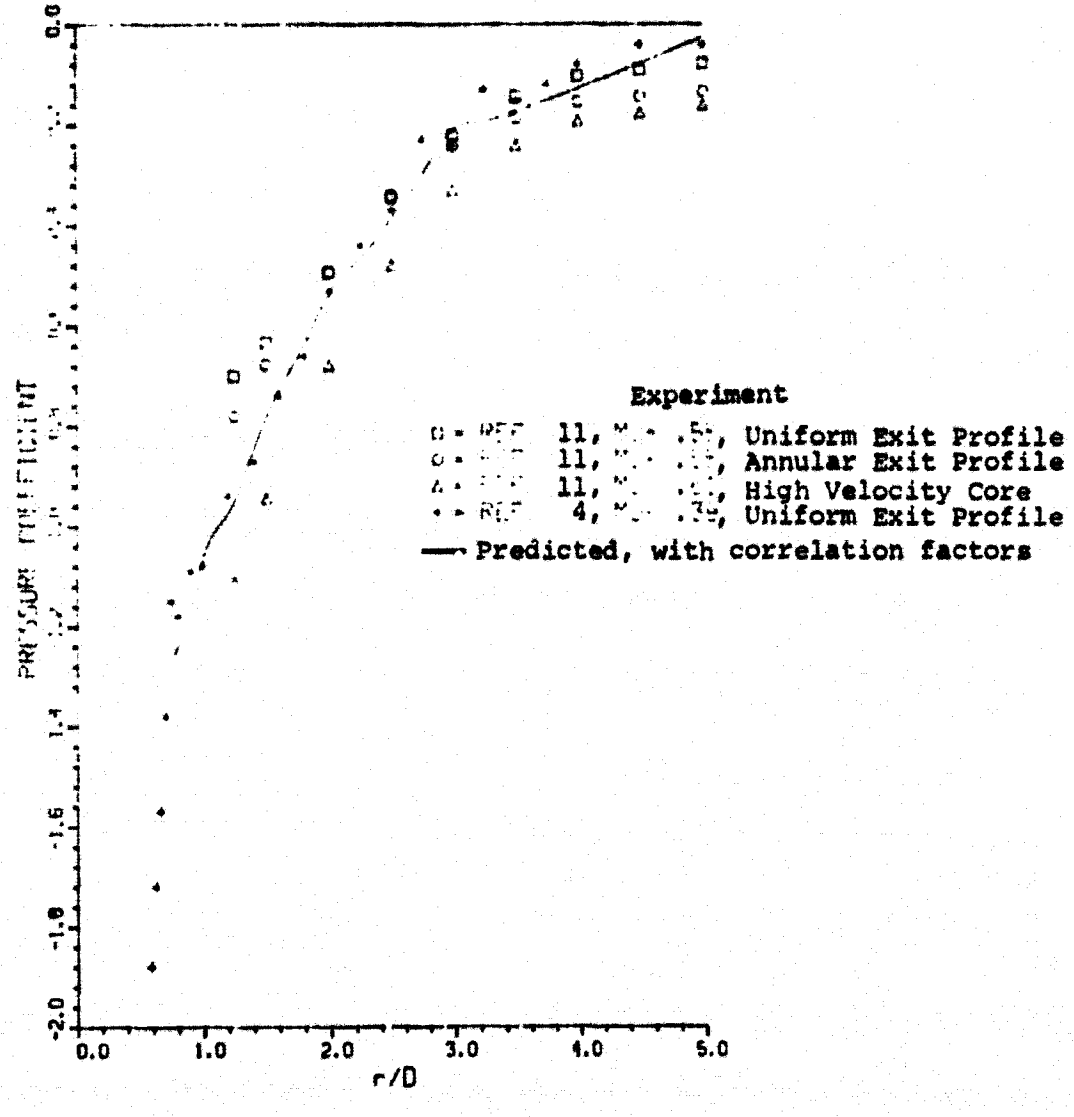

(d) $\beta = 180°$

Figure 24.- Concluded.

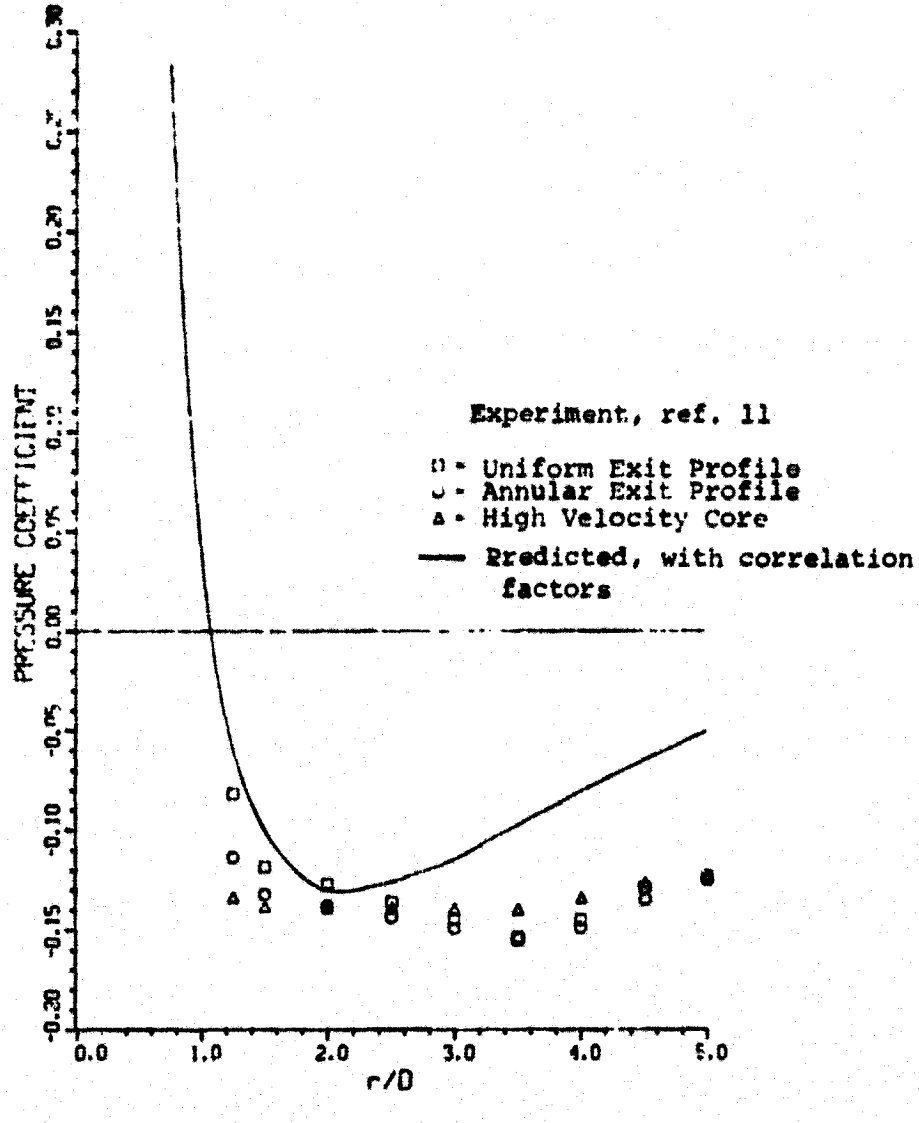

(a) $\beta = 0^\circ$

Figure 25.- Comparison of predicted and measured plate pressure distributions showing effects of nonuniform exit profile, R = 8.

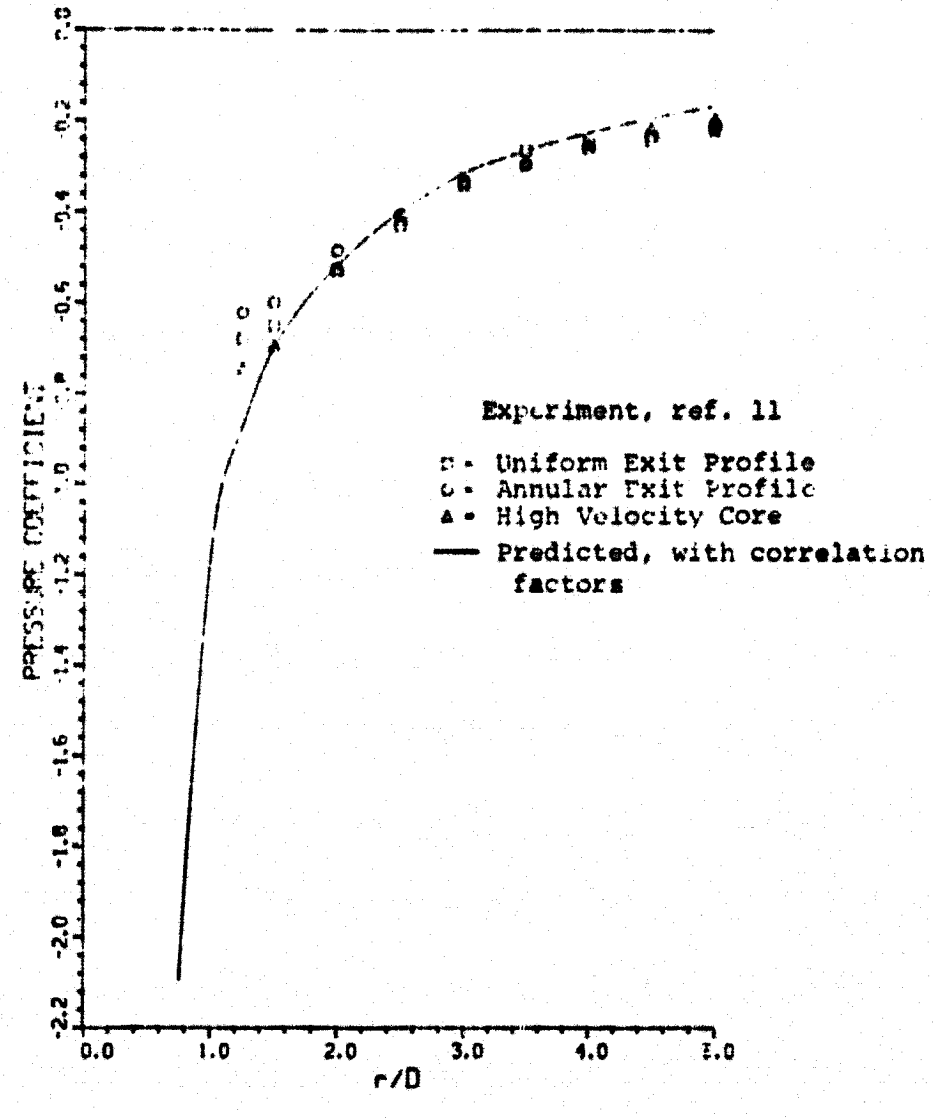

(b) $\beta = 60^{\circ}$

Figure 25.- Continued.

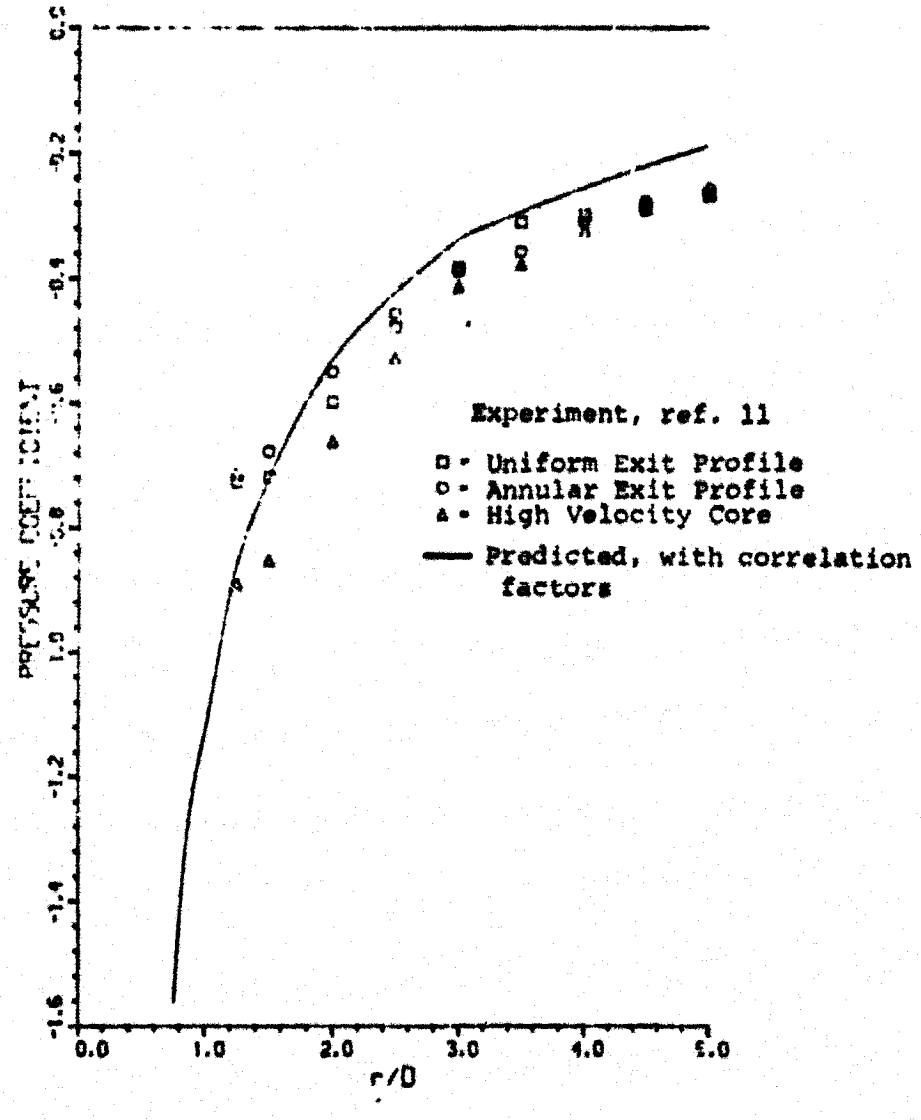

(c) $\beta = 120^{\circ}$

Figure 25.- Continued.

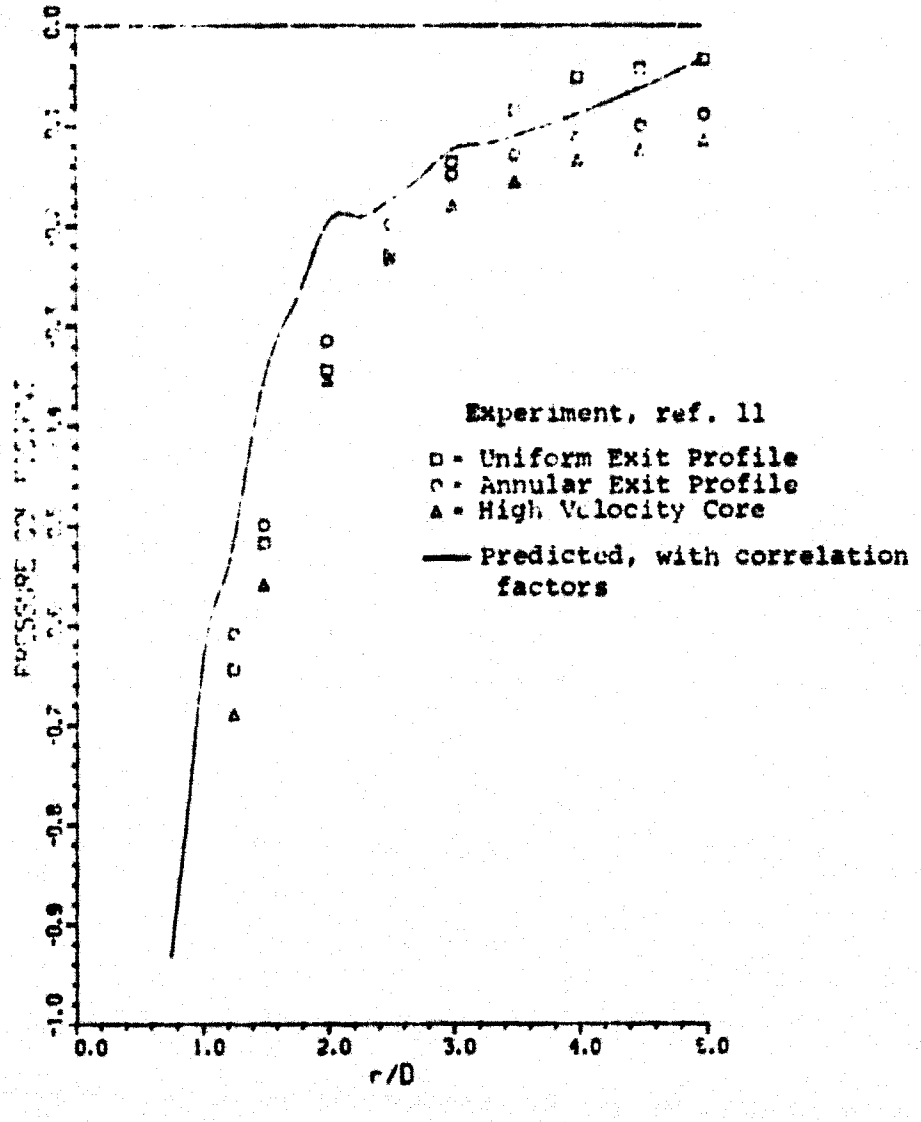

(d) $\beta = 180^{\circ}$

Figure 25.- Concluded.

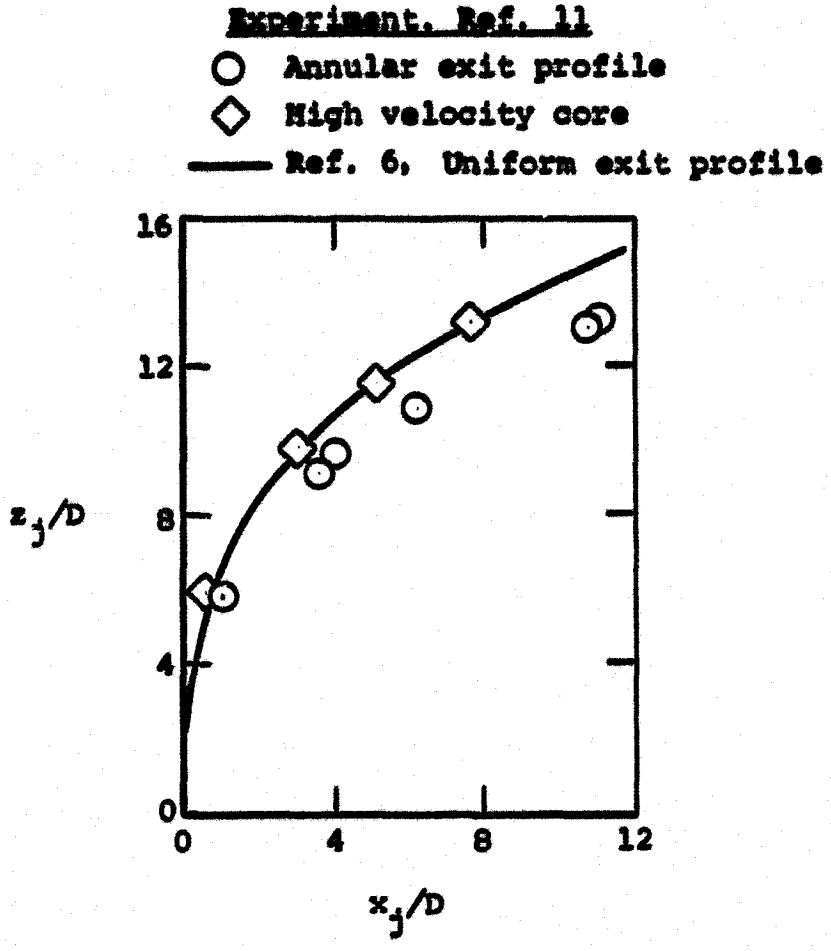

Figure 26.- Effect of jet exit profile on measured jet centerline trajectories, R = 8.

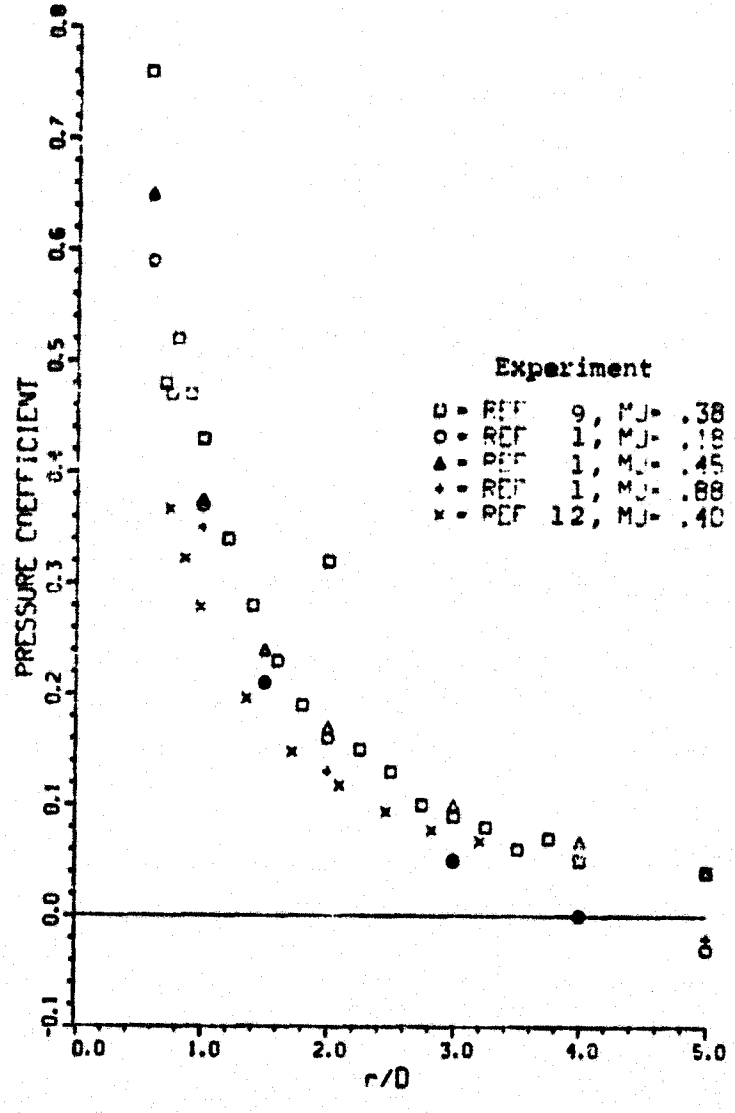

(a) $\beta = 0^{\circ}$

Figure 27.- Effect of jet exit and freestream Mach number combination on measured plate pressure distributions, R = 2.5.

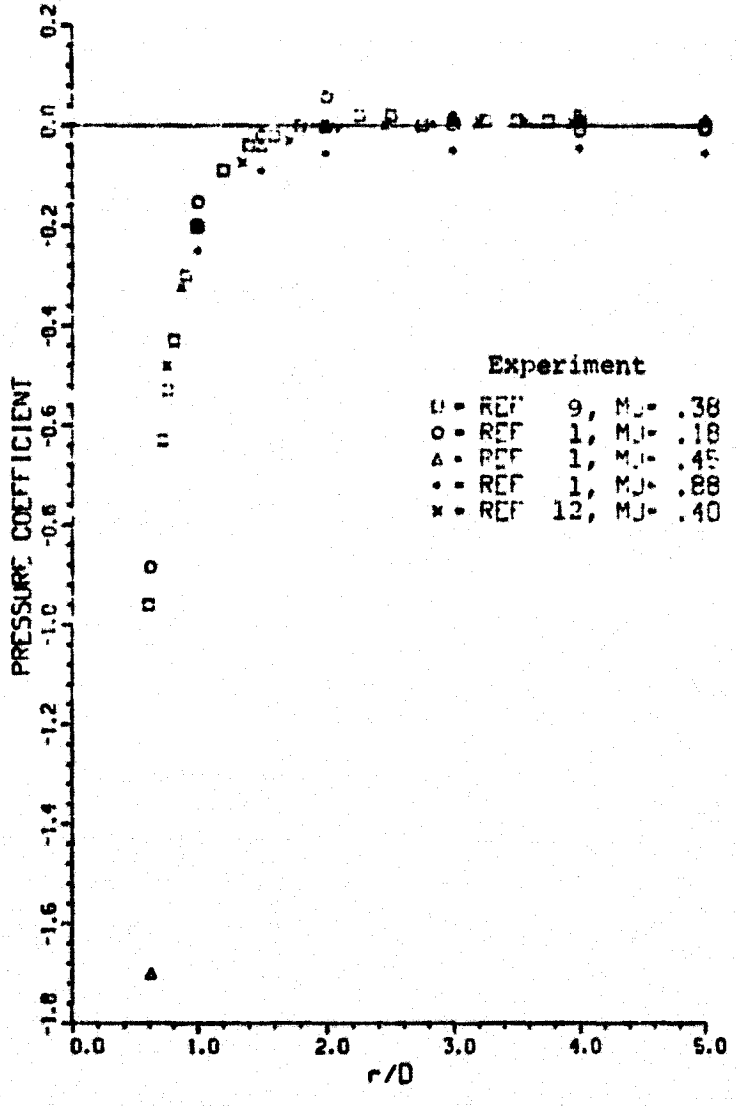

(b) $\beta = 60^{\circ}$

Figure 27.- Continued.

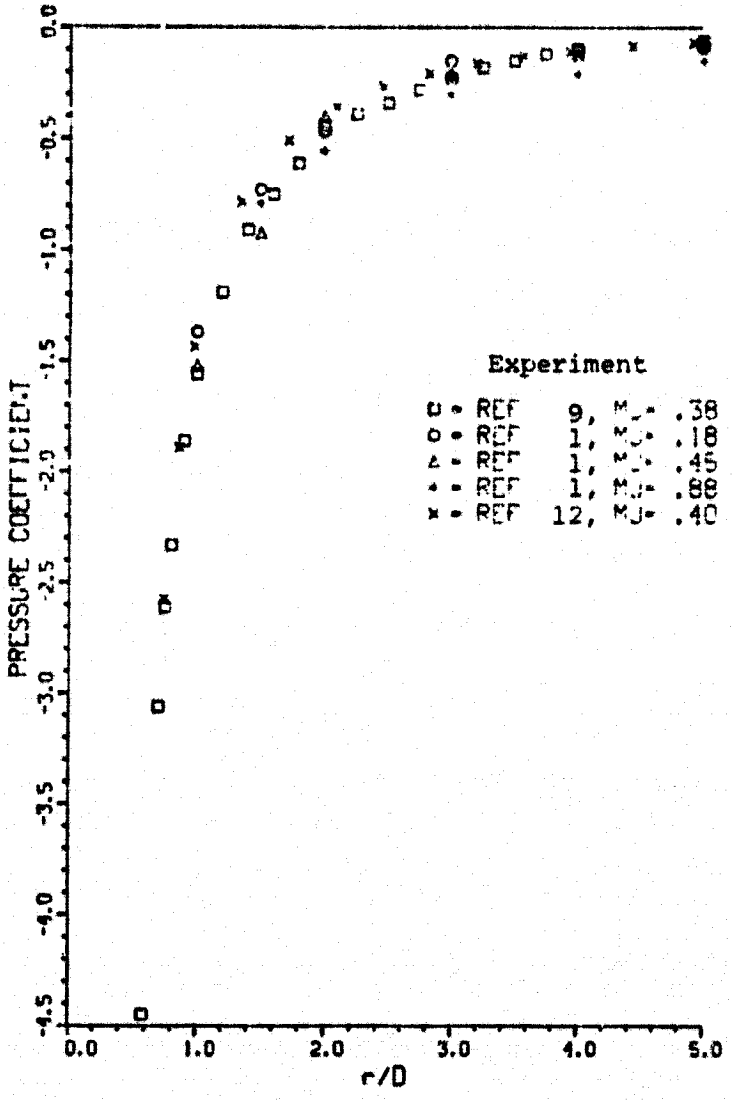

(c) $\beta = 120^{\circ}$

Figure 27.- Continued.

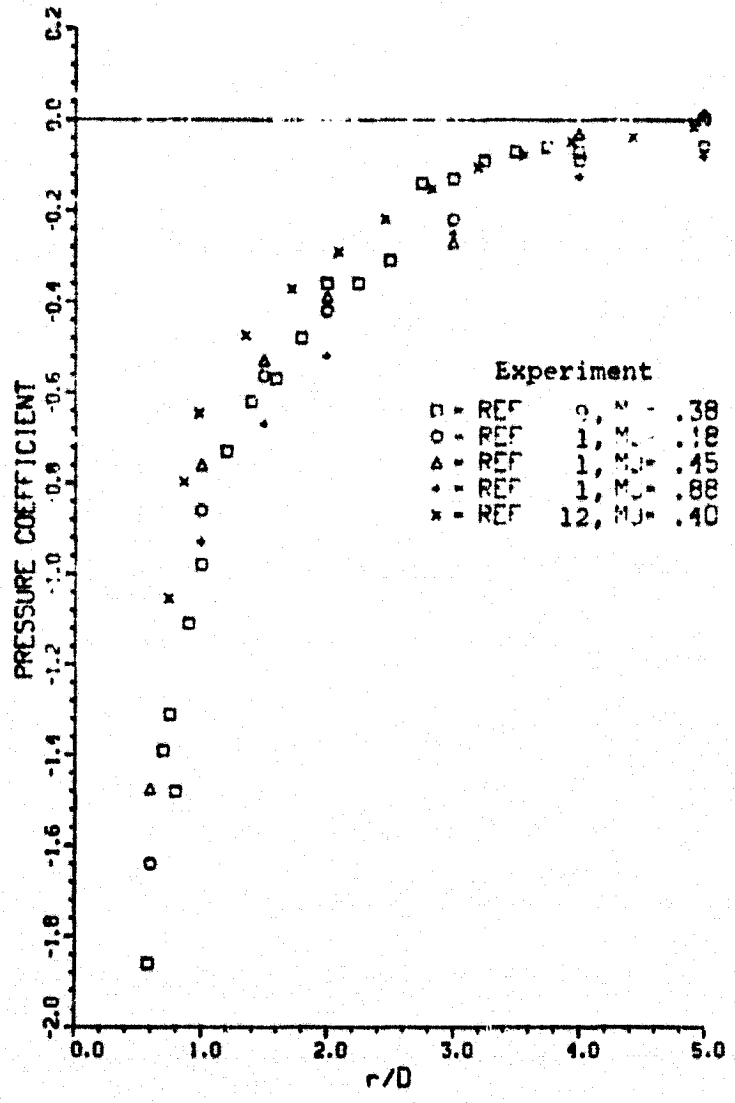

(d) $\beta = 180^{\circ}$

Figure 27.- Concluded.

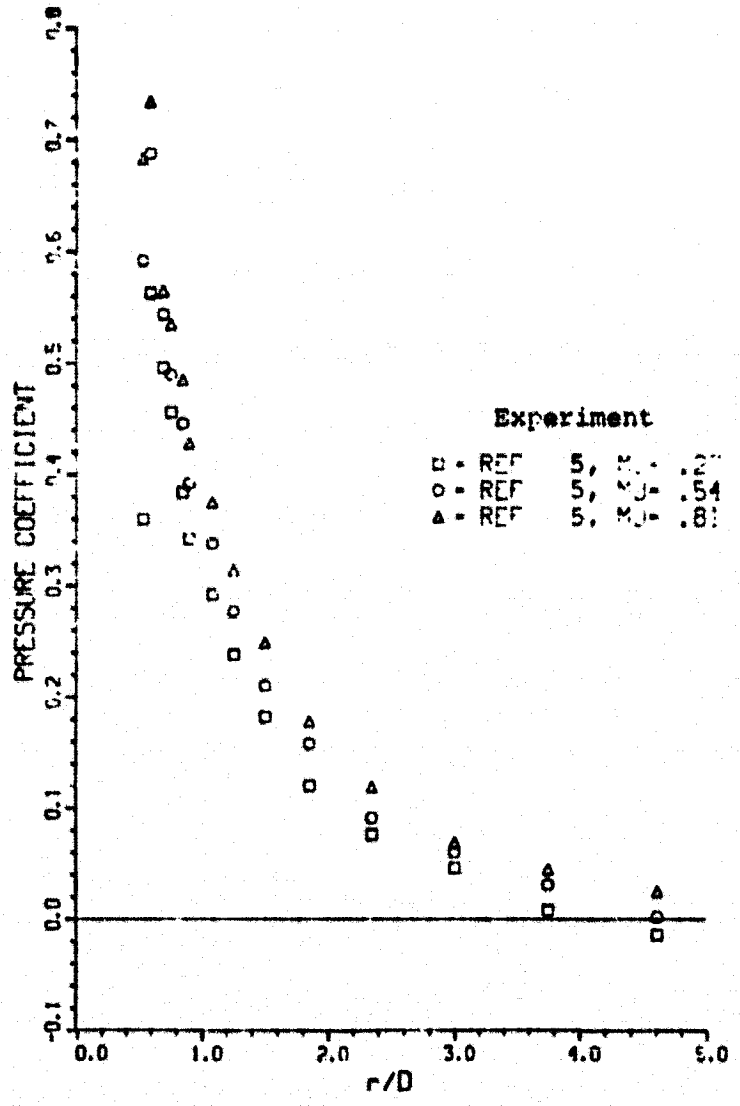

(a) $\beta = 0^{\circ}$

Figure 28.- Effect of jet exit and free-stream Mach number combination on measured plate pressure distributions, R = 3.0.

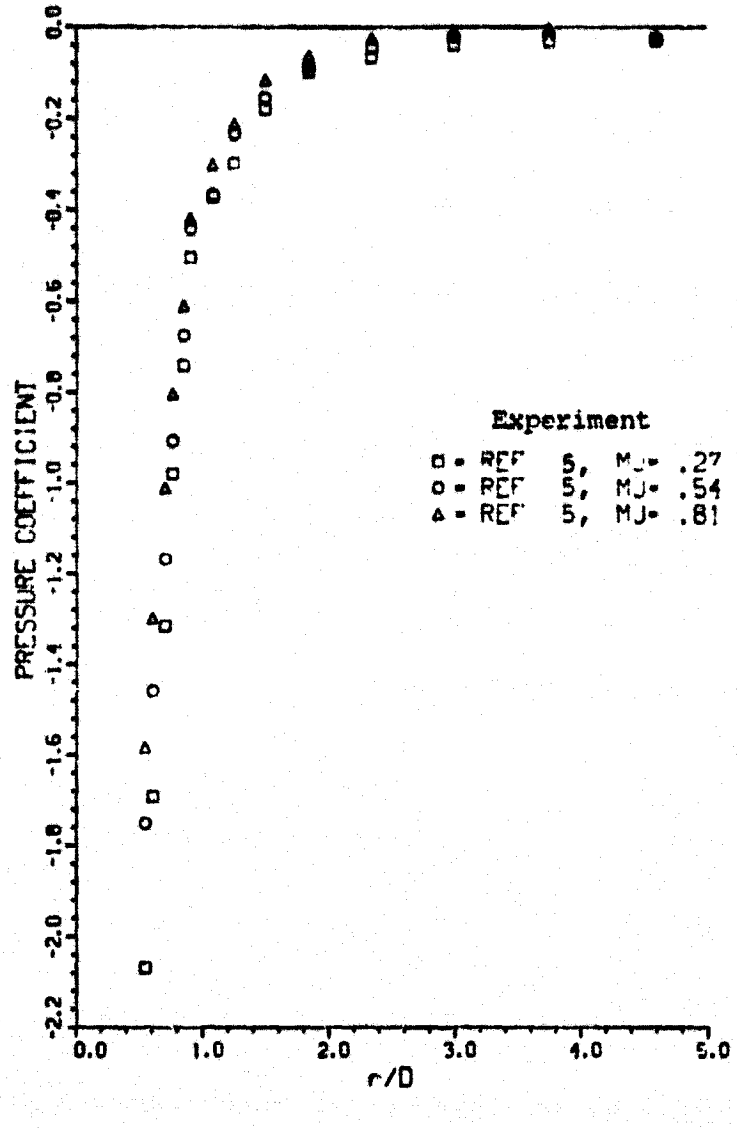

(b) $\beta = 60^{\circ}$

Figure 28.- Continued.

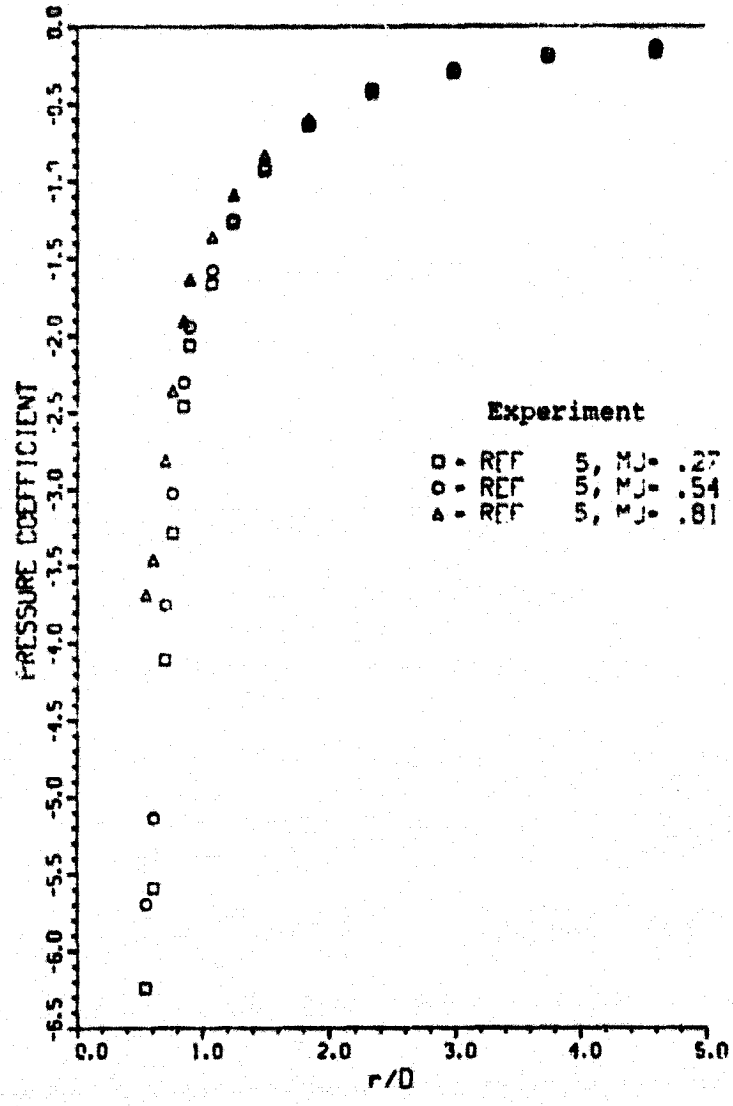

(c) $\beta = 120^{\circ}$

Figure 28.- Continued.

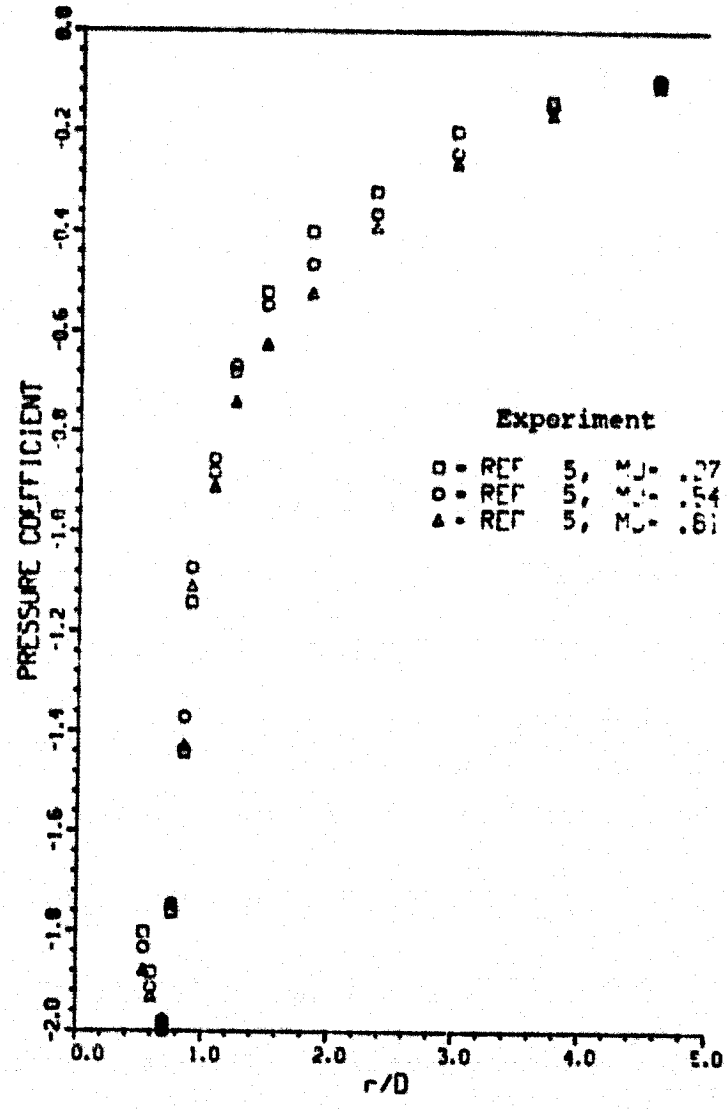

(d) $\beta = 180^{\circ}$

Figure 28.- Concluded.

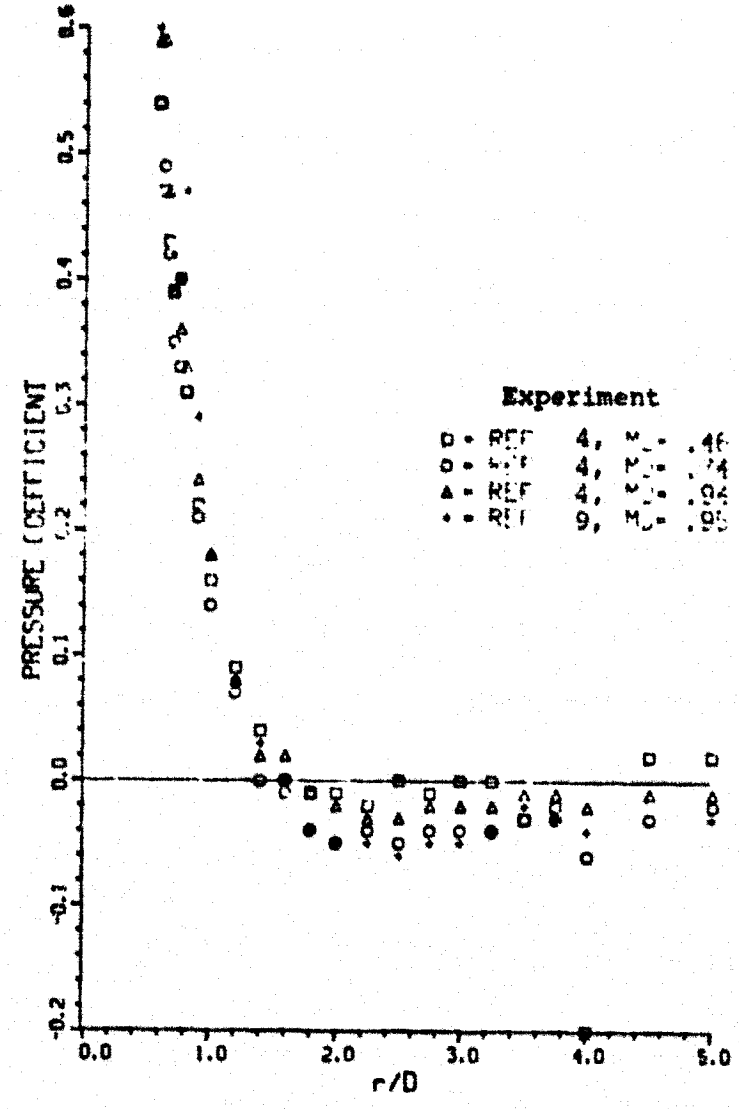

(a) $\beta = 0^\circ$

Figure 29.- Effect of jet exit and free-stream Mach number combination on measured plate pressure distributions, R = 6.0.

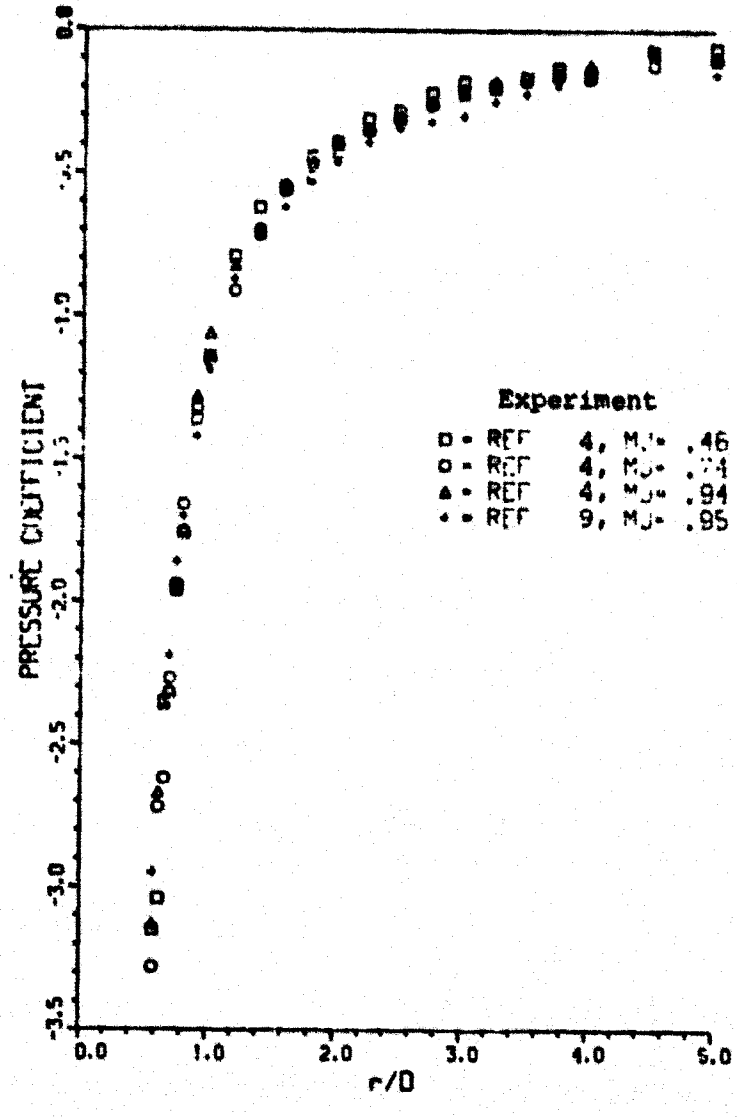

(b) $\beta = 60^{\circ}$

Figure 29.- Continued.

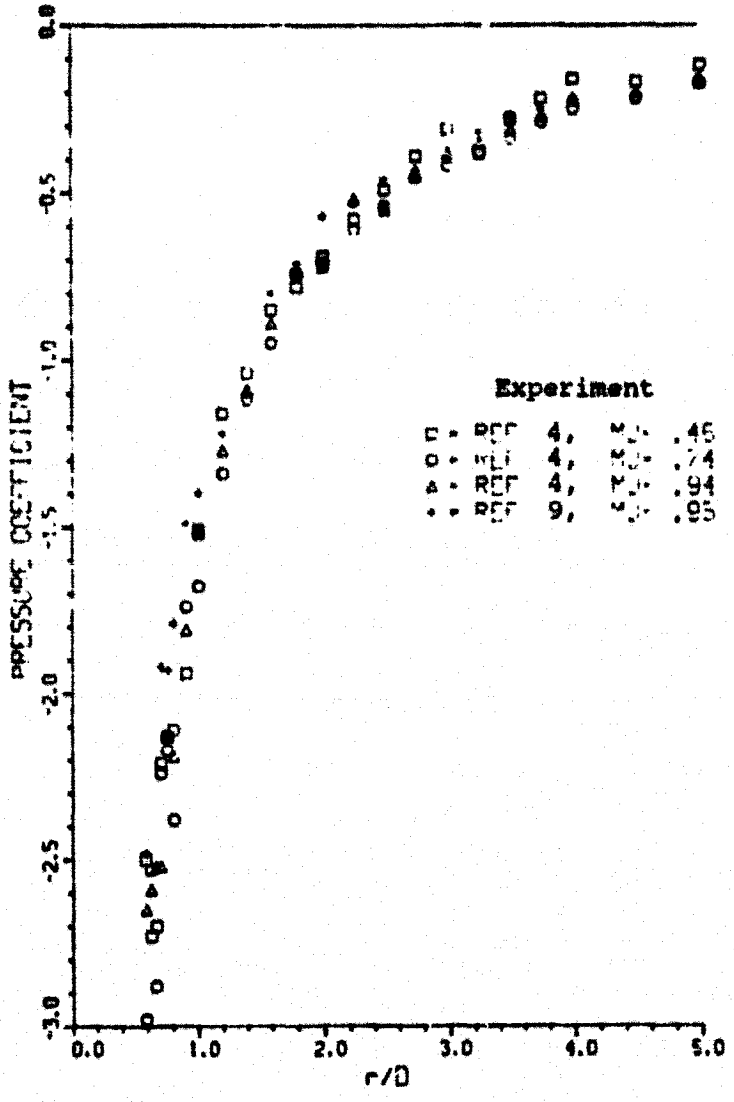

(c) $\beta = 120^{\circ}$

Figure 29.- Continued.

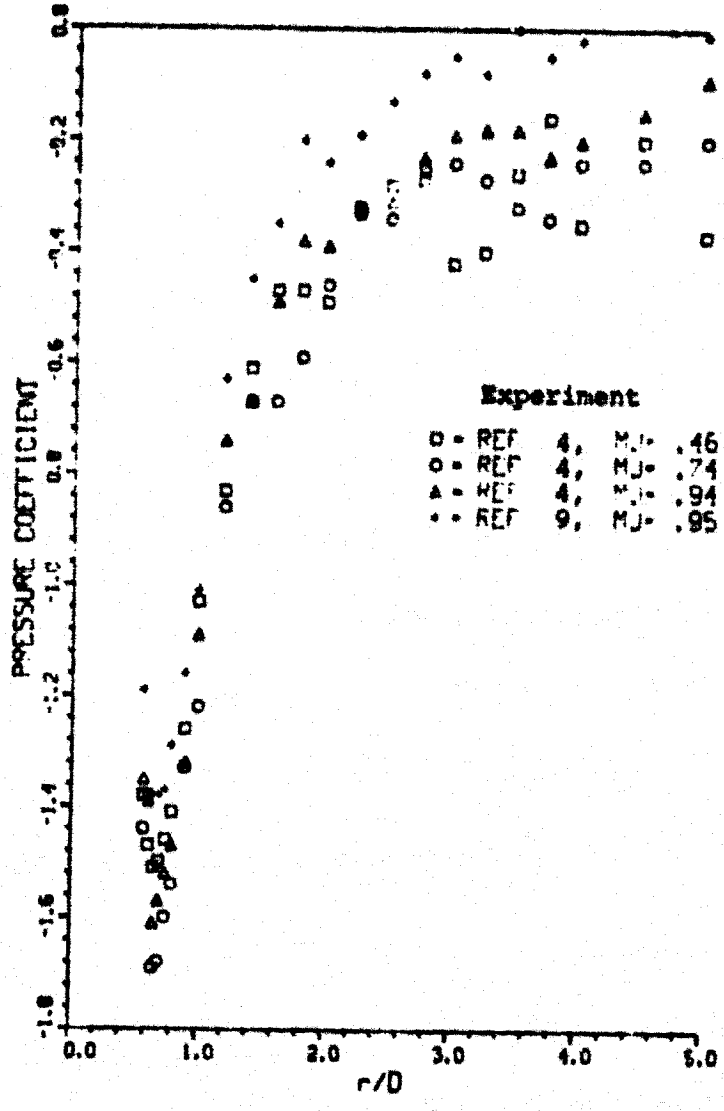

(d) $\beta = 180^{\circ}$

Figure 29.- Concluded.

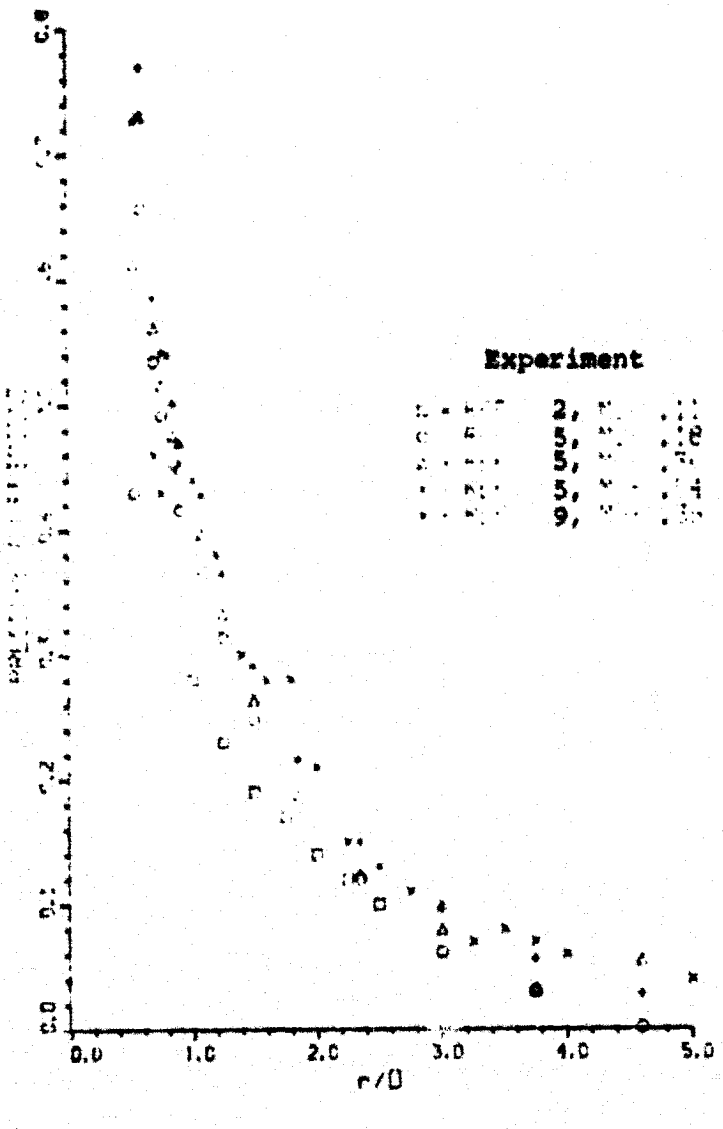

(a) $\beta = 0^{\circ}$

Figure 30.- Effect of jet exit and free-stream Mach number combination on measured plate pressure distributions, R = 2.0.

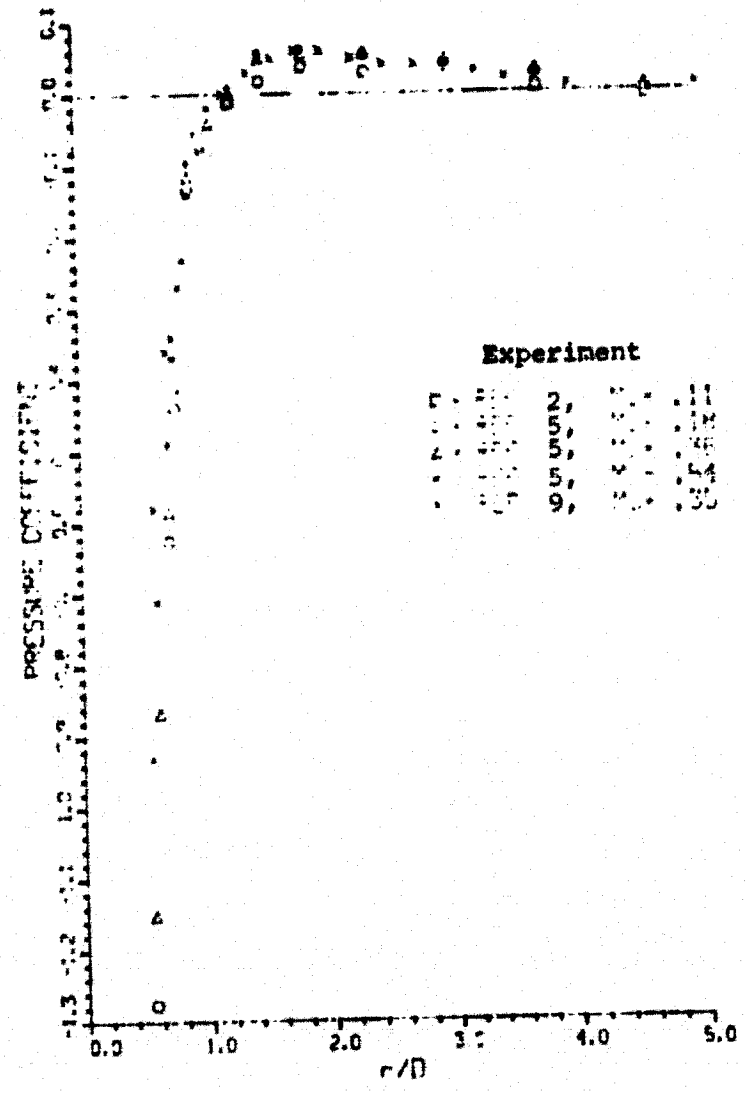

(b) $\beta = 60^{\circ}$

Figure 30.- Concluded.

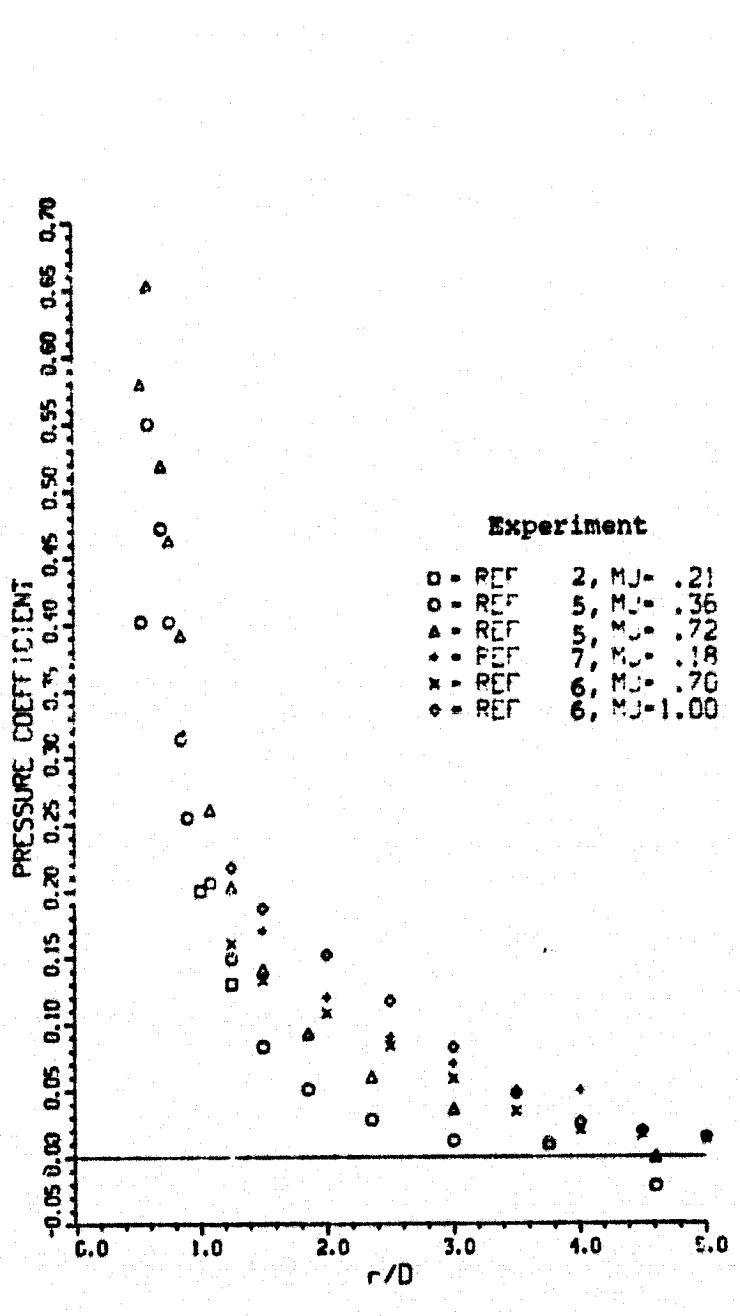

(a) $\beta = 0^{\circ}$

Figure 31.- Effect of jet exit and free-stream Mach number combination on measured plate pressure distributions, R = 4.0.

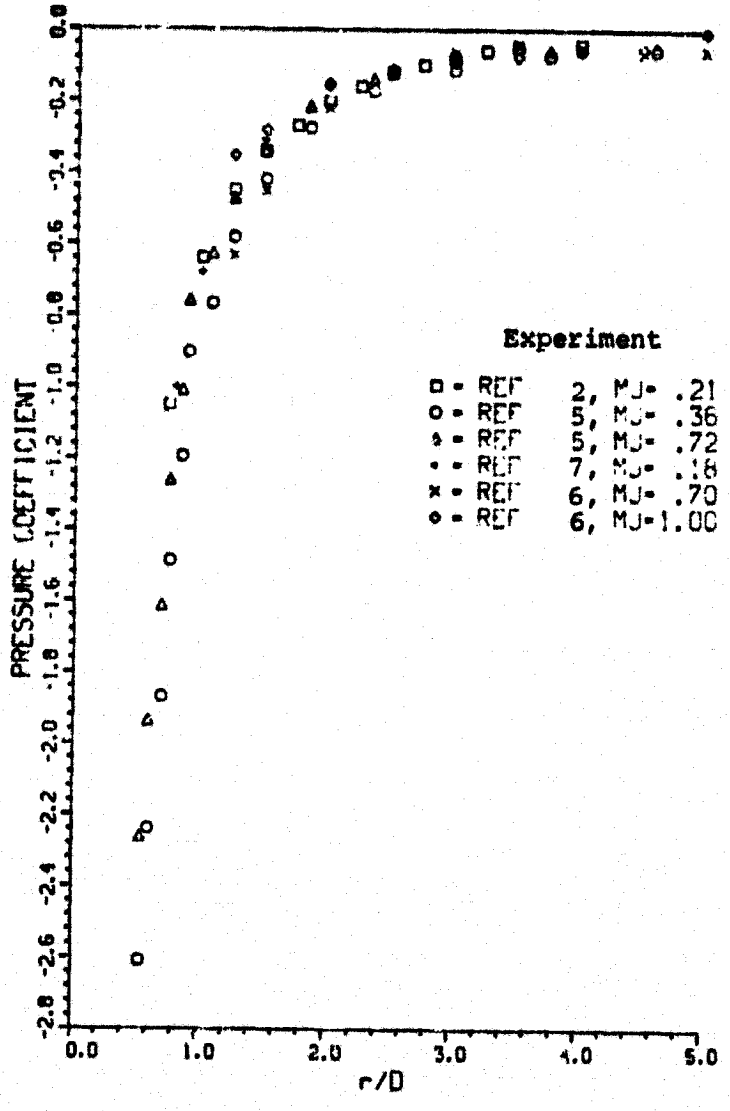

(b) $\beta = 60^{\circ}$

Figure 31.- Concluded.

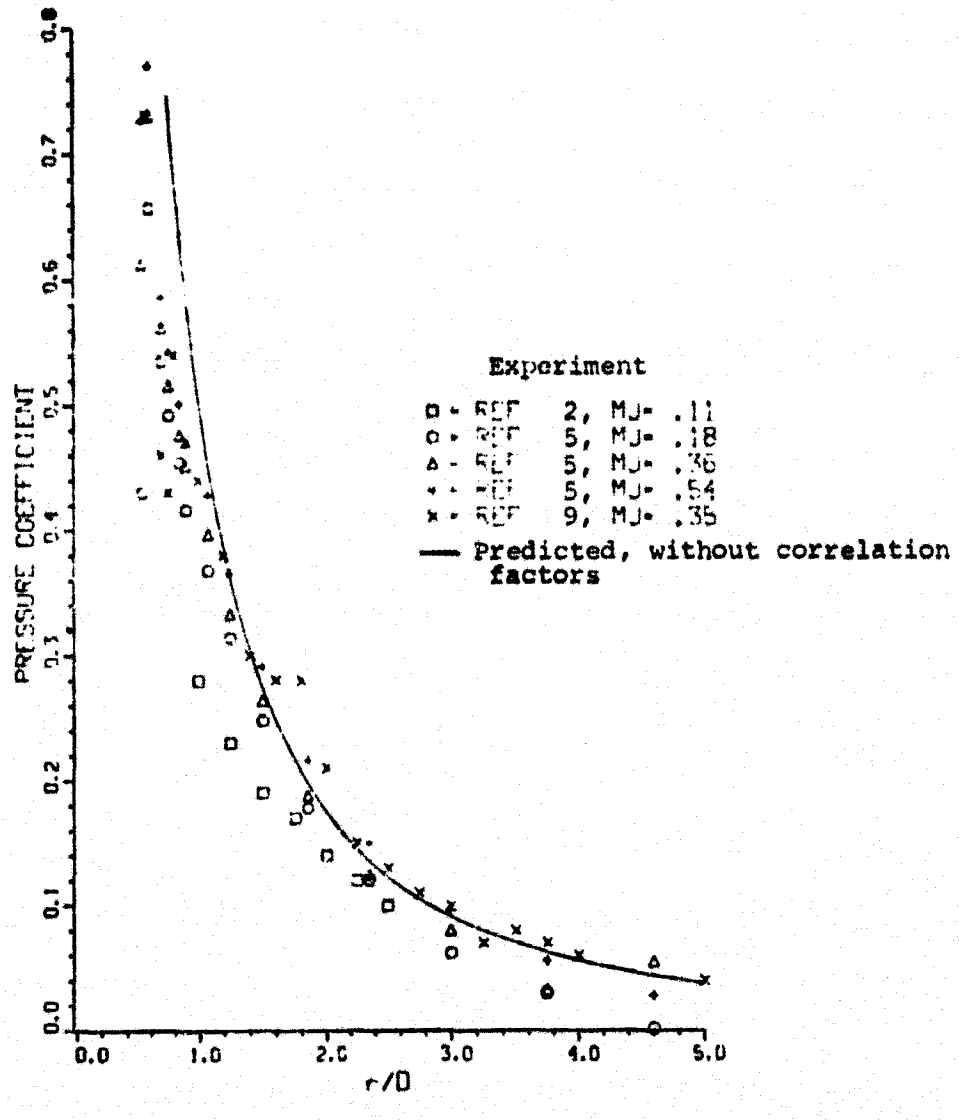

(a) $\beta = 0^{\circ}$

Figure 32.- Comparison of predicted and measured plate pressure distributions, R = 2.0.

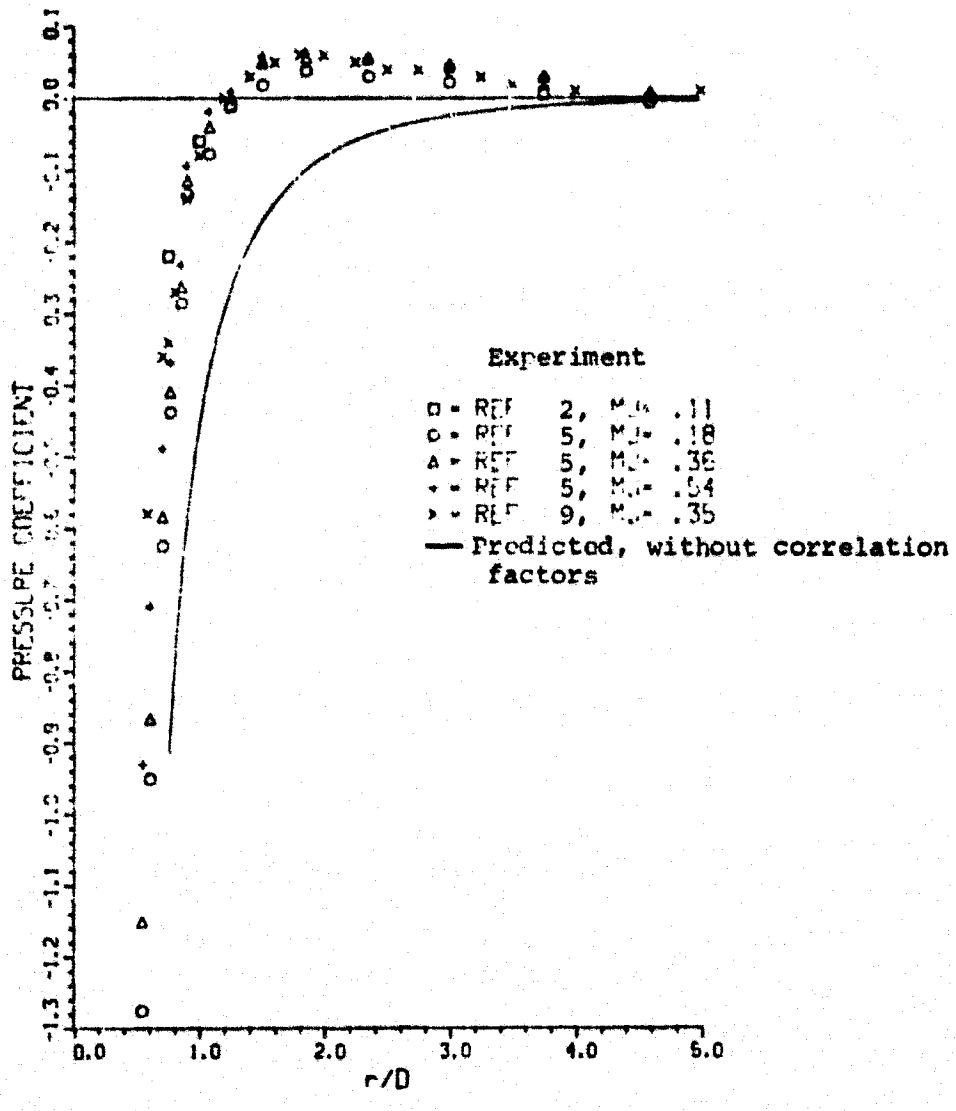

(b) $\beta = 60^{\circ}$

Figure 32.- Concluded.

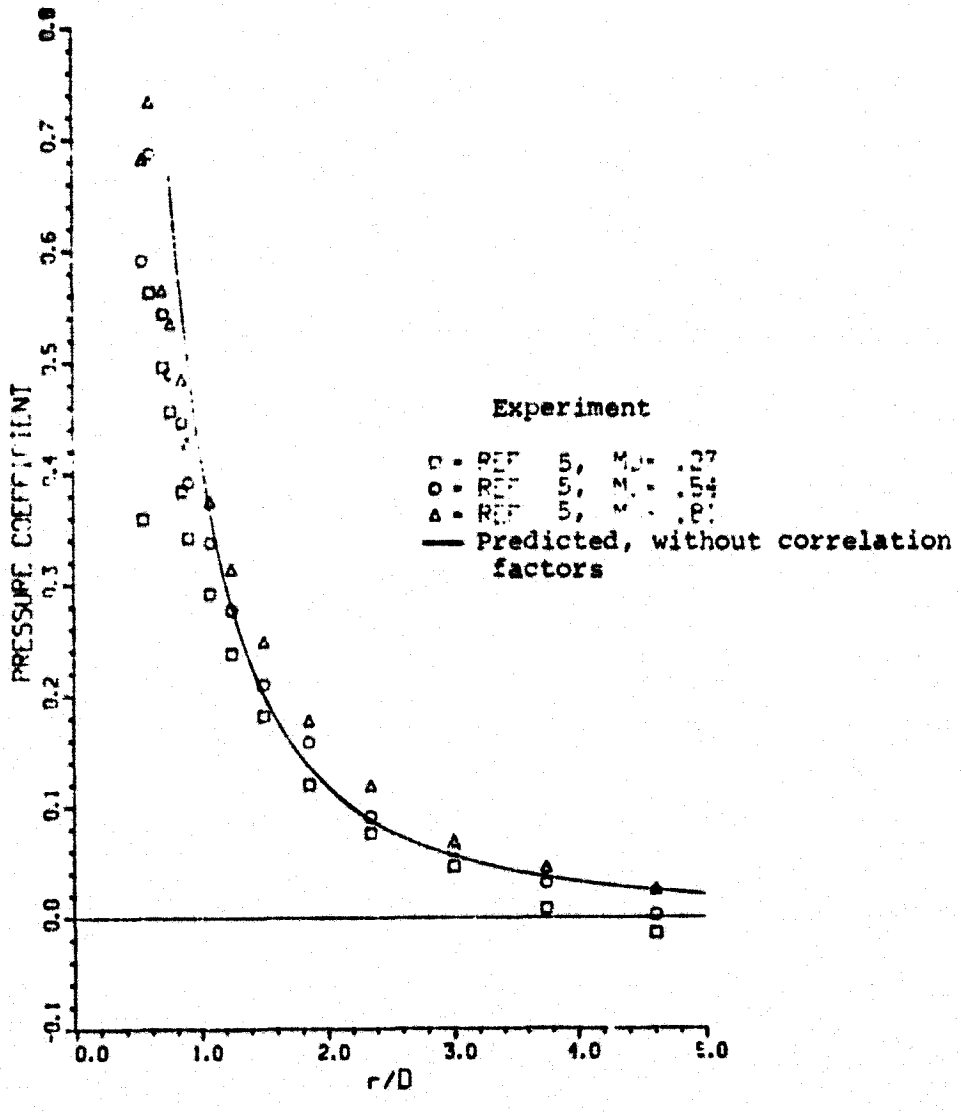

(a) $\beta = 0^{\circ}$

Figure 33.- Comparison of predicted and measured plate pressure distributions, R = 3.0.

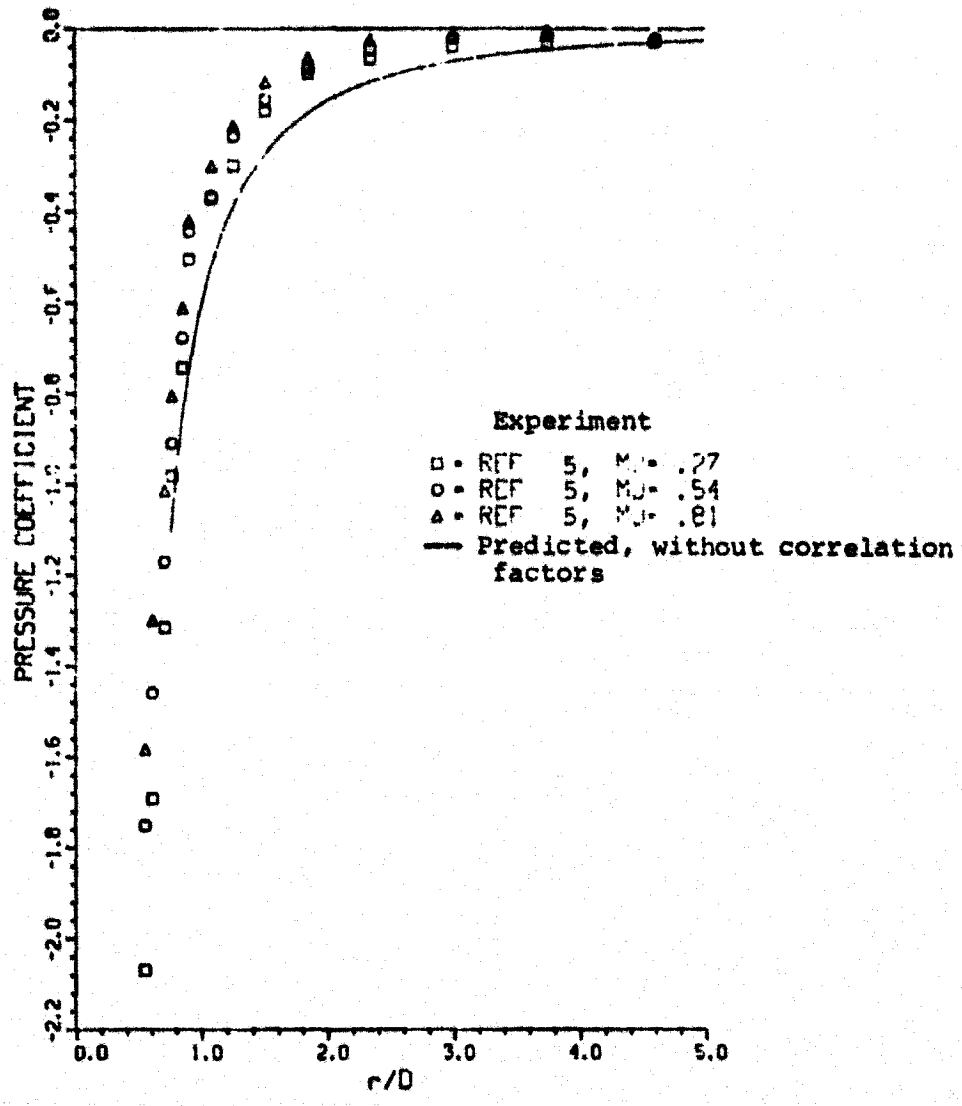

(b) $\beta = 60^{\circ}$

Figure 33.- Concluded.

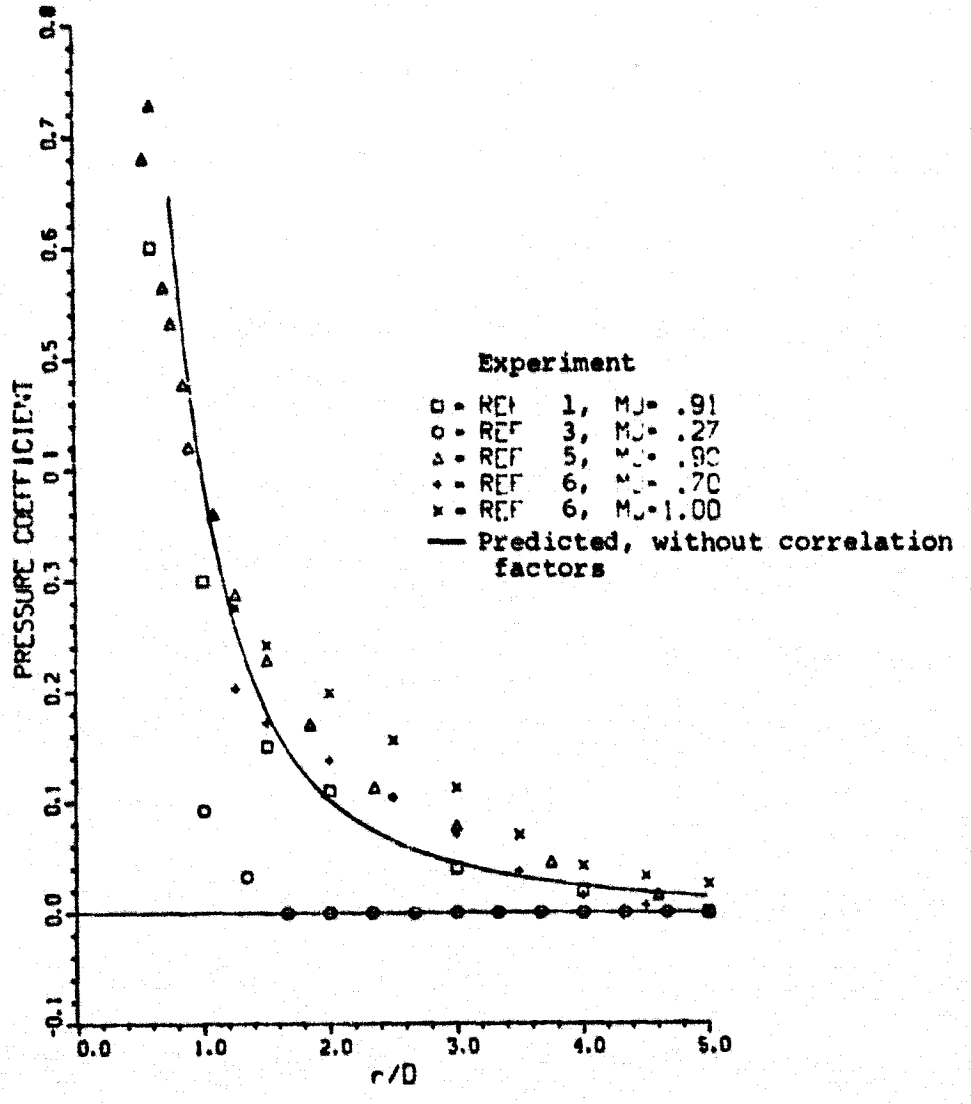

(a) $\beta = 0^{\circ}$

Figure 34.- Comparison of predicted and measured plate pressure distributions, R = 3.33.

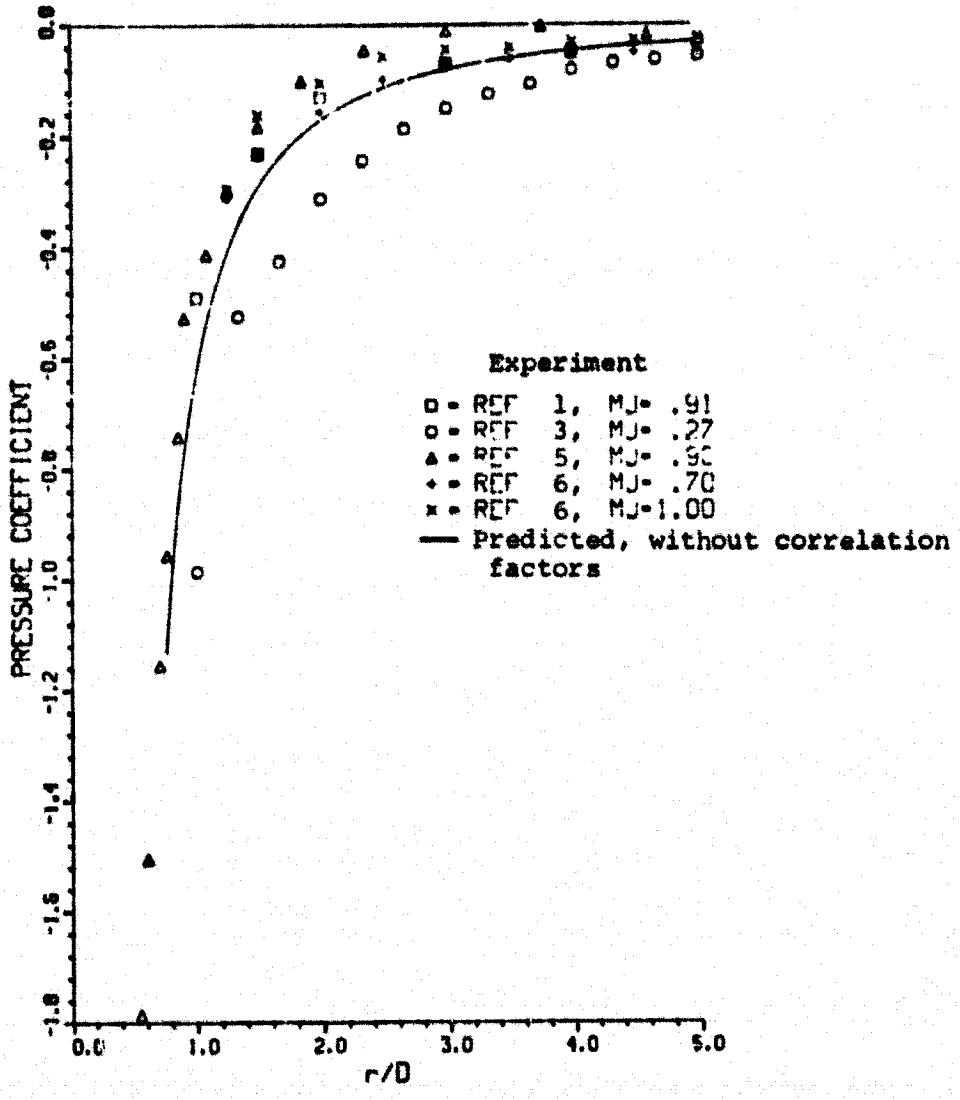

(b) $\beta = 60^{\circ}$

Figure 34.- Concluded.

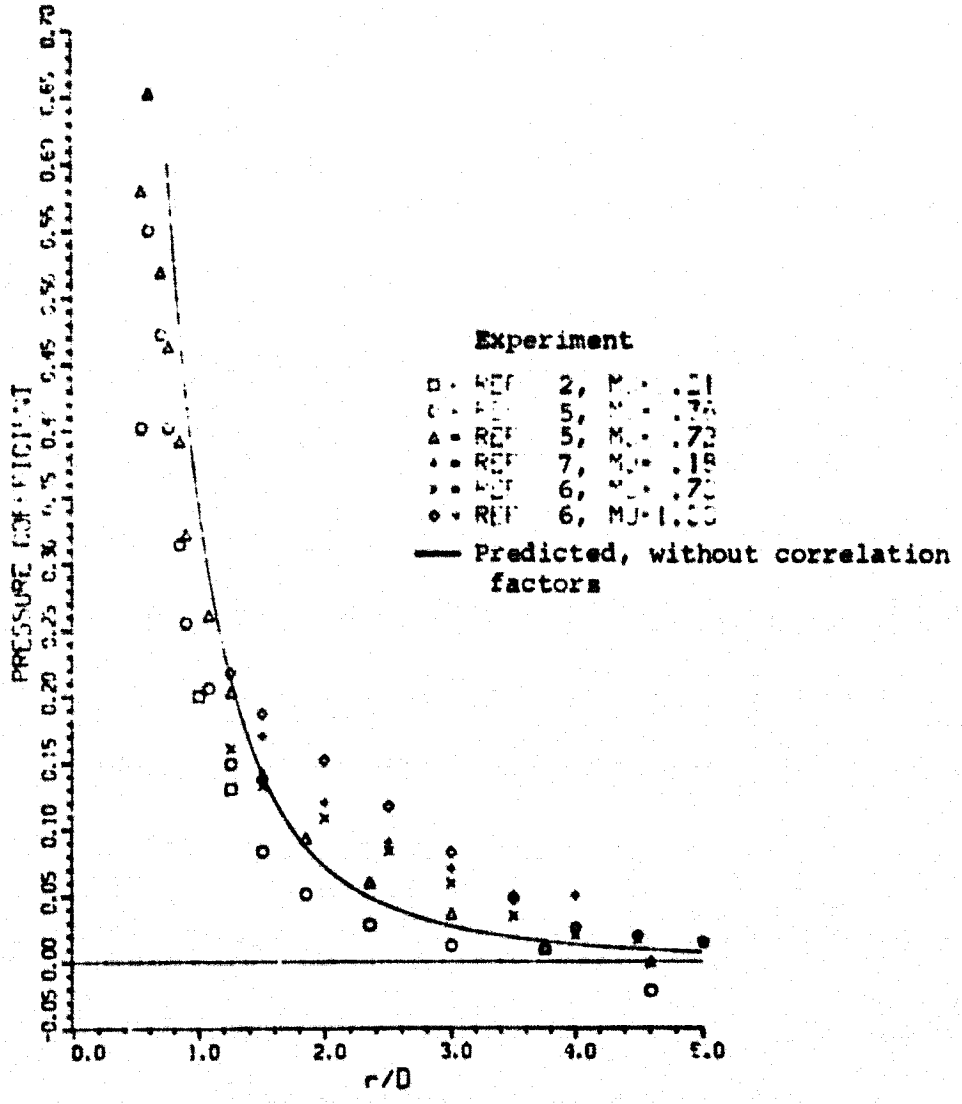

(a) $\beta = 0^{\circ}$

Figure 35.- Comparison of predicted and measured plate pressure distributions, R = 4.0.

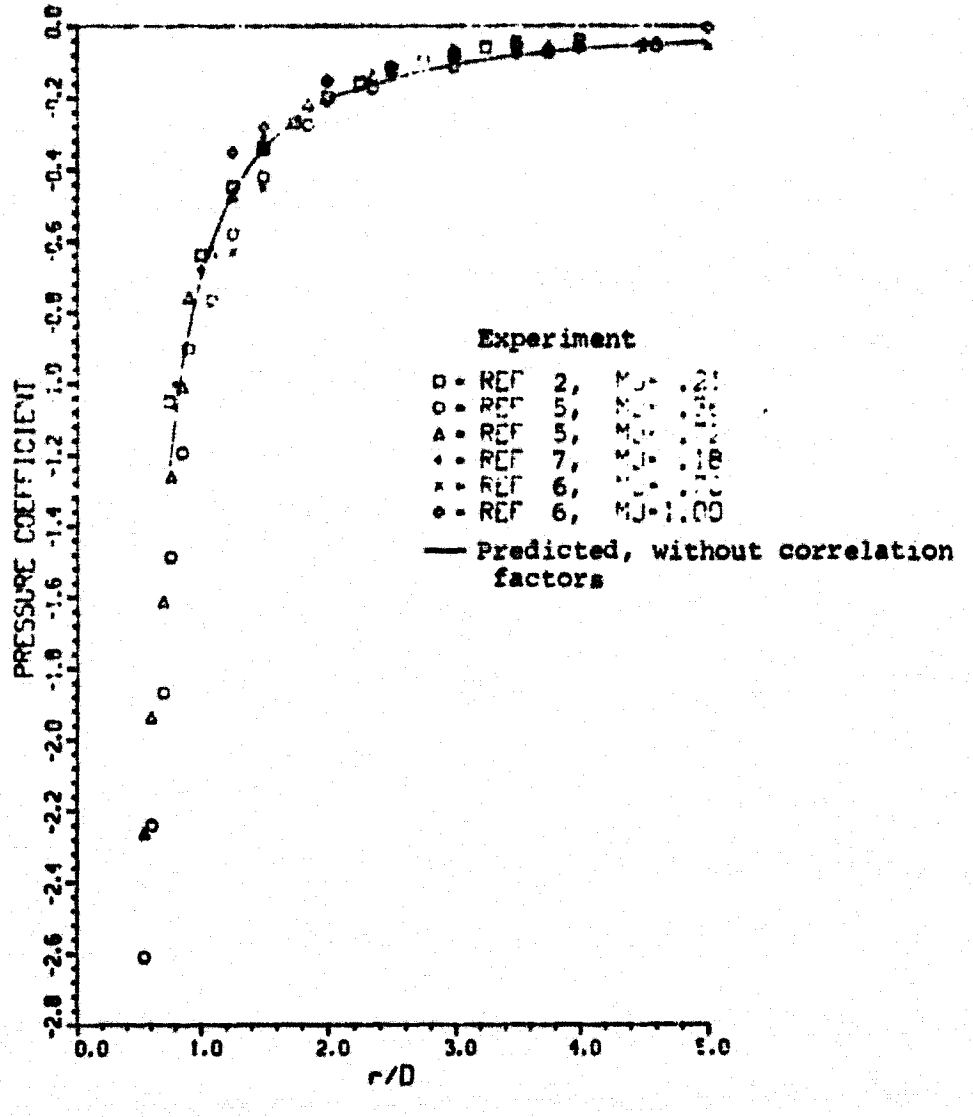

(b) $\beta = 60^{\circ}$

Figure 35.- Concluded.

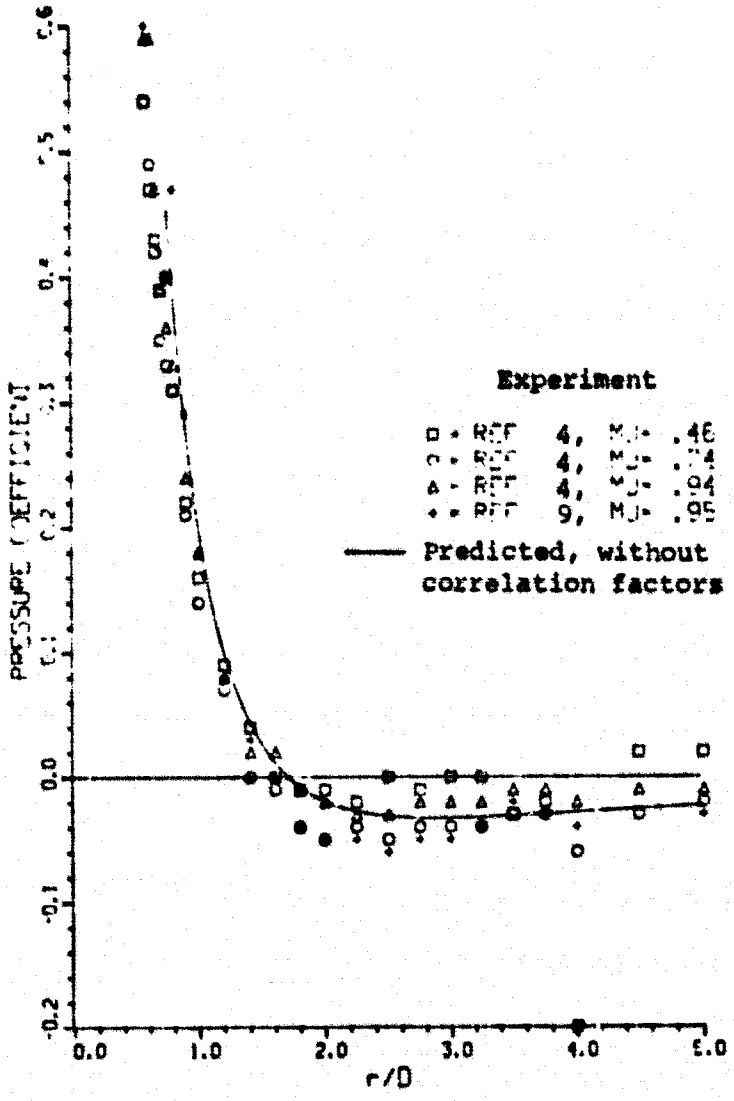

(a) $\beta = 0^{\circ}$

Figure 36.- Comparison of predicted and measured plate pressure distributions, R = 6.0.

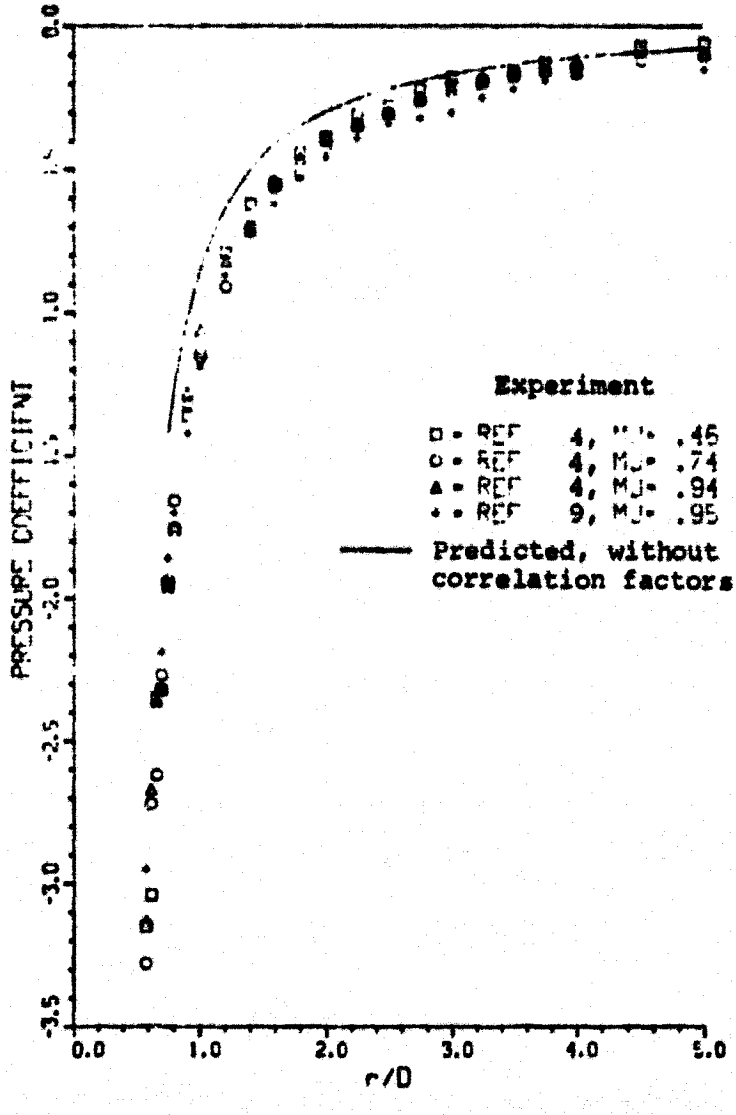

(b) $\beta = 60^{\circ}$

Figure 36.- Concluded.

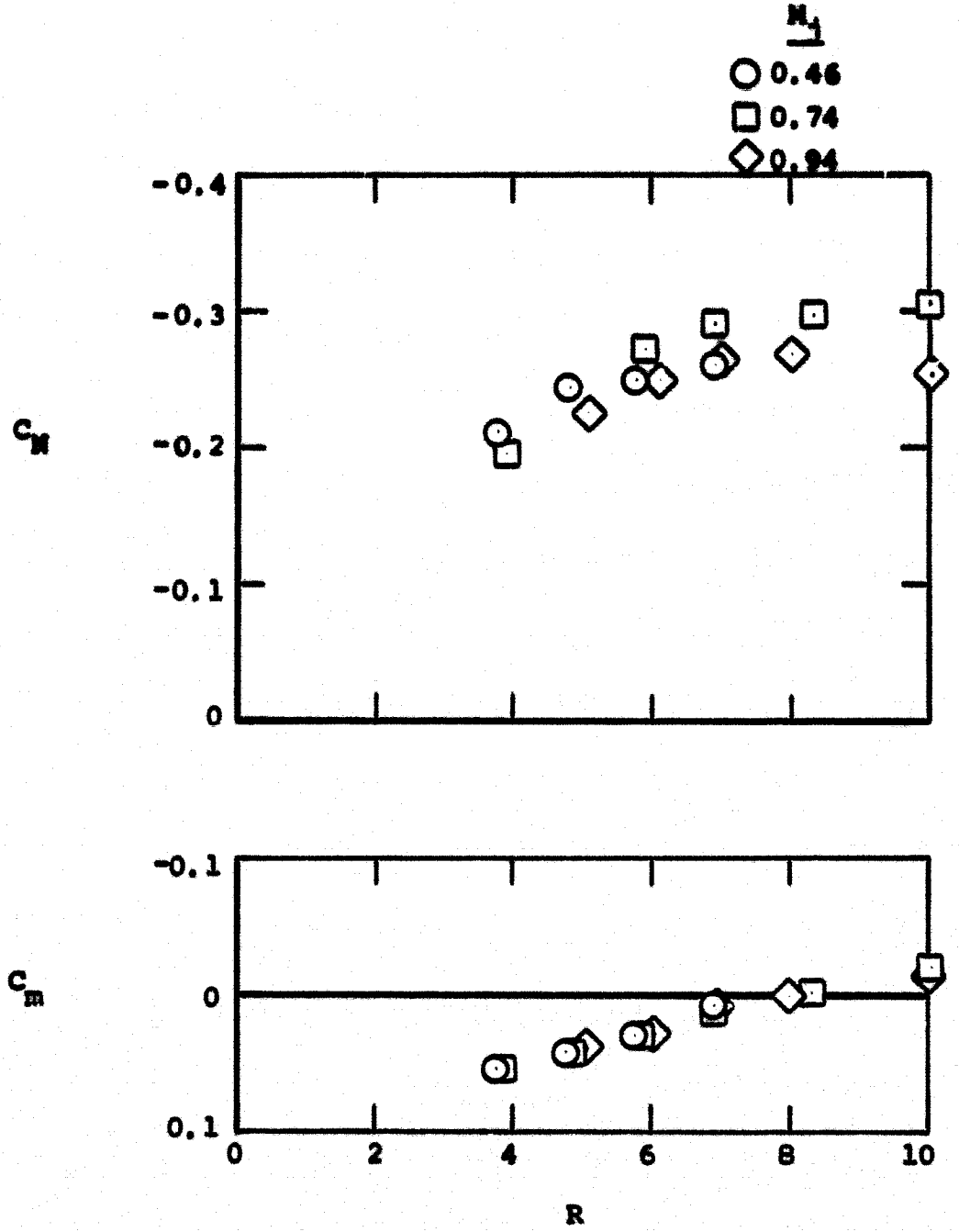

(a) Reference 4 data, r_{max} = 5.25 D

Figure 37.- Normal-force and pitching-moment coefficients on a finite circular plate obtained from measured pressure distributions.

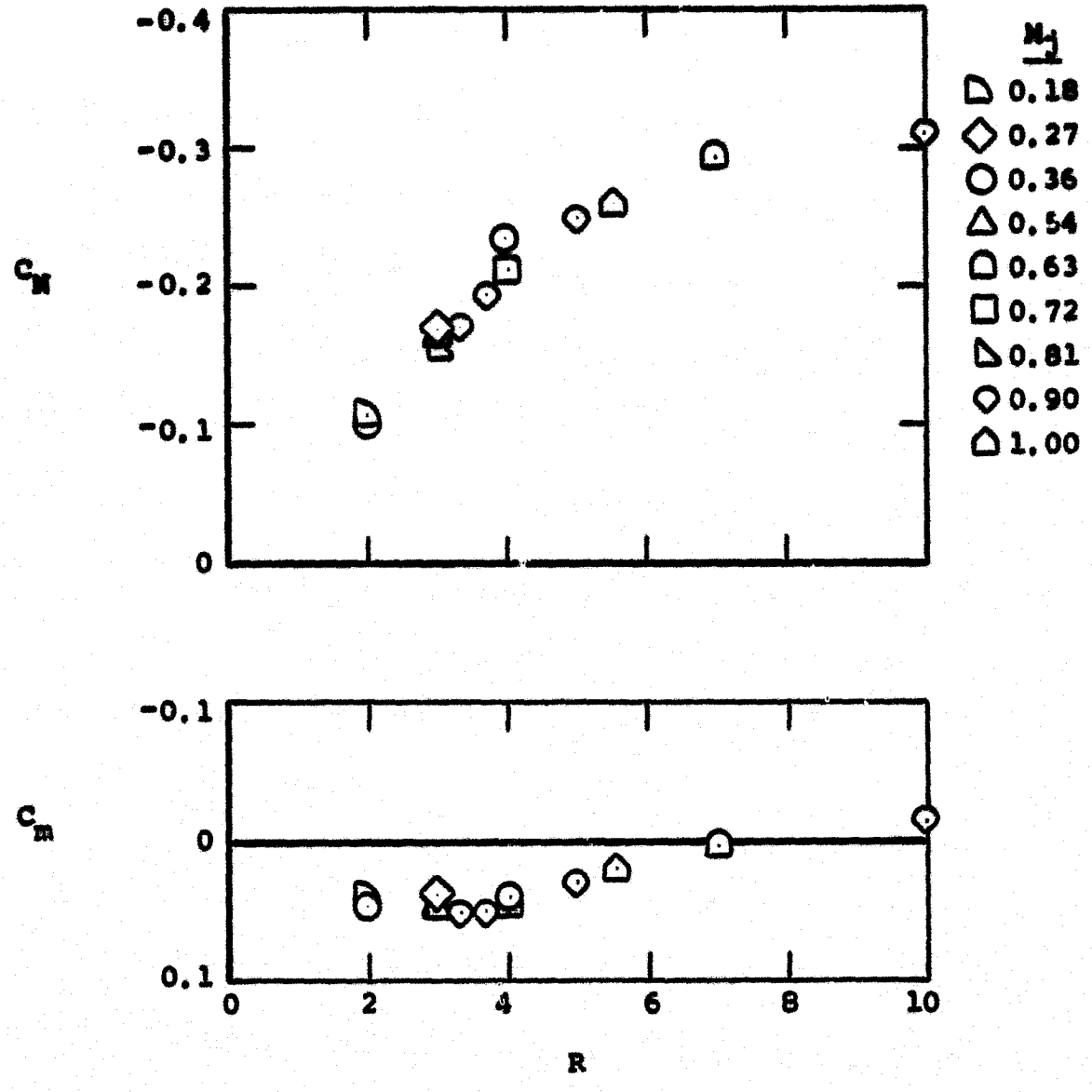

(b) Reference 5 data, r_{max} = 5.025D

Figure 37.- Continued.

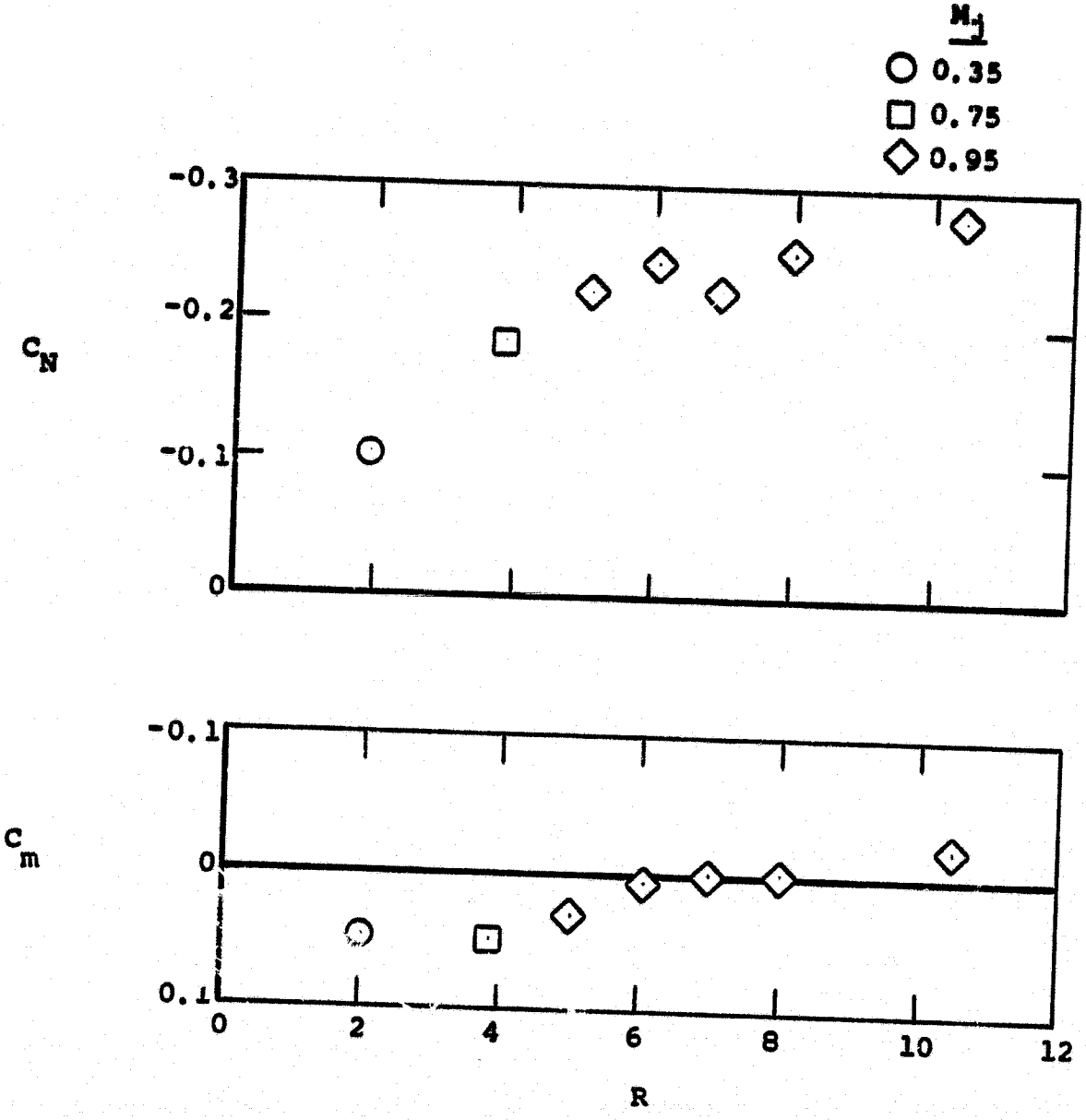

(c) Reference 9 data, r_{max} = 5.5 D.

Figure 37.- Concluded.

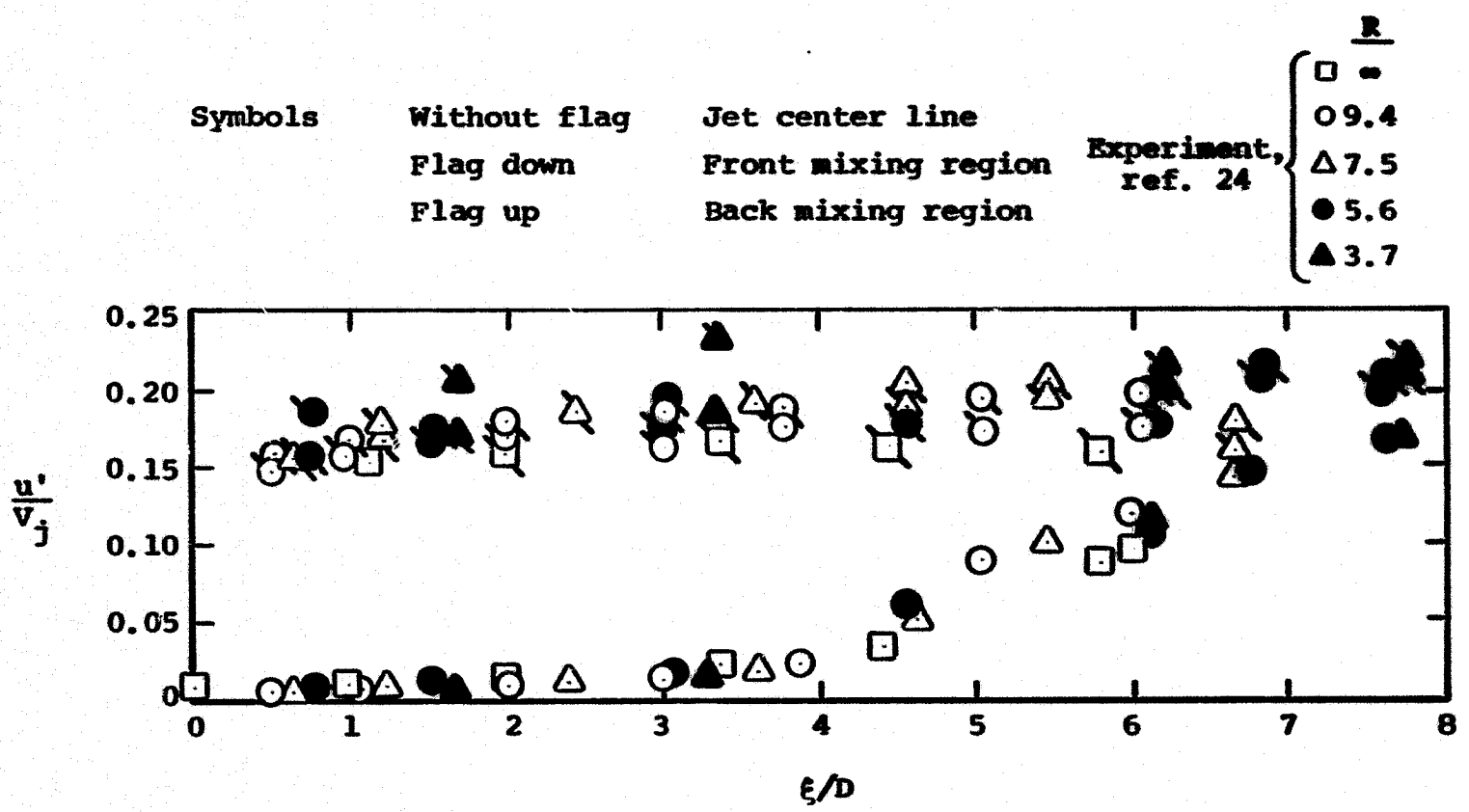

Figure 38.- Axial distribution of turbulent intensity.

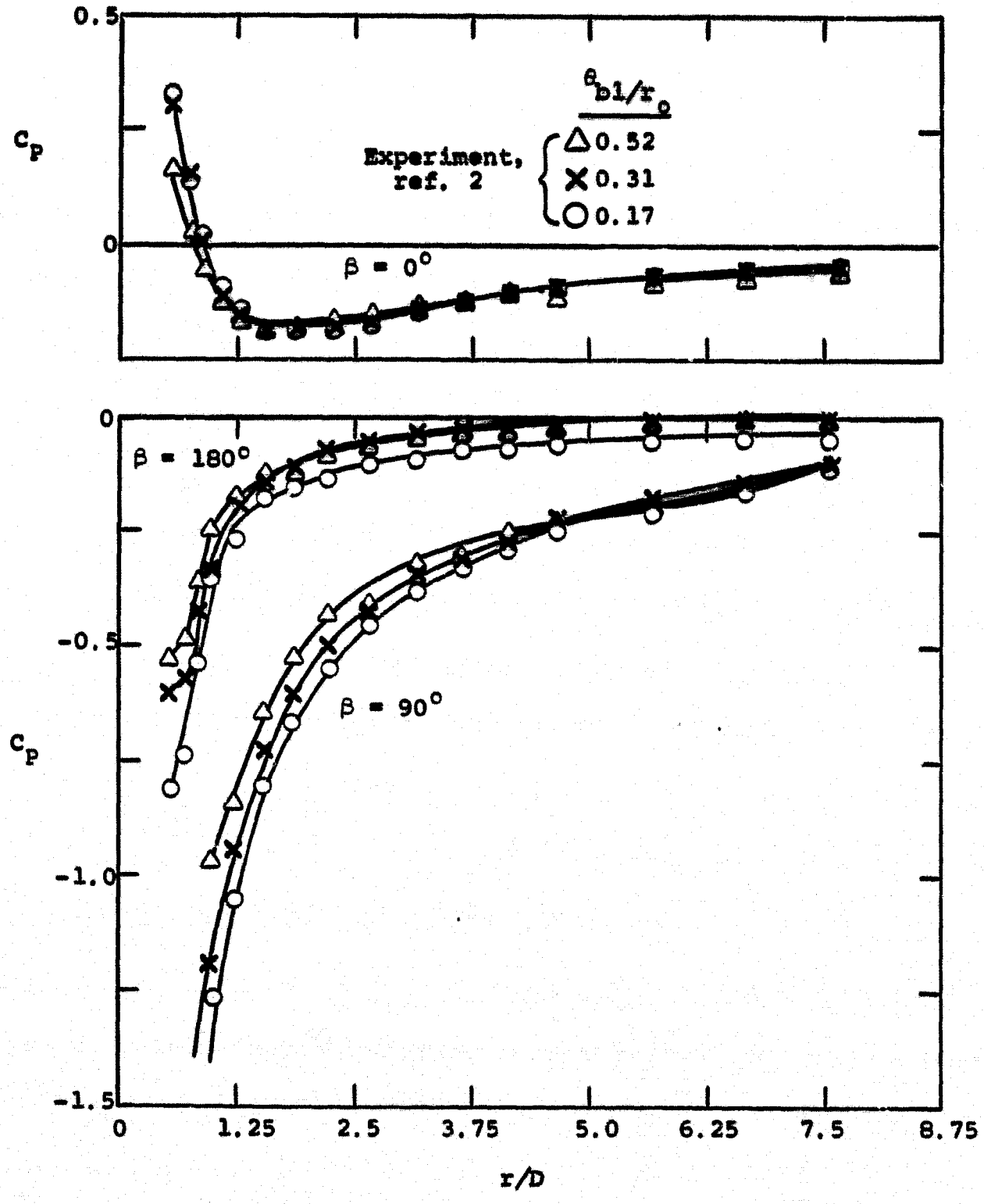

Figure 39.- Effect of boundary-layer thickness on measured surface pressure distribution, R = 8.

APPENDIX A

SUMMARY OF SURFACE PRESSURE DISTRIBUTION DATA

The appendix contains a summary of information on surface pressure distribution data for jets exhausting from a flat plate into a subsonic free stream. The information is listed in Table A-I for the jet velocity ratio range $1.0 \leq R \leq 12.0$. The jet velocity ratio is followed in the table by the reference number (from reference list in text), the definition of R used in that reference, and pertinent experimental parameters. These parameters are free-stream and jet-exit Mach numbers (M_∞ and M_j, respectively), free-stream Reynolds numbers based on jet-exit diameter and run length, (Re_D and Re_ℓ, respectively), the jet-exit diameter and run length (D and ℓ, respectively), and the length and width of the plate (L and W, respectively). Also included is a column which indicates any additional information on jet characteristics available for the given reference. The symbols used in the last column are defined in Table A-II.

TABLE A-I. - DATA SUMMARY TABLE

R	Reference No.	Definition of R	M_∞	M_j	Free Stream Reynolds Number		D (in.)	ℓ (in.)	Plate Dimensions		Jet Characteristics Data Available
					Re_{D_6} ($\times 10^{-6}$)	Re_{ℓ_6} ($\times 10^{-6}$)			L (in.)	W (in.)	
1.0	1	V_j/V_∞	.18	.18	.10	2.01	1.0	20.0	40.0	24.0	
1.25			.14	.18	.08	0.70	1.0	8.5	17.0	4.5	
			.14	.18	.08	1.65		20.0	40.0	24.0	
			.35	.44	.19	3.82		20.0	40.0	24.0	
1.67			.11	.18	.06	0.54		8.5	17.0	4.5	
			.11	.18	.06	1.26		20.0	40.0	24.0	
			.27	.45	.15	1.28		8.5	17.0	4.5	
			.27	.45	.15	3.02		20.0	40.0	24.0	
1.98	9	M_j/M_∞	.178	.353	.205	1.85	2.0	18.0	54.0	48.0	EVP
2.0	2	$\sqrt{q_j/q_\infty}$	.05	.11	.03	0.893	1.0	30.0	84.0	72.0	

TABLE A-I. - CONTINUED

R	Reference No.	Definition of R	M_∞	M_j	Free Stream Reynolds Number		D (in.)	ℓ (in.)	Plate Dimensions		Jet Characteristics Data Available
					Re_{D_6} ($\times 10^{-6}$)	Re_{ℓ_6} ($\times 10^{-6}$)			L (in.)	W (in.)	
2.0	4	M_j/M_∞	.09	.18	.212	1.91	4.0	36.0	96.0	108.0	EVP, PC
	4		.18	.36	.425	3.82	4.0	36.0	96.0	108.0	EVP, PC
	5		.09	.18	.24	1.99	4.7	38.9	98.8	99.2	
			.18	.36	.50	4.14					
			.27	.54	.74	6.12					
2.01	11	$\sqrt{q_{j_e}/q_\infty}$	.27	.55	.153	3.47	1.0	22.75	54.0*	54.0	EVP
2.18	12	V_{j_e}/V_∞	.18	.40	.091	2.151	1.02	24.0	48.0	36.0	
2.21	12	V_{j_e}/V_∞		.40	.090	2.111	1.02	24.0	48.0	36.0	
2.20	4	M_j/M_∞		.39	.425	3.82	4.0	36.0	96.0	108.0	EVP, PC
2.22	11	$\sqrt{q_{j_e}/q_\infty}$	.25	.55	.138	3.14	1.0	22.75	54.0*	54.0	EVP

*Circular Plate

TABLE A-I. - CONTINUED

R	Reference No.	Definition of R	M_∞	M_j	Free Stream Reynolds Number		D (in.)	L (in.)	Plate Dimensions		Jet Characteristics Data Available
					Re_{D_6} ($\times 10^{-6}$)	Re_{ℓ_6} ($\times 10^{-6}$)			L (in.)	W (in.)	
2.23	11	$\sqrt{q_{j_e}/q_\infty}$	.27	.605	.153	3.47	1.0	22.75	54.0*	54.0	EVP
2.27	12	V_{j_e}/V_∞	.18	.40	.095	2.230	1.02	24.0	48.0	36.0	
2.37	↓	↓	.17	↓	.092	2.164	↓	↓	↓	↓	↓
2.37	↓	↓	.17	↓	.091	2.138	↓	↓	↓	↓	↓
2.38	3	V_j/V_∞	.08	.19	.017	0.811	0.375	18.0	36.0	26.0	PC, CDR
2.44	9	M_j/M_∞	.157	.384	.181	1.63	2.0	18.0	54.0	48.0	EVP
2.47	11	$\sqrt{q_j/q_\infty}$	.25	.605	.138	3.14	1.0	22.75	54.0*	54.0	EVP
2.50	12	V_{j_e}/V_∞	.16	.40	.090	2.119	1.02	24.0	48.0	36.0	EVP, PC, CDR, CT
2.50	1	V_j/V_∞	.07	.18	.04	0.84	1.0	20.0	40.0	24.0	
2.50	1	V_j/V_∞	.18	.45	.10	0.85	1.0	8.5	17.0	4.5	

*Circular Plate

TABLE A-I. - CONTINUED

R	Reference No.	Definition of R	M_∞	M_j	Free Stream Reynolds Number		D (in.)	L (in.)	Plate Dimensions		Jet Characteristics Data Available
					Re_{D_6} ($\times 10^{-6}$)	Re_{L_6} ($\times 10^{-6}$)			L (in.)	W (in.)	
2.50	1	V_j/V_∞	.18	.45	.10	2.01	1.0	20.0	40.0	24.0	
2.50	1	V_j/V_∞	.35	.88	.19	3.82	↓	20.0	40.0	24.0	
2.51	11	$\sqrt{q_{j_e}/q_\infty}$	.22	.55	.122	2.78	↓	22.75	54.0*	54.0	EVP
2.59	12	V_{j_e}/V_∞	.15	.40	.087	2.101	1.02	24.0	48.0	36.0	↓
2.61	12	V_{j_e}/V_∞	.154	.40	.084	1.923	1.02	24.0	48.0	36.0	↓
2.78	11	$\sqrt{q_{j_e}/q_\infty}$	.22	.065	.122	2.78	1.0	22.75	54.0*	54.0	↓
2.80	4	M_j/M_∞	.16	.44	.377	3.40	4.0	36.0	96.0	108.0	EVP, PC
2.85	3	V_j/V_∞	.08	.23	.017	.811	0.375	18.0	36.0	26.0	
2.85	11	$\sqrt{q_{j_e}/q_\infty}$	.19	.55	.107	2.44	1.0	22.75	54.0*	54.0	EVP
2.87	11	$\sqrt{q_{j_e}/q_\infty}$	.25	.71	.140	3.17	1.0	22.75	54.0*	54.0	EVP

*Circular Plate

TABLE A-I. - CONTINUED

R	Reference No.	Definition of R	M_∞	M_j	Free Stream Reynolds Number		D (in.)	ℓ (in.)	Plate Dimensions		Jet Characteristics Data Available
					Re_{D_6} ($\times 10^{-6}$)	Re_{ℓ_6} ($\times 10^{-6}$)			L (in.)	W (in.)	
3.0	5	M_j/M_∞	.09	.27	.24	1.99	4.7	30.9	98.8	99.2	
↓	↓	↓	.18	.54	.50	4.14	↓	↓	↓	↓	
↓	↓	↓	.27	.81	.74	6.12	↓	↓	↓	↓	
3.17	11	$\sqrt{q_{j_e}/q_\infty}$	.19	.605	.107	2.44	1.0	22.75	54.0*	54.0	EVP
3.33	1	V_j/V_∞	.13	.45	.08	0.66	1.0	8.5	17.0	4.5	
↓	↓	↓	.13	.45	.08	1.55	↓	20.0	40.0	24.0	
↓	↓	↓	.27	.90	.15	1.28	↓	8.5	17.0	4.5	
↓	↓	↓	.27	.90	.15	3.02	↓	20.0	40.0	24.0	
↓	3	↓	.08	.27	.017	0.811	0.375	18.0	36.0	26.0	PC, CDR
↓	5	M_j/M_∞	.27	.90	.74	6.12	4.7	38.9	98.8	99.2	

*Circular Plate

TABLE A-I. - CONTINUED

R	Reference No.	Definition of R	M_∞	M_j	Free Stream Reynolds Number		D (in.)	ℓ (in.)	Plate Dimensions		Jet Characteristics Data Available
					Re_{D_6} ($\times 10^{-6}$)	Re_{ℓ_6} ($\times 10^{-6}$)			L (in.)	W (in.)	
3.34	6	$\sqrt{q_j/q_\infty}$	.21	.70	.118	2.69	1.0	22.75	54.0*	54.0	EVP
3.34	11	$\sqrt{q_{j_e}/q_\infty}$	.21	.71	.120	2.72					EVP
3.35	6	$\sqrt{q_j/q_\infty}$	.30	1.0	.168	3.82					EVP, PC
3.36	11	$\sqrt{q_{j_e}/q_\infty}$	.16	.55	.091	2.08					EVP
3.68	11	$\sqrt{q_{j_e}/q_\infty}$	.165	.605	.092	2.10					EVP
3.70	5	M_j/M_∞	.27	1.0	.74	6.12	4.7	38.9	98.8	99.2	
3.8	4		.11	.44	.259	2.33	4.0	36.0	96.0	108.0	EVP, PC
3.84	9		.194	.744	.223	2.01	2.0	18.0	54.0	48.0	EVP
3.88			.193	.749	.222	2.0					
3.89			.193	.751	.222	2.0					

*Circular Plate

TABLE A-I. - CONTINUED

R	Reference No.	Definition of R	M_∞	M_j	Free Stream Reynolds Number		D (in.)	ℓ (in.)	Plate Dimensions		Jet Characteristics Data Available
					Re_{D_6} ($\times 10^{-6}$)	Re_{ℓ_6} ($\times 10^{-6}$)			L (in.)	W (in.)	
3.9	4	M_j/M_∞	.19	.75	.448	4.03	4.0	36.0	96.0	108.0	EVP, PC
3.9	12	V_{je}/V_∞	.10	.40	.054	1.274	1.02	24.0	48.0	36.0	EVP,CT,PC, CDR
3.97	6	$\sqrt{q_j/q_\infty}$	.176	.70	.099	2.257	1.0	22.75	54.0*	54.0	EVP
4.0	6	$\sqrt{q_j/q_\infty}$	.25	1.0	.141	3.212	1.0	22.75	54.0*	54.0	EVP
	4	M_j/M_∞	.09	.36	.212	1.91	4.0	36.0	96.0	108.0	EVP, PC
	4		.18	.72	.425	3.82	4.0	36.0	96.0	108.0	EVP, PC
	5		.09	.36	.24	1.99	4.7	38.9	98.8	99.2	
	7	$\sqrt{q_j/q_\infty}$	.044	.18	.052	0.621	2.0	24.0	48.0	66.0	EVP, CT
	2	$\sqrt{q_j/q_\infty}$	.05	.22	.030	0.893	1.0	30.0	84.0	72.0	
	5	M_j/M_∞	.18	.72	.50	4.14	4.7	38.9	98.8	99.2	

*Circular Plate

TABLE A-I. - CONTINUED

R	Reference No.	Definition of R	M_∞	M_j	Free Stream Reynolds Number		D (in.)	ℓ (in.)	Plate Dimensions		Jet Characteristics Data Available
					Re_D ($\times 10^{-6}$)	Re_ℓ ($\times 10^{-6}$)			L (in.)	W (in.)	
4.01	11	$\sqrt{q_{j_e}/q_\infty}$	.25	1.0	.140	3.19	1.0	22.75	54.0*	54.0	EVP, CT
4.03	11	$\sqrt{q_{j_e}/q_\infty}$	.18	.71	.099	2.26	1.0	22.75	54.0*	54.0	EVP, CT
4.36	12	V_{j_e}/V_∞	.09	.40	.045	1.064	1.02	24.0	48.0	36.0	EVP
4.42	↓	↓	.08	↓	.044	1.044	↓	↓	↓	↓	↓
4.54	↓	↓	.09	↓	.046	1.093	↓	↓	↓	↓	↓
4.74	↓	↓	.09	↓	.046	1.071	↓	↓	↓	↓	↓
4.74	↓	↓	.08	↓	.045	1.057	↓	↓	↓	↓	↓
4.80	4	M_j/M_∞	.09	.45	.212	1.91	4.0	36.0	96.0	108.0	EVP, PC
4.90	4	M_j/M_∞	.15	.74	.354	3.18	4.0	36.0	96.0	108.0	EVP, PC, CT
4.98	6	$\sqrt{q_j/q_\infty}$	.20	1.0	.113	2.572	1.0	22.75	54.0*	54.0	EVP, PC

*Circular Plate

TABLE A-I. - CONTINUED

R	Reference No.	Definition of R	M_∞	M_j	Free Stream Reynolds Number		D (in.)	ℓ (in.)	Plate Dimensions		Jet Characteristics Data Available
					Re_D ($\times 10^{-6}$)	Re_ℓ ($\times 10^{-6}$)			L (in.)	W (in.)	
4.99	12	V_{j_e}/V_∞	.08	.40	.044	1.039	1.02	24.0	48.0	36.0	EVP
4.99	11	$\sqrt{q_{j_e}/q_\infty}$	.18	.71	.080	1.82	1.0	22.75	54.0*	54.0	EVP
5.0	1	V_j/V_∞		.90	.10	0.85		8.5	17.0	8.5	
	1	V_j/V_∞			.10	2.01		20.0	40.0	24.0	
	4	M_j/M_∞			.425	3.82	4.0	36.0	96.0	108.0	EVP, PC
	5	M_j/M_∞			.50	4.14	4.7	38.9	98.8	99.2	
	6	$\sqrt{q_j/q_\infty}$	.14	.70	.079	1.186	1.0	22.75	54.0*	54.0	EVP
5.05	11	$\sqrt{q_{j_e}/q_\infty}$	.20	1.0	.111	2.53	1.0	22.75	54.0*	54.0	
5.07	9	M_j/M_∞	.186	.945	.214	1.92	2.0	18.0	54.0	48.0	
5.09	11	$\sqrt{q_{j_e}/q_\infty}$	.11	.55	.060	1.37	1.0	22.75	54.0*	54.0	

*Circular Plate

TABLE A-I. - CONTINUED

R	Reference No.	Definition of R	M_∞	M_j	Free Stream Reynolds Number		D (in.)	L (in.)	Plate Dimensions		Jet Characteristics Data Available
					Re_D ($\times 10^{-6}$)	Re_ℓ ($\times 10^{-6}$)			L (in.)	W (in.)	
5.1	4	M_j/M_∞	.19	.95	.448	4.03	4.0	36.0	96.0	108.0	EVP, PC
5.18	12	V_{j_e}/V_∞	.08	.40	.044	1.039	1.02	24.0	48.0	36.0	EVP
5.21	12	V_{j_e}/V_∞	.08	.40	.040	0.952	1.02	24.0	48.0	36.0	EVP
5.56	5	M_j/M_∞	.18	1.0	.50	4.14	4.7	38.9	98.8	99.2	
5.8	4	↓	.08	.46	.189	1.70	4.0	36.0	96.0	108.0	EVP, PC
5.9	↓	↓	.12	.74	.283	2.55	↓	↓	↓	↓	EVP, PC, CT
6.1	↓	↓	.15	.94	.354	3.18	↓	↓	↓	↓	EVP, PC
6.12	9	↓	.154	.946	.177	1.59	2.0	18.0	54.0	48.0	EVP
6.51	12	V_{j_e}/V_∞	.06	.40	.032	0.760	1.02	24.0	48.0	36.0	↓
6.53	6	$\sqrt{q_j/q_\infty}$	.107	.70	.060	1.370	1.0	22.75	54.0*	54.0	↓

*Circular Plate

TABLE A-I. - CONTINUED

R	Reference No.	Definition of R	M_∞	M_j	Free Stream Reynolds Number		D (in.)	ℓ (in.)	Plate Dimensions		Jet Characteristics Data Available
					Re_{D_6} ($\times 10^{-6}$)	Re_{ℓ_6} ($\times 10^{-6}$)			L (in.)	W (in.)	
6.53	12	V_{j_e}/V_∞	.06	.40	.030	0.707	1.02	24.0	48.0	36.0	EVP
6.58	12	V_{j_e}/V_∞	.06	.40	.030	0.694	1.02	24.0	48.0	36.0	
6.61	6	$\sqrt{q_j/q_\infty}$	.15	1.0	.085	1.94	1.0	22.75	54.0*	54.0	
6.63	11	$\sqrt{q_{j_e}/q_\infty}$	.18	.71	.060	1.37					
6.80	11	$\sqrt{q_{j_e}/q_\infty}$	.15	1.0	.083	1.88					
6.81	12	V_{j_e}/V_∞	.06	.40	.031	0.726	1.02	24.0	48.0	36.0	
6.9	4	M_j/M_∞	.07	.46	.157	1.42	4.0	36.0	96.0	108.0	EVP, PC
			.09	.63	.212	1.91					
			.11	.74	.259	2.33					
7.0			.13	.94	.307	2.76					EVP, PC, CT

*Circular Plate

TABLE A-I. - CONTINUED

R	Reference No.	Definition of R	M_∞	M_j	Free Stream Reynolds Number		D (in.)	ℓ (in.)	Plate Dimensions		Jet Characteristics Data Available
					Re_{D_6} ($\times 10^{-6}$)	Re_{ℓ_6} ($\times 10^{-6}$)			L (in.)	W (in.)	
7.0	5	M_j/M_∞	.09	.63	.24	1.99	4.7	38.9	98.8	99.2	
7.02	9	M_j/M_∞	.134	.943	.154	1.39	2.0	18.0	54.0	48.0	EVP
7.10	12	V_{j_e}/V_∞	.06	.40	.030	0.703	1.02	24.0	48.0	36.0	
7.11			.06			0.707					
7.49			.05			0.696					
7.76			.05		.029	0.691					
7.77	6	$\sqrt{q_j/q_\infty}$	.09	.70	.051	1.152	1.0	22.75	54.0*	54.0	
7.81	12	V_{j_e}/V_∞	.05	.40	.026	0.633	1.02	24.0	48.0	36.0	EVP, PC, CT, CDR
7.89	11	$\sqrt{q_{j_e}/q_\infty}$	.09	.71	.051	1.15	1.0	22.75	54.0*	54.0	EVP, CT
8.0	2	$\sqrt{q_j/q_\infty}$	.05	.44	.030	0.893	1.0	30.0	84.0	72.0	

*Circular Plate

TABLE A-I. - CONTINUED

R	Reference No.	Definition of R	M_∞	M_j	Free Stream Reynolds Number		D (in.)	ℓ (in.)	Plate Dimensions		Jet Characteristics Data Available
					Re_{D_6} ($\times 10^{-6}$)	Re_{ℓ_6} ($\times 10^{-6}$)			L (in.)	W (in.)	
8.0	4	M_j/M_∞	.12	.93	.283	2.55	4.0	36.0	96.0	108.0	EVP, CT
↓	7	$\sqrt{q_{j_e}/q_\infty}$	.044	.36	.052	0.621	2.0	24.0	48.0	66.0	EVP, CT, CDR
↓	9	M_j/M_∞	.117	.938	.135	1.21	2.0	18.0	54.0	48.0	EVP
8.02	11	$\sqrt{q_{j_e}/q_\infty}$	.125	1.0	.070	1.60	1.0	22.75	54.0*	54.0	EVP, PC, CDR
8.04	6	$\sqrt{q_{j_e}/q_\infty}$	.125	1.0	.070	1.595	1.0	22.75	54.0*	54.0	EVP, CT
8.07	9	M_j/M_∞	.117	.943	.135	1.21	2.0	18.0	54.0	48.0	EVP
8.14	9	↓	.117	.949	.137	1.24	2.0	18.0	54.0	48.0	EVP
8.3	4	↓	.09	.74	.212	1.91	4.0	36.0	96.0	108.0	EVP, PC
8.72	12	V_{j_e}/V_∞	.05	.40	.024	0.529	1.02	24.0	48.0	36.0	EVP
8.78	12	V_{j_e}/V_∞	.05	.40	.022	0.511	1.02	24.0	48.0	36.0	EVP

*Circular Plate

TABLE A-I. - CONTINUED

R	Reference No.	Definition of R	M_∞	M_j	Free Stream Reynolds Number		D (in.)	ℓ (in.)	Plate Dimensions		Jet Characteristics Data Available
					Re_{D_6} ($\times 10^{-6}$)	Re_{ℓ_6} ($\times 10^{-6}$)			L (in.)	W (in.)	
9.08	12	V_{j_e}/V_∞	.044	.40	.023	0.543	1.02	24.0	48.0	36.0	EVP
9.11	↓	↓	.044	↓	↓	0.542	↓	↓	↓	↓	↓
9.41	↓	↓	.043	↓	↓	0.532	↓	↓	↓	↓	↓
9.48	↓	↓	.042	↓	.022	0.526	↓	↓	↓	↓	↓
9.95	6	$\sqrt{q_j/q_\infty}$	.10	1.0	.057	1.288	1.0	22.75	54.0*	54.0	EVP, PC
9.98	12	V_{j_e}/V_∞	.04	.40	.022	0.521	1.02	24.0	48.0	36.0	EVP
10.0	4	M_j/M_∞	.07	.74	.157	1.42	4.0	36.0	96.0	108.0	EVP, PC
↓	4	↓	.09	.93	.212	1.91	4.0	36.0	96.0	108.0	EVP,PC,CT CDR
↓	5	↓	.09	.90	.24	1.99	4.7	38.9	98.8	99.2	
↓	7	$\sqrt{q_j/q_\infty}$	.044	.44	.052	0.621	2.0	24.0	48.0	66.0	EVP

*Circular Plate

TABLE A-I. - CONCLUDED.

R	Reference No.	Definition of ρ	M_∞	M_j	Free Stream Reynolds Number		D (in.)	ℓ (in.)	Plate Dimensions		Jet Characteristics Data Available
					Re_{D_6} ($\times 10^{-6}$)	Re_{ℓ_6} ($\times 10^{-6}$)			L (in.)	W (in.)	
10.18	6	$\sqrt{q_j/q_\infty}$	.07	.70	.039	0.880	1.0	22.75	54.0*	54.0	EVP
10.29	11	$\sqrt{q_{j_e}/q_\infty}$	.10	1.0	.055	1.25	↓	↓	↓	↓	↓
10.33	11	$\sqrt{q_{j_e}/q_\infty}$	.07	.71	.039	0.88	↓	↓	↓	↓	↓
10.35	12	V_{j_e}/V_∞	.04	.40	.022	0.517	1.02	24.0	48.0	36.0	↓
10.46	9	M_j/M_∞	.090	.944	.104	0.93	2.0	18.0	54.0	48.0	↓
11.11	5	M_j/M_∞	.09	1.0	.24	1.99	4.7	38.9	98.8	99.2	
11.3	2	$\sqrt{q_j/q_\infty}$	.05	.63	.03	0.893	1.0	30.0	84.0	72.0	
12.0	7	$\sqrt{q_j/q_\infty}$	.044	.53	.052	0.621	2.0	24.0	48.0	66.0	EVP, CT
12.0	8	V_j/V_∞	NR**	.53	NR**	NR**	0.5	10.0	48.0	36.0	EVP, CT, PC, CDR

*Circular Plate

**Indicates no reference to the given quantity

TABLE A-II. - DEFINITION OF SYMBOLS USED IN TABLE A-I

Symbol	Jet Characteristics for Which Information is Available
CDR	Centerline Decay Rate (velocity, dynamic pressure or total pressure)
CT	Centerline Trajectory (based on maximum velocity or dynamic pressure)
EVP	Exit Velocity Profile
PC	Potential Core Length (static or dynamic)